AN ABSTRACT OF THE THESIS OF

David D. McGehee for the degree of Master of Ocean Engineering in Ocean Engineering presented on July 17, 1997. Title: Three Applications of Wave Measurements in Coastal Engineering.

Redacted for privacy

Abstract approved: _____

Charles K. Sollitt

Three case studies are presented in which measured wave data describe the environment and provide engineering solutions. The first study details monitoring of Agat Harbor, Guam. The harbor was excavated on a coral reef and protected with a detached breakwater. Waves and water levels were recorded for several years. Data during large wave events, including three typhoons, indicate an unanticipated mode of non-linear transformation is responsible for the highest energy levels observed on the reef. The second study compares measured wave reflection and transmission at a breakwater with physical model predictions. Nondirectional wave measurements were made at four sites inside and outside of Burns Harbor, IN, which is protected by a porous rubble mound breakwater. An energy-based method was used to determine a reflection coefficient, K_R, as a function of incident wave height, by analyzing simultaneous measurements from sites in front of, and beside, the structure. The transmission coefficient of the breakwater, K_T, was similarly calculated from simultaneous measurements at sites in front of, and behind, the structure. The measured transmission characteristics were compared to the physical model results. The third study describes a potential tool for improved tsunami warnings. Four tools are described for improving the amplitude estimate of an approaching tsunami using pressure measurements in shallow water. Performance is evaluated with a pressure time series from the 4 October 1994 Shikotan tsunami measured at Kahului Harbor, HI.

Three Applications of Wave Measurements in Coastal Engineering

by

David D. McGehee

A THESIS

submitted to

Oregon State University

in partial fulfillment of
the requirements for the
degree of

Master of Ocean Engineering

Presented July 17, 1997
Commencement June 1998

Master of Ocean Engineering thesis of David D. McGehee presented on July 17, 1997

APPROVED:

Redacted for privacy

Major Professor, representing Ocean Engineering

Redacted for privacy

Chair of Department of Civil Construction, and Environmental Engineering

Redacted for privacy

Dean of Graduate School

I understand that my thesis will become part of the permanent collection of Oregon State University libraries. My signature below authorizes release of my thesis to any reader upon request.

Redacted for privacy

David D. McGehee, Author

ACKNOWLEDGMENTS

These studies were funded by Headquarters, U.S. Army Corps of Engineers (CE) through the Coastal Field Data Collection Program and the Monitoring Completed Navigation Projects Program. The Burns and Agat harbors wave data were collected by the Prototype Measurement and Analysis Branch (PMAB) of the U.S. Army Engineer Waterways Experiment Station. Analysis and plotting of the data were performed with the assistance of Mr. Patrick McKinney and Dr. Joon Rhee of PMAB. The tsunami data set was collected by the Coastal Data Information Program, a network of wave gages jointly managed and funded by the CE and the California Department of Boating and Waterways, and operated by the Scripps Institution of Oceanography (SIO). Mr. David Castel of SIO provided valuable assistance in compiling and analyzing the data. Ms. Rebecca Brooks and Ms. Terri Prickett of the CE Coastal and Hydraulics Laboratory assisted in the preparation of tables and figures. Permission was granted by the Chief of Engineers to publish this information.

CONTRIBUTION OF AUTHORS

Mr. David McGehee was the principal author for each manuscript. Dr. Charles K. Sollitt developed the concept and derived the basic equations used to estimate a tsunami's period from the temporal derivative of the sea surface slope. Mr. Stanley Boc developed the initial monitoring plan, and provided valuable logistic and administrative support for the study at Agat Harbor, Guam.

TABLE OF CONTENTS

TABLE OF CONTENTS (Continued)

LIST OF FIGURES

LIST OF FIGURES (Continued)

LIST OF TABLES

LIST OF NOTATIONS

a = tsunami amplitude;

σ = tsunami angular frequency;

t = time, origin at leading edge of wave;

p = measured pressure;

h = mean depth of sensor;

η = water surface elevation due to tsunami;

ρ = water density;

g = acceleration due to gravity;

$\overline{\eta}$ = tidal elevation;

k = wave number;

z = vertical space coordinate;

π = 3.14159;

T = tsunami period;

H = solitary wave height;

x = horizontal space coordinate;

c = wave celerity;

τ = time, origin at the passage of the wave crest;

L = wavelength;

R = wave runup;

h_s = water depth;

H_s = wave height;

P = wave power;

η^* = predicted elevation of the wave crest, constant period; and

$\eta(T)$ = predicted elevation of the wave crest, variable period.

THREE APPLICATIONS OF WAVE MEASUREMENTS IN COASTAL ENGINEERING

INTRODUCTION

Obtaining a single ocean wave measurement with any instrument more accurate than the human eye is a costly undertaking. Extending those measurements for months or years, and insuring continuance through extremes of weather, is so expensive that only the government or the offshore oil industry attempt it on a regular basis. As a result, many coastal projects are designed using hindcast wave "data" generated from more readily available wind data, with an inevitable decrease in accuracy. When measurements are available, it is imperative to maximize the information derived. This thesis presents three instances where that is attempted - two case studies and one proposed application.

The studies cover a broad spectrum of interest and energy - wind waves affecting harbor operations, with periods on the order of seconds; seiche modes on the order of minutes, that turn out to dominate a coral reef's hydraulics; and tsunamis, with periods approaching an hour. The common theme in these three studies is the continuum of thought required to bridge the gap from observation to understanding. A natural process may be initially observed visually, but the underlying physics of hydraulic phenomenon are seldom obvious. To obtain a better grasp of the phenomenon, a *data collection* plan is developed, including a selection (or design) of a sensor/instrument system and a signal processing system. To improve our grasp of the data, a *data analysis* scheme is used to compile, reduce, and/or display the data and its interrelationships. If we are successful, visualization of the analyzed data will allow us to *interpret* the data in terms of the original phenomenon. Ideally, a sound engineering decision results.

The inherent risk in this process is confusing our interpretation with nature. The instrument both illuminates and filters what it measures; the analysis both reveals and distorts the data. This is avoided through understanding of the limitations and artifacts imposed each

time we step further away from the prototype, and towards our conceptual model. From that perspective, the human eye may be the optimum window on reality.

Agat Harbor Monitoring Study

David D. McGehee and Stanley Boc

Technical Report CHL-97-22,
U.S. Army Corps of Engineers,
Waterways Experiment Station, Vicksburg, MS,
September, 1997, in press.

AGAT HARBOR MONITORING STUDY

INTRODUCTION

The Monitoring Completed Coastal Projects (MCCP) Program was established by Headquarters, U.S. Army Corps of Engineers (HQUSACE) in 1981 to evaluate the performance of the Corps in planning, design, construction, and operation and maintenance of selected Civil Works coastal projects. The program was renamed Monitoring Completed Navigation Projects (MCNP) in October 1996. The MCNP is funded by the Operations and Maintenance (O&M) Division HQUSACE, and is managed by the U.S. Army Engineer Waterways Experiment Station (WES) Coastal Engineering Research Center (CERC). Oversight is provided by a Field Review Group composed of representatives of Corps Divisions with coastal interests, Technical Monitors from HQUSACE, and the Coastal Engineering Research Board. The program's objective is to acquire information through intensive monitoring of coastal projects for improving:

a. Project purpose and attainment.

b. Design procedures.

c. Construction methods.

d. Operation and maintenance techniques.

Potential projects are nominated by coastal Districts and selected for monitoring during an annual Program Review attended by the Field Review Group. Selection is based on the potential for improving general procedures for application at other sites or for solving site-specific problems. Agat Harbor was nominated for inclusion in the MCCP by the

U.S. Army Engineer Division, Pacific Ocean (POD) and accepted for inclusion in the program in 1986. Monitoring and documentation were joint efforts between CERC and POD.

PROJECT DESCRIPTION

Site Description: Agat Harbor is located on the western side of the island of Guam (Figure 1). Mean tide range is 0.4 m (1.4 ft).[1] Agat is fringed by coral reefs characterized by a broad, shallow flat with a near-uniform depth of 0.3 m mean lower low water (mllw) (i.e., nearly exposed at low tide) that extends about 1 km offshore. The face of the reef is live coral with a near vertical slope down to approximately -6 m. The face is extremely porous and rough due to the health and size of the coral, and is an excellent dissipator of wave energy. Further offshore, water depth increases rapidly at an average bottom slope of 0.2.

Agat is in the lee of the island with respect to the predominant easterly trade winds, so incident waves are usually low. Waves that do approach from the west break at the reef face, so the reef flat and harbor are quiescent the majority of the time. The island is routinely exposed to typhoons. Typhoon conditions can only be estimated, but conditions on the reef flat and the backshore will be violent.

The harbor was designed and built by the POD and the Port Authority of Guam (U.S. Army Engineer District (USAED), Honolulu 1981). Construction was completed in 1990. The harbor basin was excavated from the reef flat that runs for miles along the western shore (Figure 2). It is protected by a detached 300-m long rubble-mound breakwater. A 36-m wide by 4.2-m deep and approximately 300-m long entrance channel was excavated from the harbor across the reef flat. The channel enters the -6 m depth outside the reef face at a "notch" in the reef plan that is likely a natural channel through the reef. Figure 3 shows the channel under construction, before excavation of the basin; Figure 4 shows the completed project prior to construction of berthing and shoreside facilities.

---

[1] The original design and survey data were provided in English units. Data collected for this study are reported in metric units, with the exception of some overwater distances, which are provided in nautical miles, following nautical convention.

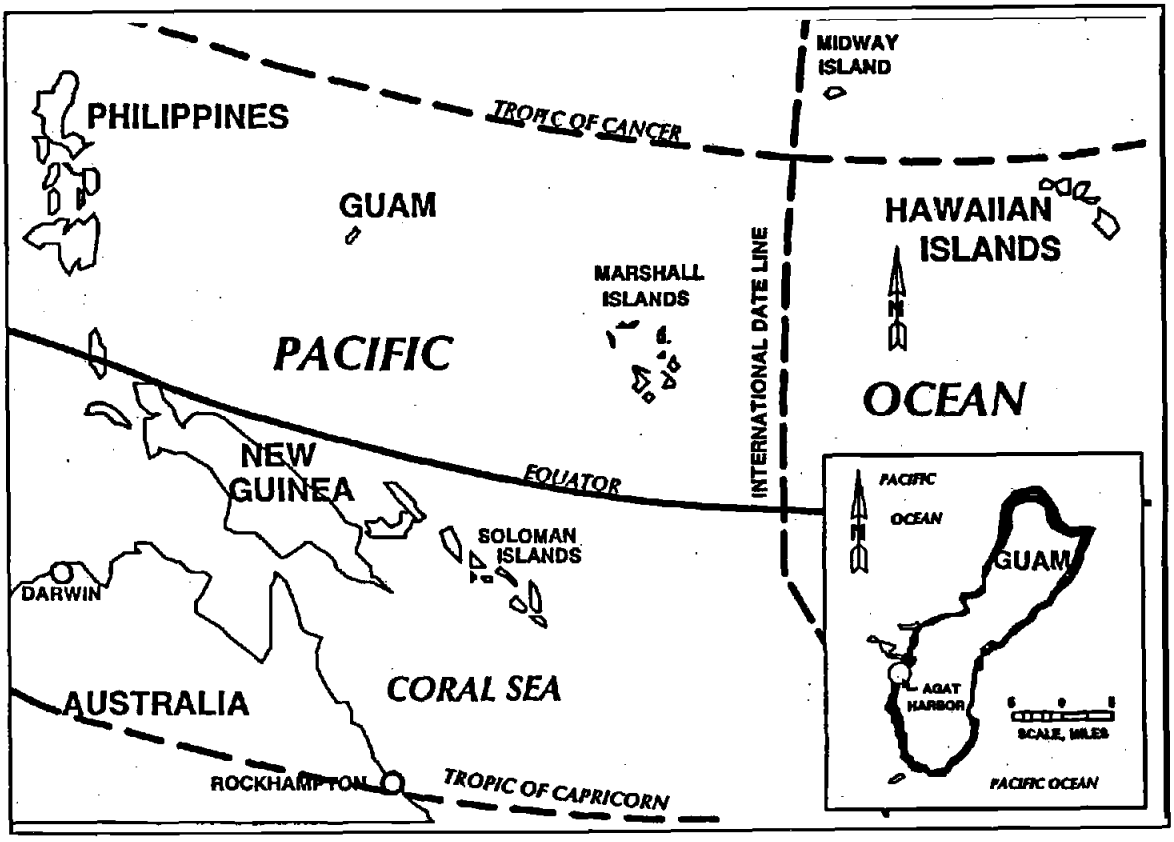

Figure 1. Location and site map of Agat Harbor, Guam

Design Criteria: The objectives of the project, as stated in the project report (USAED, Honolulu 1981), were to improve commercial and recreational boating facilities for Agat and improve socioeconomic opportunities for the people of Guam, while minimizing alteration of the reef environment. The technical criteria developed in that report for the harbor were:

a. The entrance channel should provide for two-way traffic and be navigable during all weather and sea conditions except during periods of severe storms, and the berthing area should be protected from severe storm waves during all conditions.

b. The plan should include a turning basin adequate for maneuvering of the design vessel and provisions for berthing and shoreside facilities.

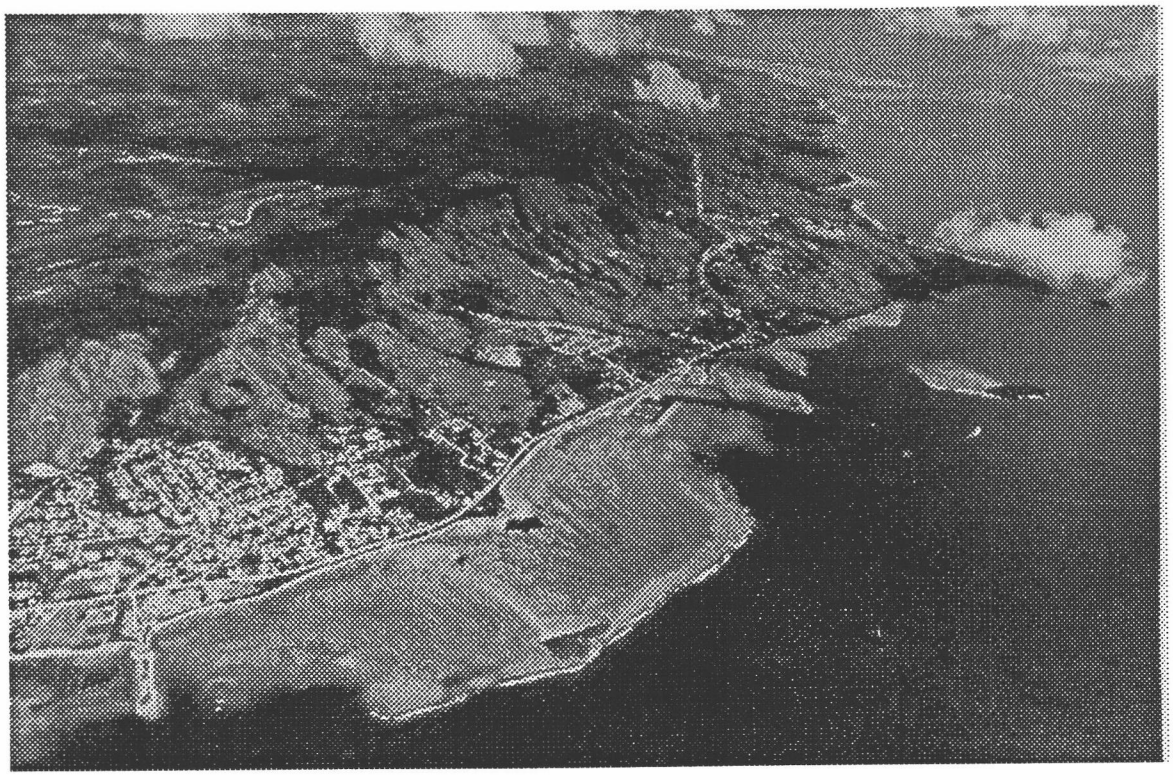

Figure 2. Aerial view of southwestern coast of Guam

c. Protective structures should be designed to withstand a severe combination of meteorological and oceanographic conditions that are characteristic of the study area (i.e., typhoon conditions).

d. The improvement design should limit design wave heights in the berthing area to less than 0.6 m.

e. The plan of improvement should be designed to accommodate a 20-m-long design vessel with a 5-m beam and a 1.8-m draft.

Design Methods: Harbor plan. A preliminary harbor plan was developed by POD based on analysis of cost, economic benefit, and environmental impact. A more conservative plan with extensions to both ends of the detached breakwater and to the south revetted mole was

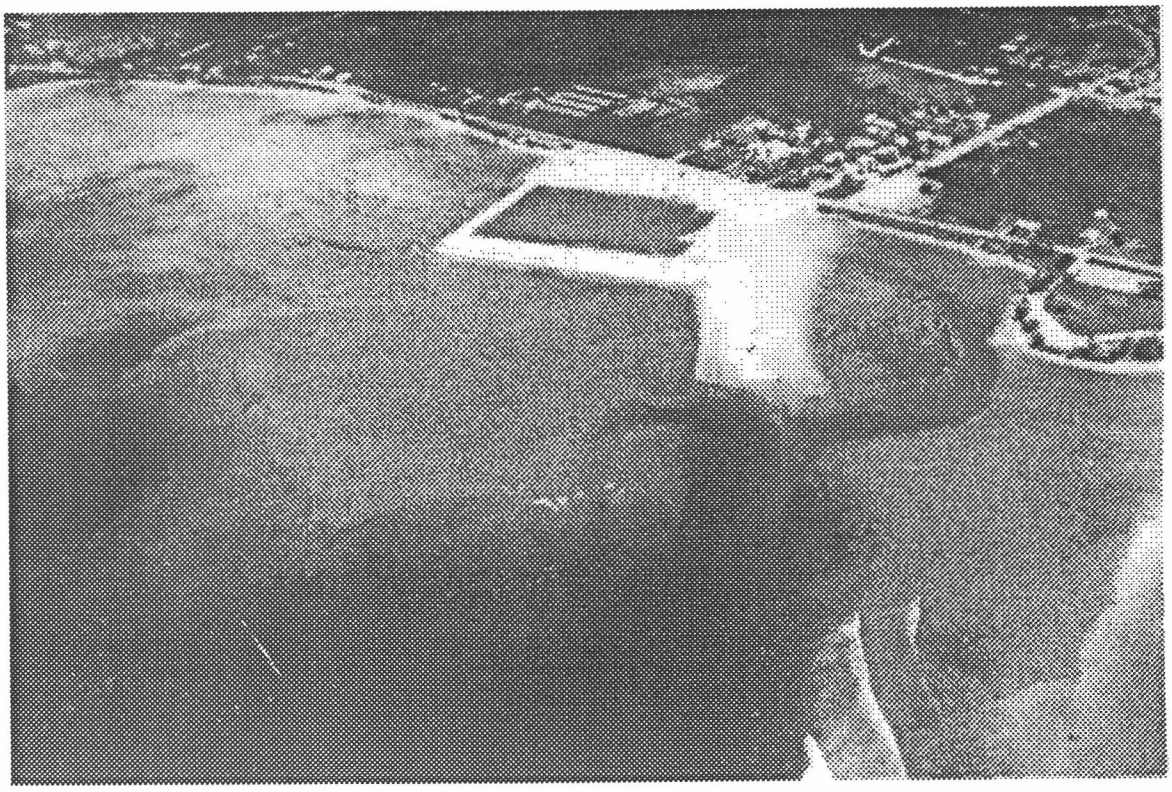

Figure 3. Agat Harbor channel under construction

suggested by CERC. The response of the harbor basins for these initial two, plus three other alternative plans, was modeled at CERC using the HARBS numerical model. The HARBS model is a finite element model that represents the harbor geometry inside a semicircular domain bounded by the shoreline on the landward side and a semicircular region of constant water depth on the seaward side. It assumes steady-state input conditions from a linear (small-amplitude), monochromatic wave; mild bottom slopes; and no current (Chen and Houston 1986).

Amplification factors were calculated for incident energy in 1-sec interval period bands from 8 to 20 sec and approaching from three incident angles. Output was reported at 32 locations (grid elements) within the harbor for the two initial and three alternative plans. The outer boundary of the numerical grid was within the reef flat. Three water levels were tested: 0.72 m, 1.4 m, and the design condition. The recommended Plan extended the north end of the detached breakwater by 45 m from the original design (Farrar and Chen 1987).

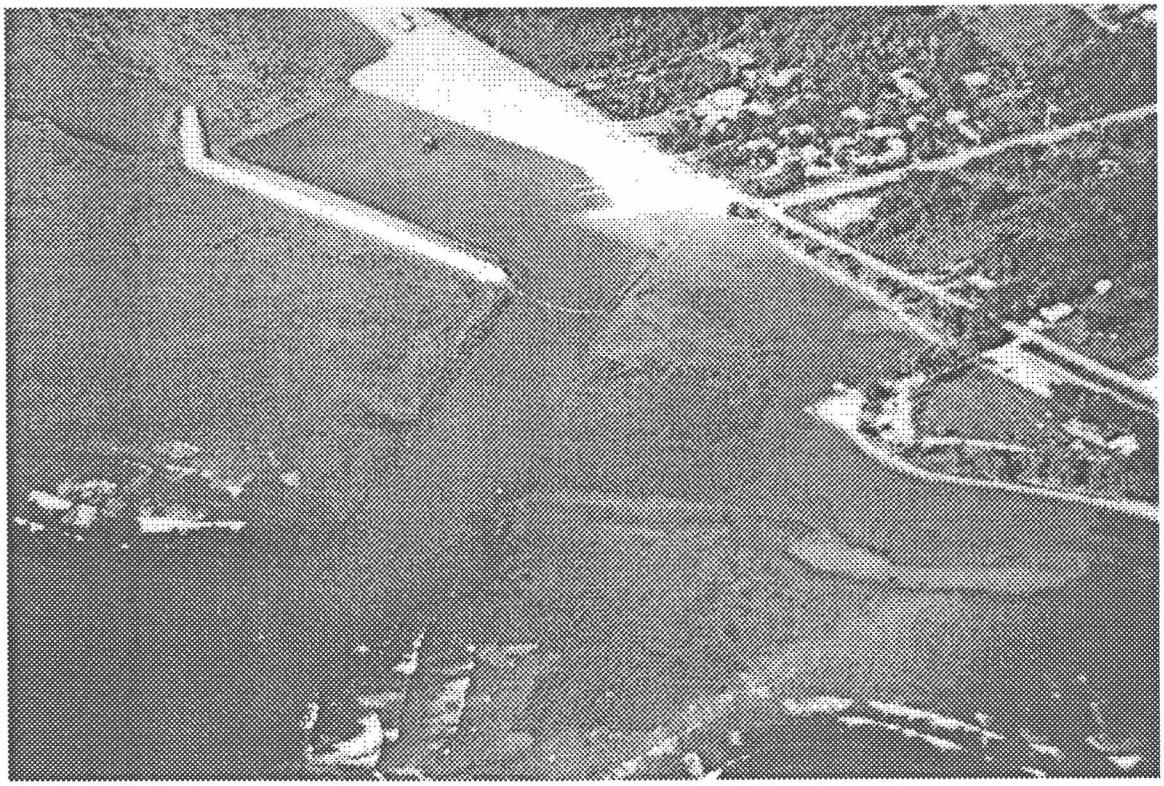

Figure 4. Agat Harbor under construction

Breakwater. Breakwater design was accomplished using standard practices found in the 1977 *Shore Protection Manual*. The Hudson formula was used to select the armor size for the design wave height, which was defined as the depth-limited breaking wave at the structure toe, or 0.78 h, where h = water depth. The design depth assumed for the constructed plan was 2.5 m, derived from a mean higher high water level of 0.7 m, plus an estimated combined surge and wave setup of 1.4 m, over a reef flat with an average elevation of 0.3 m. The resulting design wave is 1.9 m.

MONITORING PLAN

Objectives: Agat Harbor was selected for monitoring because it has potential for providing information about an environment for which little engineering data exist. Design guidance

on wave characteristics on coral reefs needs improvement, as most data on wave shoaling and breaking are derived from observations of waves approaching sandy shorelines. Figure 5 contrasts the offshore profile at Agat with the typical equilibrium beach profile. Wave transformation across this regime can be expected to be markedly different than across sand beaches. Even less information is available on maximum surge levels behind reef shorelines. How these factors affected the selection of the design parameters was an important but difficult question. The answer required observations during conditions at or near the design wave and surge conditions or at least conditions sufficiently energetic to cause structural damage. Unless a typhoon approached from the west during monitoring, there would be no opportunity to assess breakwater stability. Shoaling of the channel at the entrance was not expected because it was cut through limestone, and exited the live reef face where the water depth was well below project depth. Neither were impacts on adjacent shorelines anticipated,

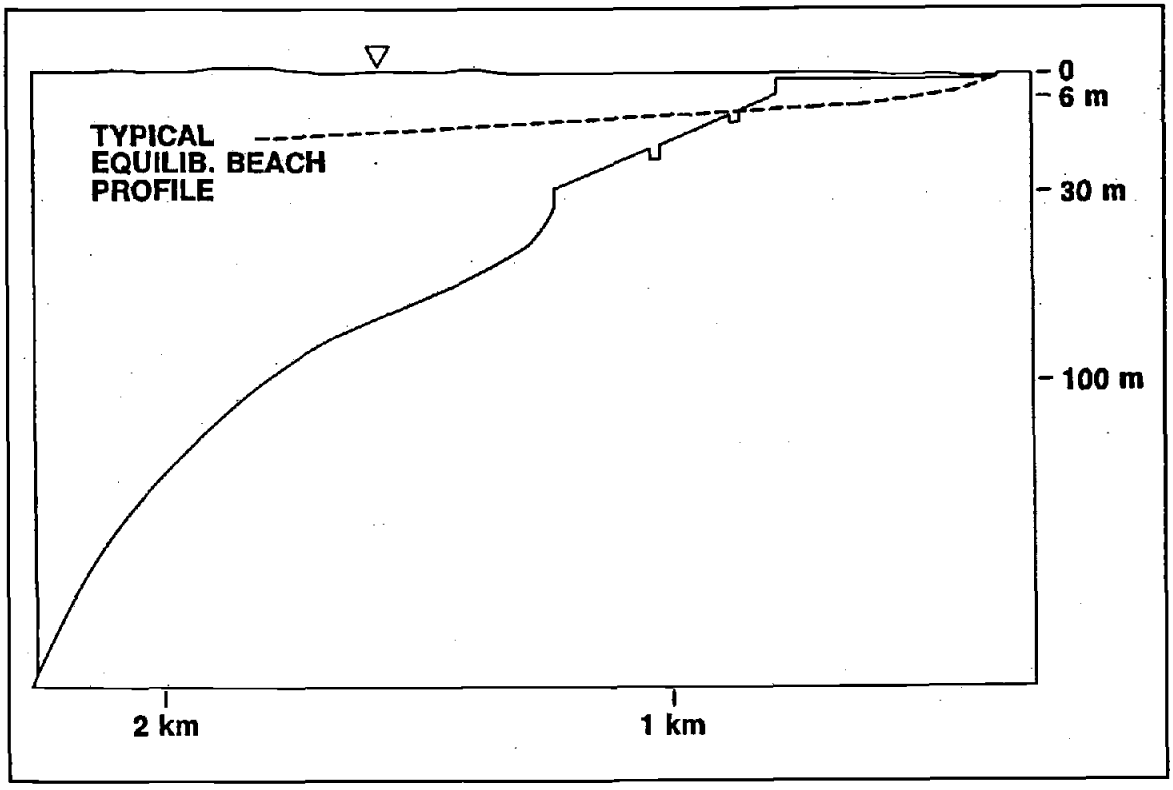

Figure 5. Idealized reef and sand beach profiles

since there was little erodible material on the reef flat and upland areas. Nevertheless, the monitoring plan included periodic inspections of the structure and surrounding shoreline. The major issues to be addressed in the study were:

a. Deepwater incident wave climate for the region around Guam.

b. Wave transformation across coral reefs as a function of depth and distance from the reef face.

c. Wave and surge levels behind coral reefs during large wave events (distant storms to the west would produce large incident waves, even without a local typhoon).

d. Validation of the HARBS model.

e. Wave transformation down steep-sided channels.

f. Response of project and adjacent shoreline.[2]

Monitoring Elements: A monitoring plan was developed to examine these issues through analysis of data collected over a 3-year observation period (Boc and McGehee 1989). Elements of the monitoring effort are related to the study issues. As is usually the case with coastal engineering field studies, the "ideal" monitoring plan had to be modified to accommodate instrumentation, logistic, and economic constraints. The elements of the plan, referenced by letter to the issues are as follows:

a. Directional wave energy spectra and surface winds from an offshore site.

---

[2] An additional issue, g, "Wave-induced circulation on a reef flat," is discussed on pages 41 and 42.

b. Wave energy spectra at several locations on a shore-normal transect across the reef flat.

c. Wave conditions and water elevations at the structure; harbor response during large wave events.

d. (1) Directional wave energy spectra at the outer boundary of the model.

(2) Wave energy spectra at several sites within the harbor.

e. Wave energy spectra at the outer and inner ends of the channel.

f. Periodic site inspections and aerial photographs of the harbor and surroundings.

Element *a* requires a long, continuous record to obtain the distribution of calm conditions as well as the extreme events that describe the wave climate. Elements *b-e* require a range of conditions above some threshold of interest, ideally including the modeled incident conditions. In order to capture a sufficient range of conditions, including episodic events, it was considered desirable to monitor these sites continuously over the course of the study. Periodic measurements or experiments were not considered initially because of the difficulty of synchronizing measurements with events of interest and because these events develop rapidly, making it difficult to fix instruments securely in place before conditions become too violent for placement.

The preferred position for measuring the incident climate is directly offshore of Agat in deep water. These depths are attained relatively close to shore, but instrument constraints, discussed below under "System Design; Data management," forced a position further offshore. Initially, a site southwest of the island (1A) was selected; a second site to the northwest (1B) was designated to improve performance.

Gauge placement in the channel and harbor posed no particular logistic restrictions, allowing sites to correspond to the channel beginning and end (Sites 5A and 5B), and with three of the HARBS model grid points (Sites 4B and 4D). Site 5A also represents incident wave conditions approaching the reef face. Three sites were selected on the reef flat: 2A, directly behind the reef face; 2B, at 25 percent of the distance from the face to the shore; and a third, 4A, at 50 percent. By selecting the third site on the reef flat at the transverse position of the breakwater, but displaced to the side to avoid reflected energy, one site serves both elements *b* and *c*. By using a directional gauge, and selecting a position at the outer boundary of the HARBS model, it also serves plan element *d*(1). Figure 6 shows the planned layout of the gauges.

SYSTEM DESIGN

General requirements: Agat Harbor is a recreation and fishing marina with frequent boat traffic. In addition, tourists and fishermen regularly wade over the reef flat area. Any instrument left in situ must not pose a risk or obstruction to the public, yet it must be protected from accidental or deliberate encounters. Electrical power at the site is occasionally lost during normal weather events, and will likely fail for days after a typhoon. Travel time from Vicksburg, MS, added to the advance permission required for government employees to travel overseas, makes technical support from CERC a long lead-time option. The system should be as automated as possible, and yet serviceable by local technical support. Equipment must be protected from, or designed to withstand, high temperature and humidity conditions.

Wave and wind measurements in deep water are most efficiently obtained from a surface-following buoy. The National Data Buoy Center (NDBC) has developed a standard, 3-m-diameter buoy that provides directional wave information every hour, as well as wind speed and direction, air pressure, and air and sea surface temperatures (Steele et al. 1990). It is a rugged, self-contained observation platform designed to operate up to 2 years under battery and solar power.

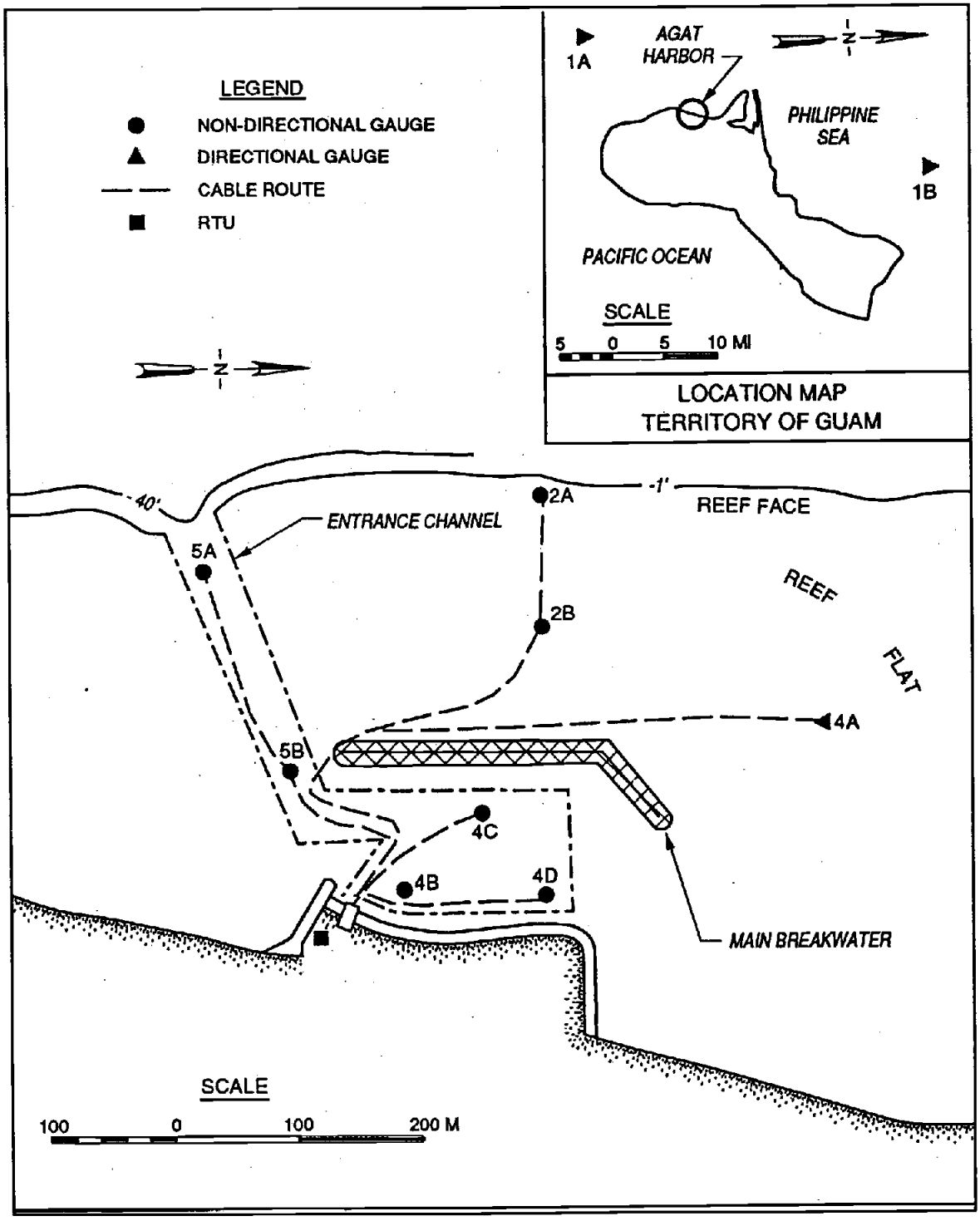

Figure 6. Plan of nearshore gauge locations

Individual, self-contained instruments were rejected for the nearshore sites for two reasons: (a) the expense of routine change-out required of the commercially available instruments over the course of the multi-year study (particularly on the deeper sites, where diving was required); and (b) the risk of loss of the instrument, and more importantly, the data, in the shallow, clear waters. An integrated system with sensors cabled to a central data processor/logger was specified for the nearshore sites to minimize the number and size of underwater components; to permit long-term, unattended operation; to ensure capture of all data prior to any sensor loss/damage; and to reduce system cost. An air-conditioned administration building at the harbor was made available by the Port Authority of Guam to house the central data management computer and power supply.

Sensors: The NDBC buoy is a discus-hull, surface-following pitch-roll-heave buoy. It measures waves with its onboard accelerometer and tilt sensors. See Steele et al. (1990) for additional information.

The basic sensor selected for the nearshore system was the pressure transducer. Mounted on the seafloor, it can accurately measure waves and water levels, is rugged enough to survive the environment without obstructing traffic, and will operate without frequent maintenance. Sensor elevation can be readily measured on the reef flat and, with more difficulty, in the channel. Three sensors arranged in a slope array produce the cross spectra used to measure directional waves. The transducers are sealed in 10-cm diameter by 25-cm long cylindrical pressure cases. Pressure is transmitted via a flexible diaphragm on one end and through an oil-filled passageway to the transducer. A copper-nickel alloy cover plate prevents biofouling of the diaphragm.

An atmospheric pressure correction must be applied to an underwater pressure measurement to produce an accurate water level. An eleventh, above-water transducer was added to the system as a barometer to provide this information.

Cables: Seven-conductor, double-armored, 1.3-cm diam cable is used to carry power to and signals from the pressure transducers. Waterproof connectors are spliced onto the cable at the transducer end to permit changing sensors, if required. The cable is allowed to self-bury

in the channel and the harbor, but on the reef flat is pinned every 200 m with 1-m long "J" clamps driven into the coral. This prevents tampering with the cable and protects against abrasion from the coral due to wave action. Sensors 5A and 5B are connected to a single cable; the remaining six sites have individual cables. The seven cables converge under the fuel dock at the southeast corner of the harbor and feed into the administration building through a conduit placed by the Port Authority during construction of the marina complex.

Mounts: The single-point transducers are mounted horizontally on 400 kg railroad wheels. A steel, hinged cylinder, containing the transducer and the cable splice, is sealed by stainless steel bolts with one-way nuts (Figure 7). The steel cylinder can only be opened by shearing the bolts.

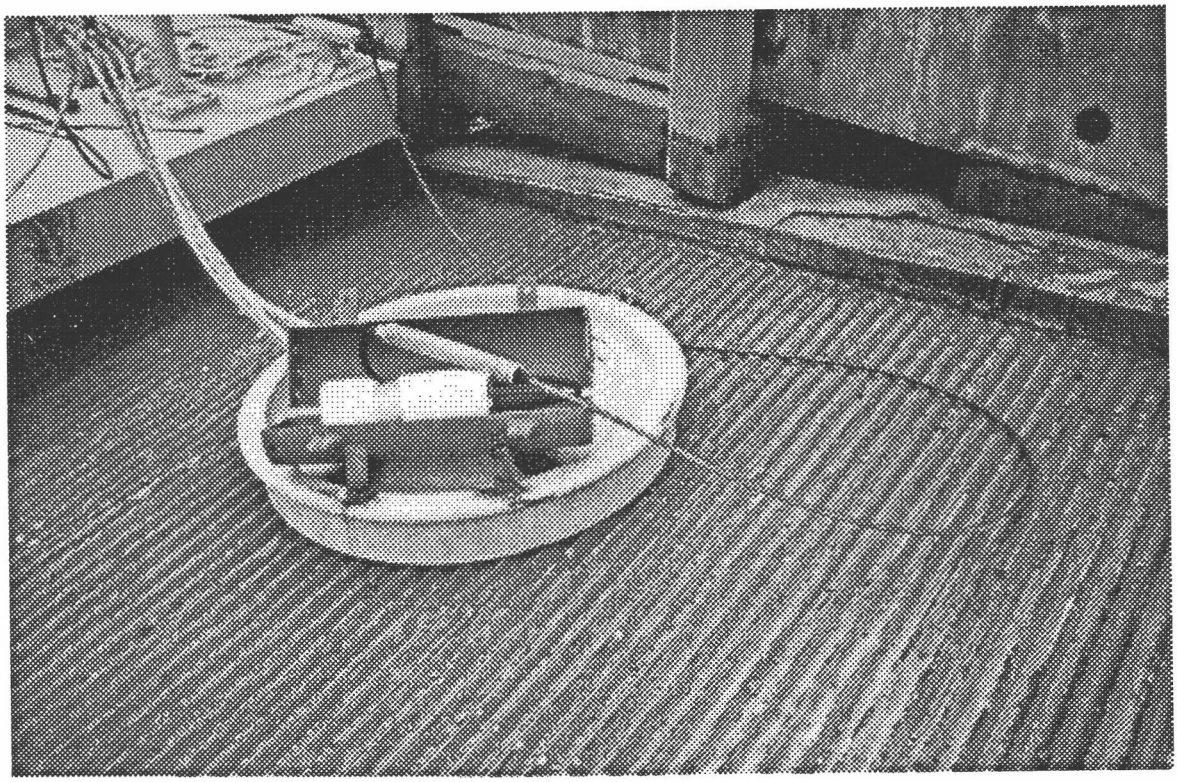

Figure 7. Single point transducers housing and mount

The slope array has three transducers mounted vertically in cylinders on radial arms welded to a central wheel (Figure 8). A larger hinged cylinder contains the electronic module described below. A single cable carries the multiplexed signal from all three transducers.

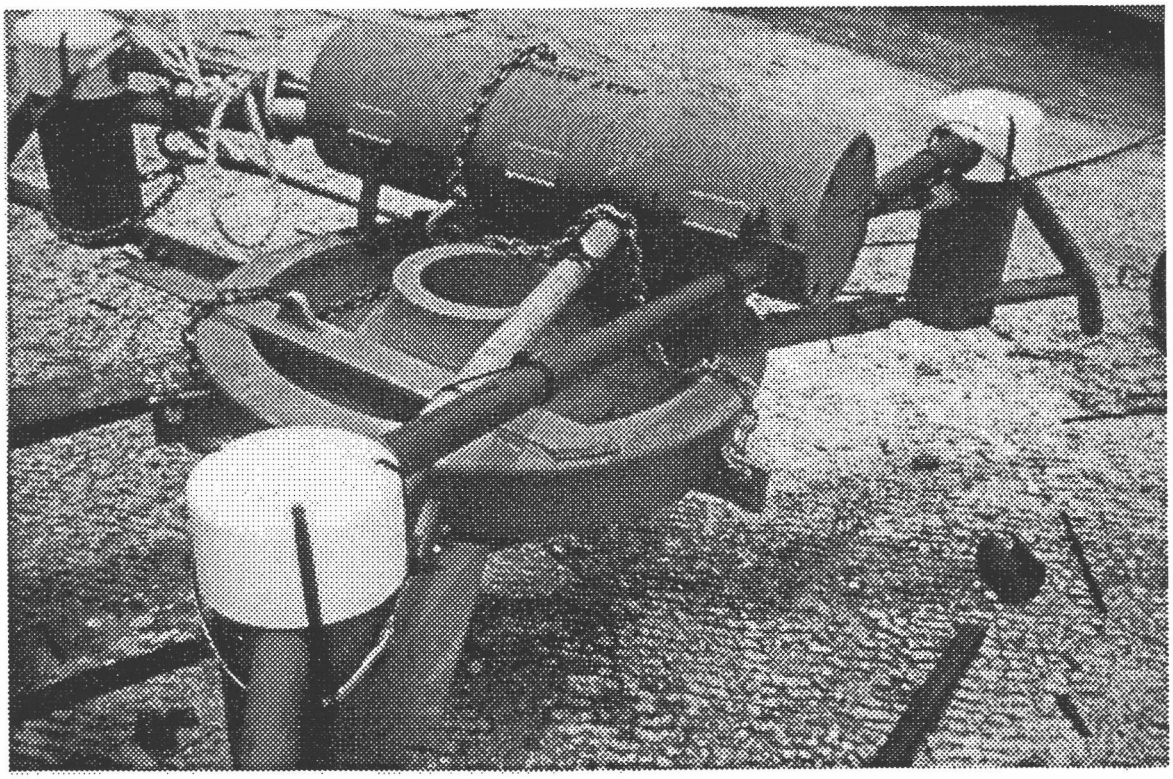

Figure 8. Slope array transducers/electronics housing and mount

Signal processing: The nearshore instrument control system features programmable data transfer and intermediate solid state buffer from remote transmitting units (RTU's) capable of handling six data channels. Three RTU's, located at the shore end of the underwater cables in watertight stainless steel enclosures, are used: GU1 controls sensors 5A, 5B, and the barometer; GU2 controls sensors 2A, 2B, 4B, 4C, and 4D; GU3 controls the slope array, 4A. The slope array contains an additional underwater module, the serial asynchronous unit (SAU), that performs A-D conversion and multiplexing of the three transducer signals. It contains a compact, single-board central processing unit (CPU) that samples the sensors and

outputs a serial data stream to the RTU. The RTU powers the transducers (or SAU), controls the sampling rate and burst interval, and transfers buffered data files to the next output device.

Data management: All time series measured by the buoy are analyzed and reduced on board, then burst-transmitted every hour via VHF radio to the GOES satellite network. This "line-of-sight" telemetry link had a direct impact on the buoy's deployment site. While the preferred position for the incident climate measurement would have been directly west of Agat, the low azimuth of the western GOES satellite at this longitude placed it below the elevation of Guam's central mountain range. Consequently, the buoy had to be placed either north or south of the island. An initial location, Site 1A, was selected about 10 n.m. west-southwest of the southern tip of the island (see Figure 6).

Onshore, data capture was designed to occur at three locations. The RTU contains battery-backed memory cards with a capacity of about 256 KB, enough for about 48 hr of data. This was considered adequate as an intermediate buffer to hold data during temporary downtime of the main data logger. The main data processor and logging device was a Digital Equipment Corporation microVax II computer running under UNIX. Records are written into its database on a 380-MB hard disc drive, and backed up onto a TK-70 cartridge tape, with a capacity of over 200 MB. Tape cartridges were scheduled to be recovered locally once a month and returned via mail to CERC for analysis and storage. Remote data retrieval via telephone was possible, but not considered as the primary method because of the cost of the telephone connection. The data management scheme is illustrated in Figure 9.

Software: There are two nested routines controlling onshore data collection and storage. Each RTU has a programmed sampling scheme, and writes an integer count associated with the measured output voltage from each sensor, along with the time word, into a directory. The microVax, in turn, queries each RTU's directory for records not previously retrieved every 20 min. It downloads these records using KERMIT, an error-free file transfer protocol, at 4,800 baud, and updates its relational database (Interbase). Attributes in the database include sensor data, such as serial number, calibration factors, and position, that permit

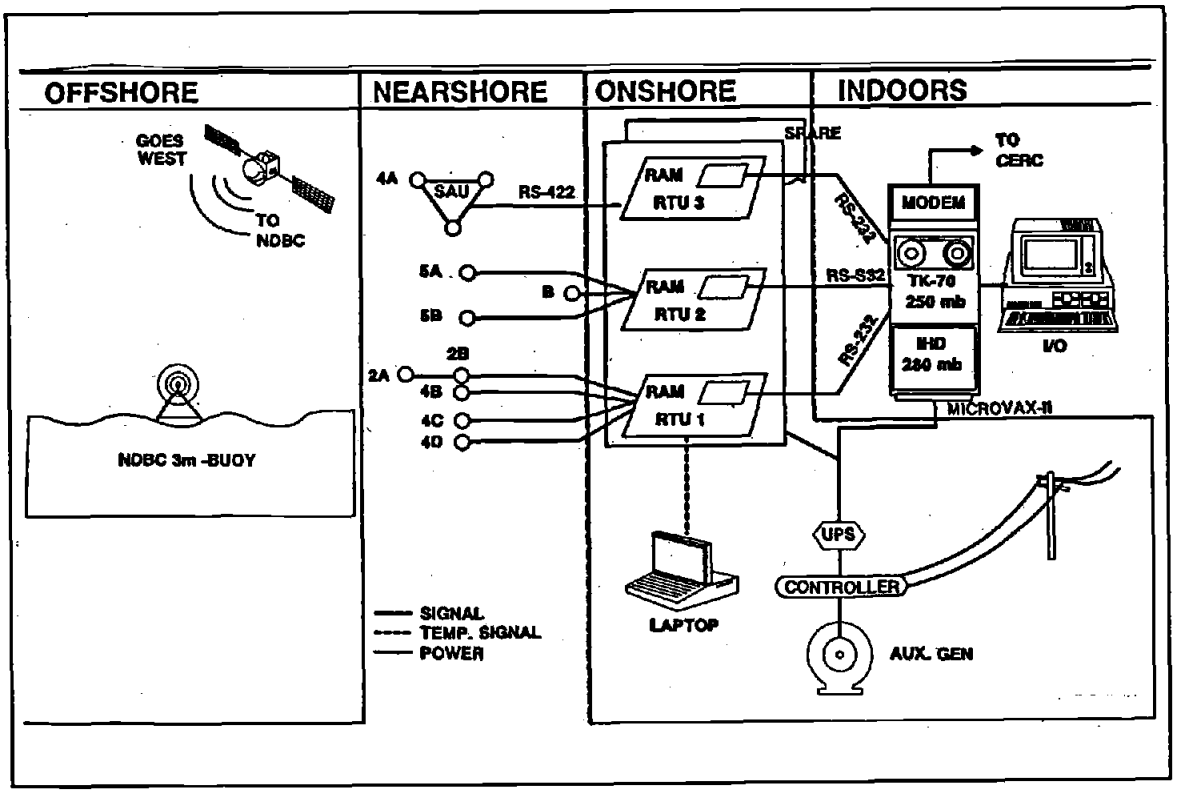

Figure 9. Data management scheme

automatic analysis of the raw time series. Once a day, the database is automatically copied onto the cartridge tape. The only manual operation required is (monthly) tape replacement.

The distributed features of the database facilitate remote access using anasynchronous DECnet link with Vax mainframe computers in Vicksburg, or any UNIX-based system running Interbase. The mainframe's database can be updated from the remote's database using Interbase record transfer commands. Similarly, changes in the database relations, or new versions of software modules, can be readily transferred to the remote computer from the mainframe.

Power supply: The primary power for the NDBC buoy is a nonrechargeable dry cell battery. The secondary power system consists of rechargeable lead-acid batteries and solar panels. The system draws continuously from both sources, but will not continue to operate after the primary battery is discharged. Typical life cycles are on the order of 18 months to 2 years.

Onshore, a major design consideration was to provide continuous power to the microVax and the RTU's for both the routine and major losses of line power. A 2-kW uninterruptable power supply is wired inline with the circuit for the system. It provides continuous, regulated voltage and will power the system for short dropouts of line voltage. If power loss lasts more than 30 sec, a 15-kW diesel generator mounted on an elevated platform adjacent to the administration building automatically starts. It has sufficient fuel to power the system for several days. Another redundant feature is a complete backup set of RTU's installed adjacent to the primary set. Switching RTU's is accomplished in a matter of minutes by switching the waterproof cable connectors.

ANALYSIS AND SAMPLING PLAN

Spectral analysis of discrete samples of surface elevation is an accepted method for obtaining useful wave parameters from a random sea. It is based on linear superposition, and thus restricted to first-order wave theory. Transformation into the frequency domain produces a power spectrum that provides energy distribution in discrete frequency bins. The method generally follows CERC's Wave Data Analysis Standard (Earle, McGehee, and Tubman 1996), though the higher sampling rate produces a spectrum that differs from the CERC standard. Table 1 gives the sampling and analysis parameters for the shallow-water sites.

Table 1
Sampling and Analysis Scheme for Onshore System

Site No.	Sample Rate (Hz)	Sample Length (count;sec)	Sample Interval (hr)	Segment Length (count;sec)	Spectral Bandwidth (Hz)	Number of Bands
2A,B; 4B-D	2.5	2560;1024	2	512;204.8	0.0049	57
4A	2.5	4500;1800	2	512;204.8	0.0049	57
5A,B,C	1	3540;3540	1	256;256	0.0039	64

An energy-based significant wave height *Hmo*, is estimated using the formula

$$Hmo = 4\left[\int_o^\infty S(f)\,df\right]^{1/2} \tag{1}$$

where *S(f)*, the nondirectional energy spectrum, is band-pass filtered. The peak frequency *fp* is defined as the frequency at which *S(f)* has a maximum. If the slope of the sea surface is included, directional information can be obtained from the cross power spectrum. The cross power spectrum *Pmn* between pairs of sea-surface fluctuations at *m* and *n* is related to the surface spectrum by

$$Pmn = \int e^{iKXmn}\, S(f,\theta)\, d\theta \tag{2}$$

where K is the wave number vector, f is frequency, θ is direction, and *Xmn* is the difference between two position vectors *Xm* and *Xn*. The dominant wave direction, the mean direction from which the energy is coming at the peak frequency, can be calculated from $S(f,\theta)$, the two-dimensional sea surface spectrum (Longuet-Higgins, Cartwright, and Smith 1963).

The standard sampling scheme used by NDBC to observe wind waves is a 20-min burst of samples taken at 2.56 Hz every hour. Data are spectrally analyzed onboard the buoy which produces a directional spectrum of the wave energy with periods between 2.5 sec and 33 sec.

A site visit was conducted in June 1988 while the project was under construction. Visual observations of waves on the reef flat during calm conditions revealed a highly nonlinear cnoidal profile, characterized by discrete, widely spaced (on the order of 100 m), steep-faced crests (on the order of 10 cm high). There were no discernible troughs, but between crests the water flowed shoreward. In short, the waves more closely resembled a periodic series of bores. To adequately capture the steep crest profile, the sample rate for the reef and harbor gauges was selected to be 2.5 Hz, rather than the 1-Hz rate typically used in shallow-water sampling. That decision, because of limited memory capacity (see "System Design"), forced a corresponding reduction in sample length, which in turn, restricted the lowest observable frequency to 0.0049 Hz, or a corresponding period of about 200 sec.

While well below the wind-wave energy band, this constraint turned out to be significant later in the study.

The channel gages, 5A and 5B, were in deeper water where linear wave forms are expected, so they collected the more standard 1-Hz samples. Since they were also selected to establish the gradient between interior and exterior water levels, they operated nearly continuously (59 min/hr). Nine mean water levels per hour (6-min average) could be extracted from these time series.

SYSTEM INSTALLATION

Installation of the harbor and channel sensors could have been accomplished using local fishing/work vessels, but installation of the reef flat gauges posed a logistics problem. No local vessel was found that had the lifting capacity to deploy the 400-kg sensor mounts, carry and lay the cable, and yet draw little enough water to operate on the reef flat without risking damage to itself or the reef. The solution was a customized, outboard-powered work barge, 3.6 m by 1.8 m by 0.3 m, with an A-frame and hand-cranked winch. The vessel was designed by CERC and fabricated of No. 6061, 7-mm alumi- num plate by the Construction Services Division at WES (Figure 10). The entire instrument system and deployment equipment, including the barge, was shipped as containerized cargo to Apra Harbor, Guam. Installation was performed by CERC in August 1990. The NDBC buoy was deployed the following month using the U.S. Coast Guard buoy tender *Basswood.*

THE UNANTICIPATED MONITORING ELEMENT

It was assumed during the design of the project and development of the monitoring plan that water currents on the flat were governed by the low-amplitude tide signal. While circulation was considered from a water quality standpoint (hence the detached breakwater design), currents were assumed inconsequential in structural considerations. However, the

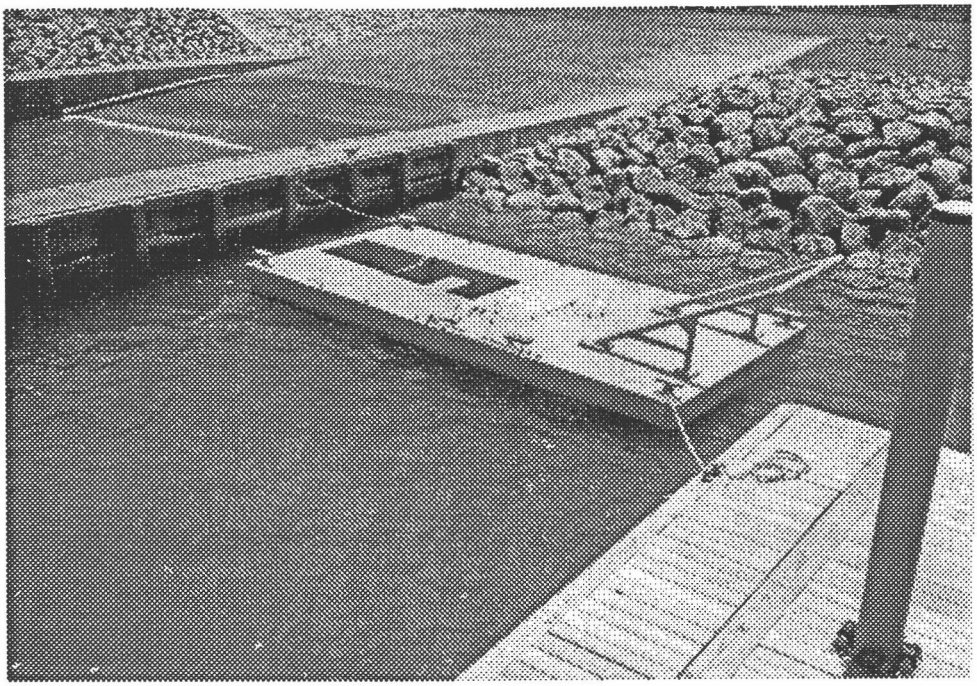

Figure 10. Custom gauge deployment barge

author's observations from shore during a site visit in July 1991 (before instruments were operative) revealed unexpectedly large currents, and provided an indication of the processes that likely govern during extreme conditions. The crude, visual estimates of waves and currents provided below describe the phenomenon.

On that occasion, a distant storm westward of the island was causing a 3- to 5-m swell to break on the reef face. Most of the incident energy was dissipated in breaking, so that incident waves reaching the breakwater were less than 1/2 m in height. Mean water depth on the reef flat was about 1 m. A significant current was evident flowing southward, parallel to shore. The current pulsated, varying in magnitude but without reversing direction, at irregular cycles of about 5 - 10 min. The current extended far enough offshore to flow around the outer breakwater, but the highest velocities occurred across the open northern side of the harbor, between the shore and the breakwater. The velocity of the water varied irregularly from less than 0.5 m/sec to over 3 m/sec, but generally was in phase with periodic oscillations of the water level in the harbor; i.e., as the water level in the harbor fell, the flow into the harbor increased in velocity. Water level fluctuations in the harbor approached 1 m. The

water level on the reef flat also varied, but with about half the amplitude of the harbor fluctuations. The lowest stage attained in the harbor was below the level of the reef flat at the northern boundary of the boat basin; at those times, a weir with a drop near 0.3 m developed as the water poured into the harbor. This condition persisted with irregular variations in amplitude and period throughout the day. When offshore wave conditions subsided to 1 - 2 m the next day, no circulation was apparent on the reef flat.

Though system installation was already under way, it was obvious that another element was needed in the monitoring plan; that is, element *g*, current measurements in the harbor and on the reef flat.

While long deployments were practical for the wave sensors (see "System Design," above), the unavailability of a reliable, long-term in situ current sensor forced another approach for element *g*. Since current measurements during energetic - but not necessarily extreme - events were desired, short-term (order of days) measurements would suffice if deployment could occur on short notice and before conditions became unsafe. One approach was use of a local contractor to deploy lightweight instruments that could be carried over the reef on foot and hand-deployed. A contract was awarded to Pacific Basin Environmental Consultants, to install and operate CERC-provided instruments. Water levels and currents were measured from battery-powered, internal recording pressure sensors and impeller-type current meters. Drogues were also provided to track surface currents. The sampling interval was set at 10 sec, effectively filtering wind-wave energy but passing energy with periods on the order of 30 sec and longer. Figure 11 shows the locations selected for placement of the pressure sensors on the reef flat north of the harbor.

MONITORING RESULTS

Performance: Design and construction of the nearshore system and buoy occurred in fiscal year (FY) 88 and FY89, while the harbor was still under construction; deployment occurred in the summer of 1990. Activation of the nearshore system was delayed until February of 1991 while awaiting completion of the administration building, in particular the electric

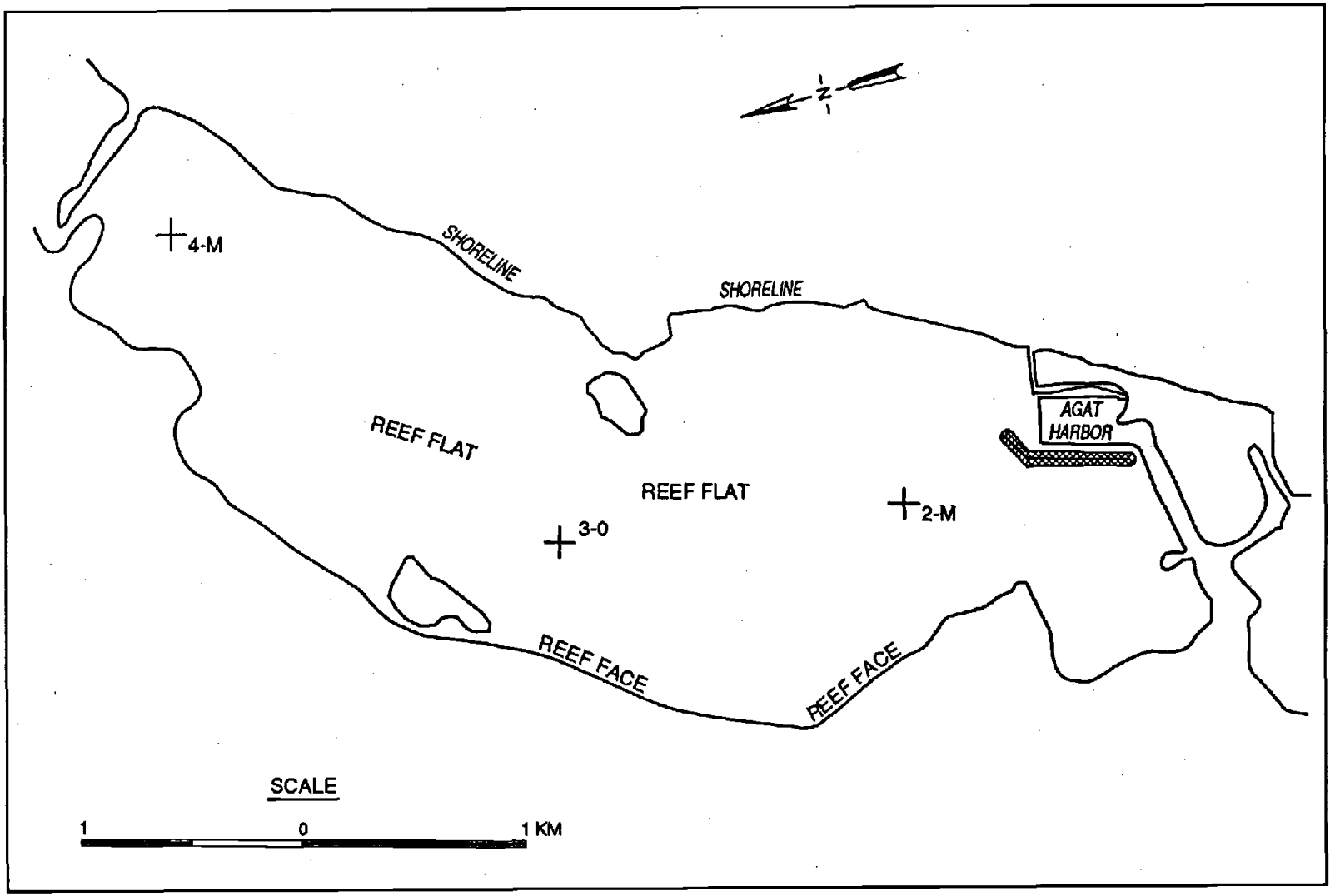

Figure 11. Short-term pressure sensor deployment sites

service. Tantalizingly, Typhoon Russ struck while the transducers sat idle on the reef flat. On 18 December 1990, it skirted the southwest side of the island, establishing ideal conditions (from the perspective of the monitoring plan's goals). If the nearshore system had been on during that storm, objectives 2-5 of the monitoring plan would have been attained 4 months after its installation. The pattern appeared to be set for the rest of the study - whenever everything was operational, conditions were likely to be mild.

A second typhoon, Omar, crossed directly over the harbor from the east on 28 August, 1992 (Figure 12). None of the wave measurement systems were operational, but some data were captured using the short-term, self-contained water level gages. Self-contained gages were also deployed at the end of October 1992 for Typhoon Brian. This time the offshore buoy and the nearshore system were operational, but because the storm track was westward, large waves ($H \cong 4m$) were not felt on the western side of the island until after the typhoon's passage. The third typhoon of the 1992 season was Typhoon Gay in late November, a relatively small storm that passed well offshore to the east. Data were recovered from the offshore buoy and the reef gages, using the solid state memory in the RTU. No other typhoons approached the island for the remainder of the study. Data collection was terminated at the end of FY93.

Periods of operation for the various instruments are shown graphically in Figure 13 as a time line, together with the offshore significant wave height to illustrate the conditions under which simultaneous data were (or weren't) recovered. Overall data recovery for the buoy was no better than 60 percent, and less than 30 percent for the nearshore system. This compares with average performances of 80 to 90 percent for most other wave stations managed by CERC and NDBC. High data return was not, in itself, required for either system; rather, it was the means intended to capture extreme events. In fact, once they malfunctioned, each system was allowed to remain idle between typhoon seasons to conserve mobilization and shipping funds (e.g., surface freight versus air freight for the buoy). Nevertheless, the lower than anticipated data return rate of the study warrants examination to extract useful lessons for future efforts.

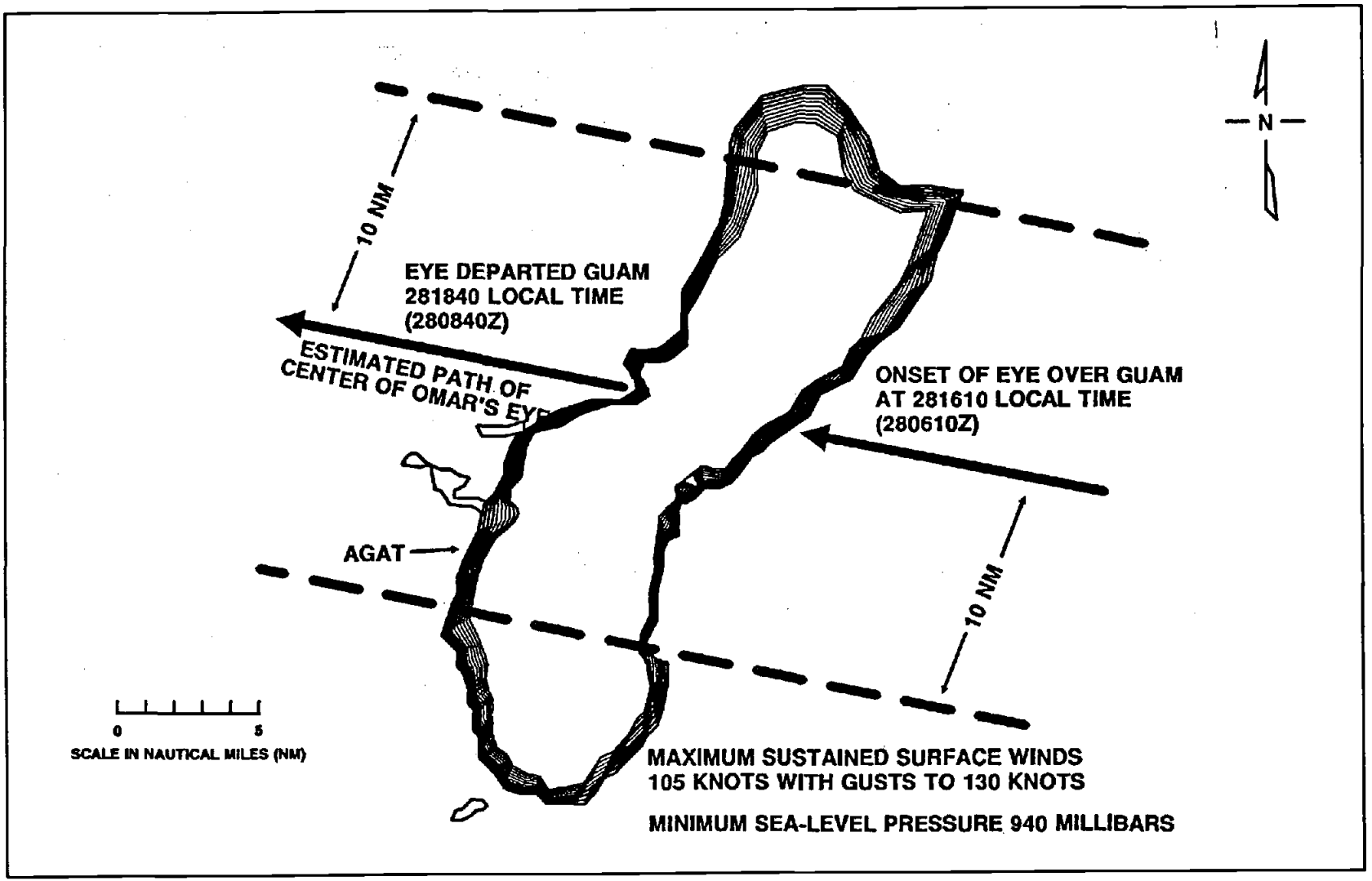

Figure 12. Typhoon Omar, Guam, 28 August 1992

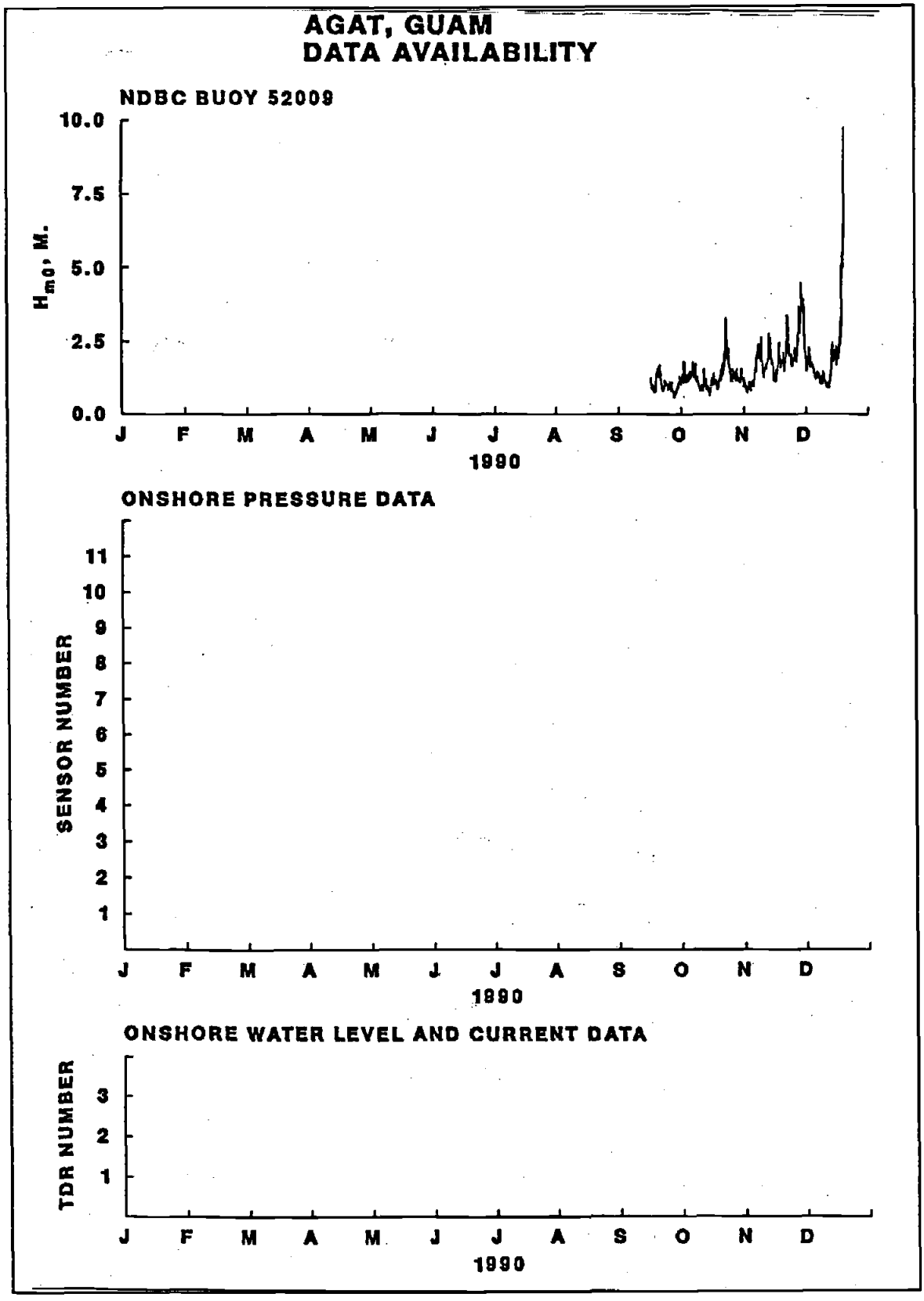

Figure 13. Data capture performance and offshore wave height, by year (Sheet 1 of 4)

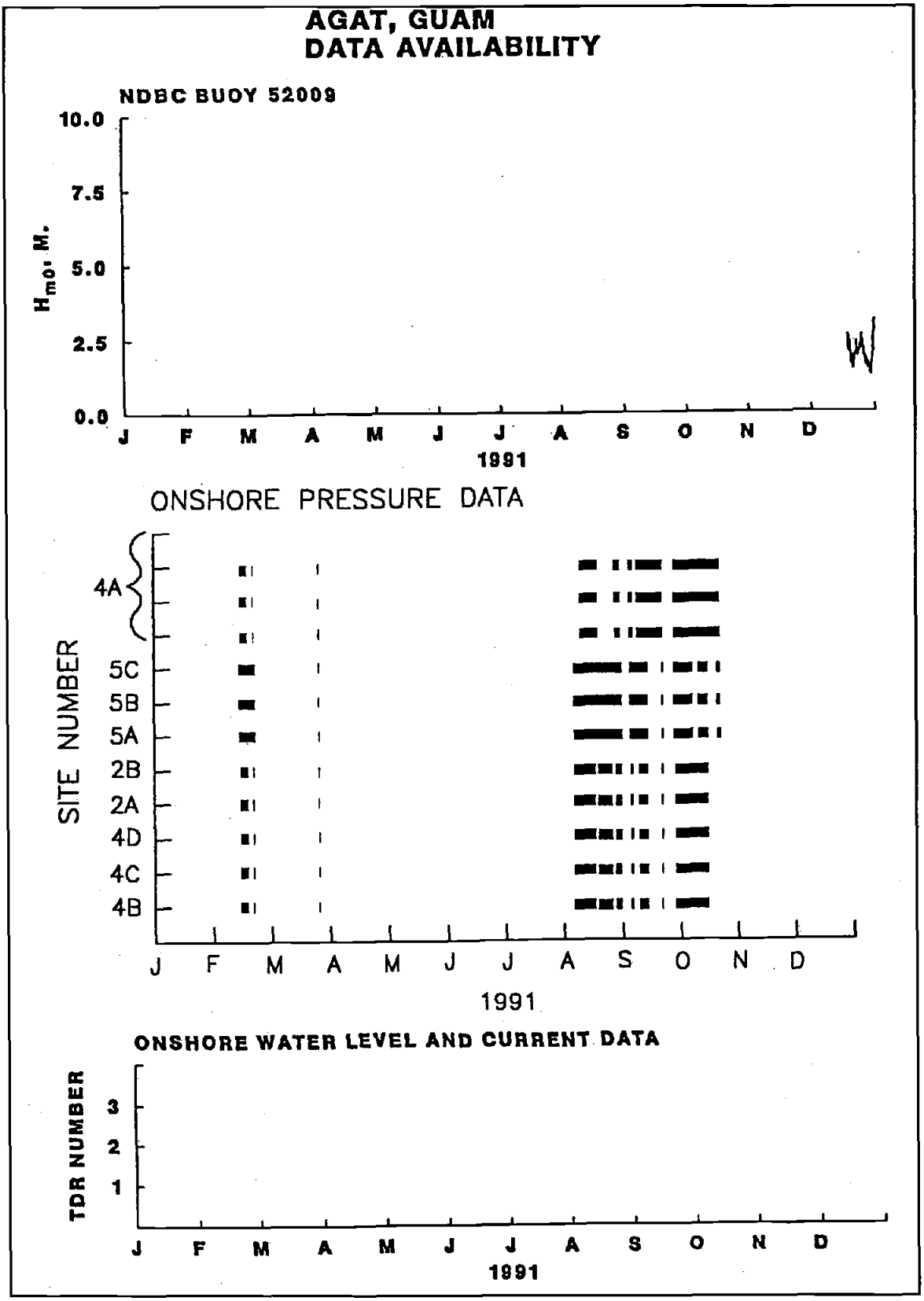

Figure 13. (Sheet 2 of 4)

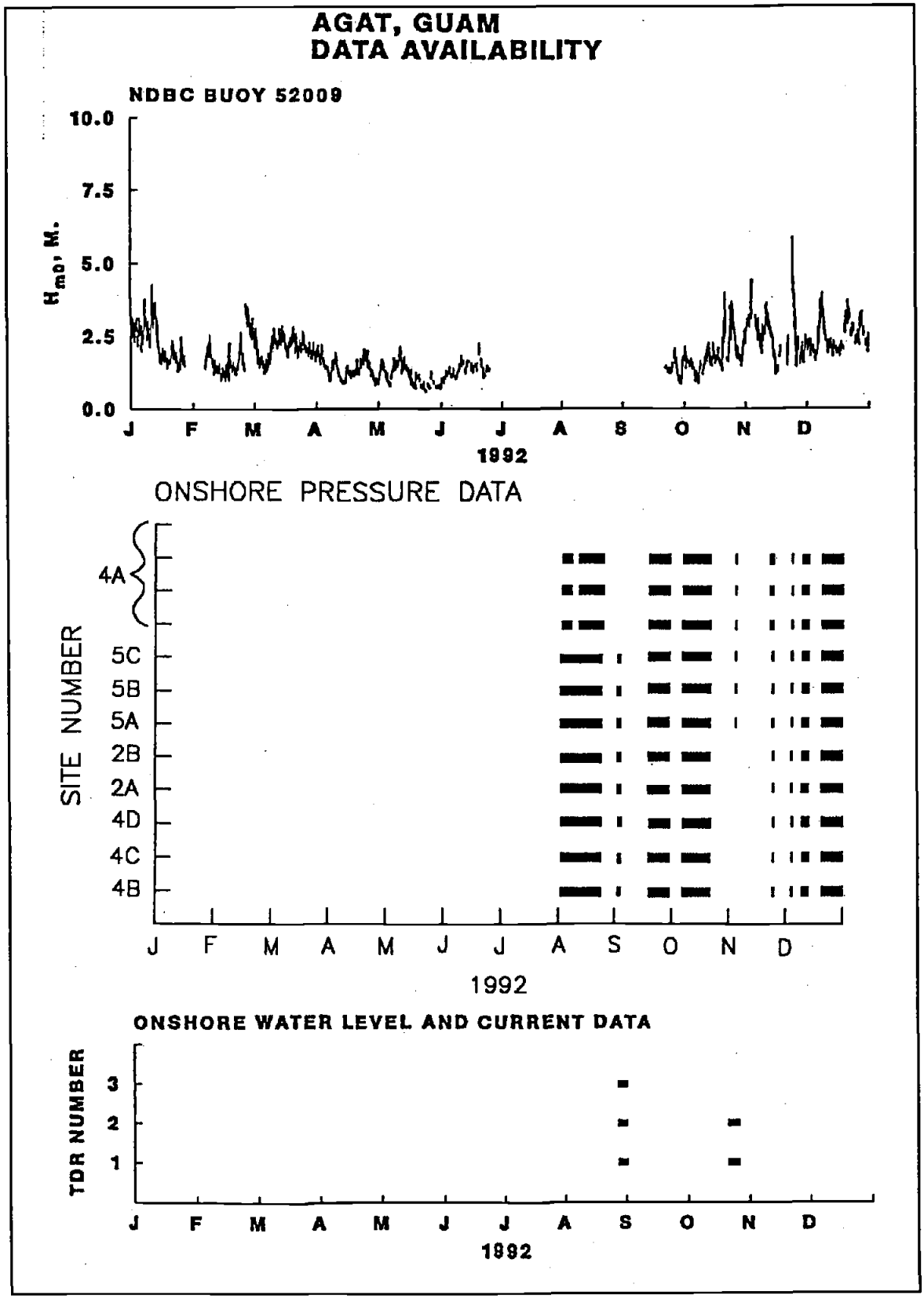

Figure 13. (Sheet 3 of 4)

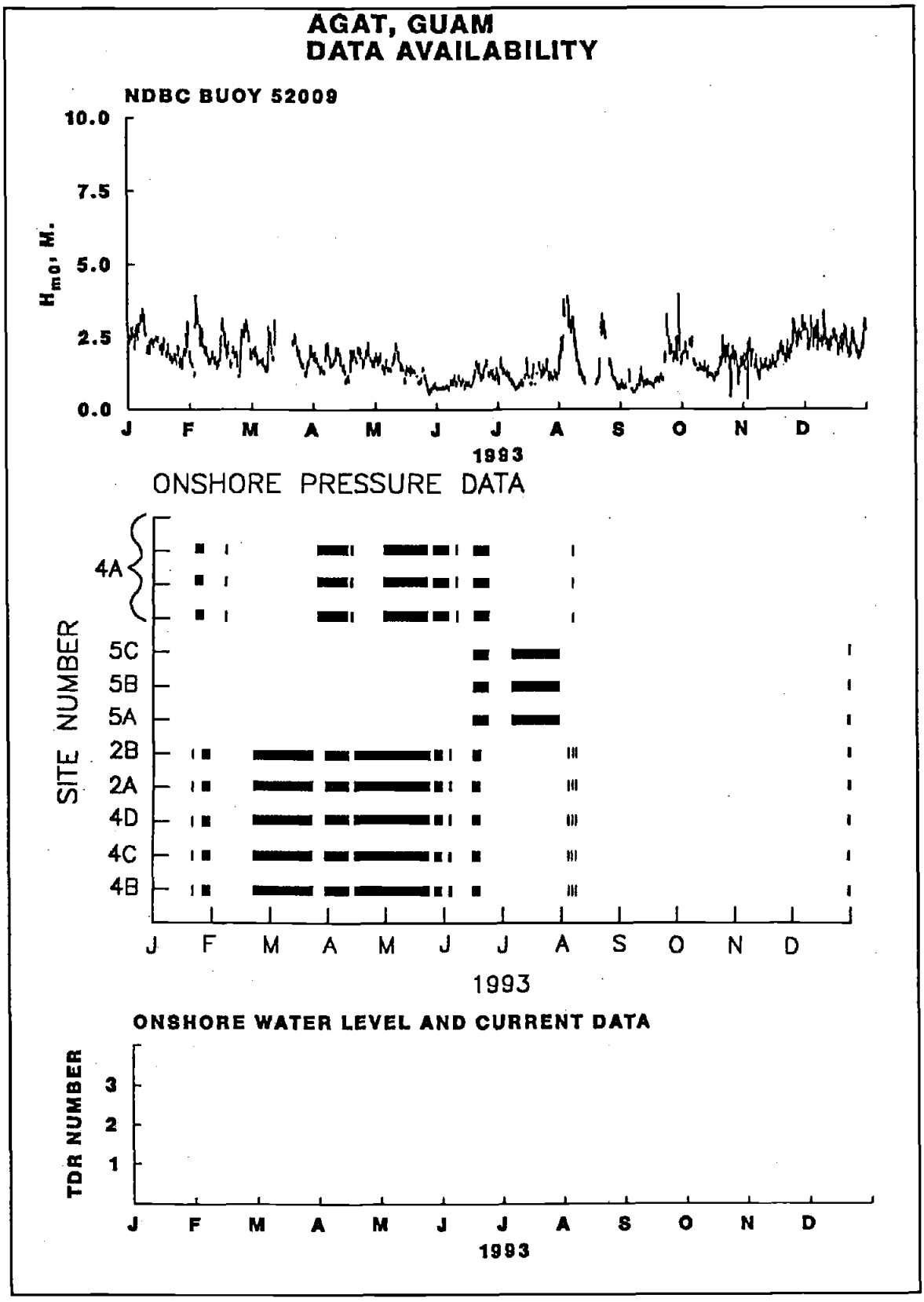

Figure 13. (Sheet 4 of 4)

Results: Results will be provided according to the lettered objectives presented earlier.

a. *Incident wave climate*. Insufficient data were recovered from station 52009 to develop a usable climate based on external analysis, but the data that were collected represent the longest directional wave record available anywhere in the Equatorial Pacific. Figure 14 is a rose plot of the mean wave heights by direction.

Unique measurements of deepwater directional spectra were obtained during the approach of a typhoon that will provide valuable "outer envelope" information for wave generation models. Figure 15 shows the path of Typhoon Russ relative to the island and the gauge. Also plotted are the

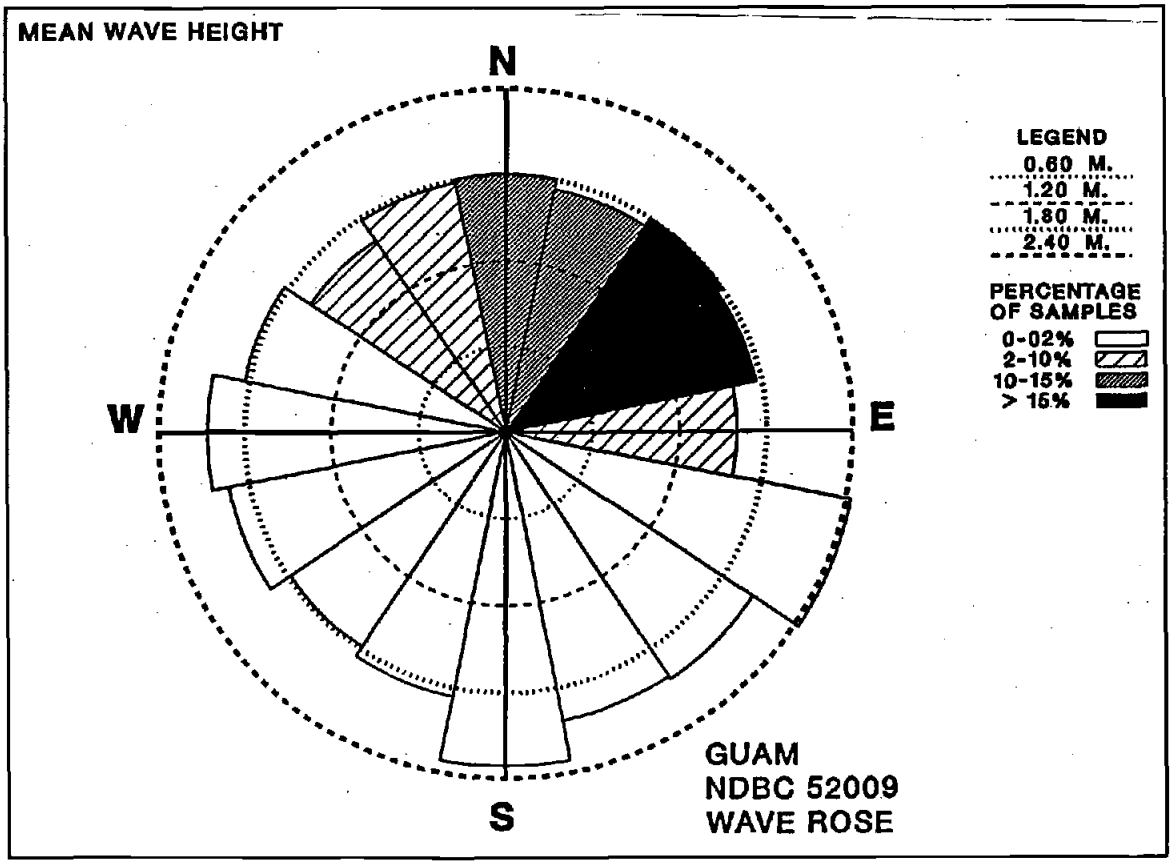

Figure 14. Rose plot of incident wave conditions

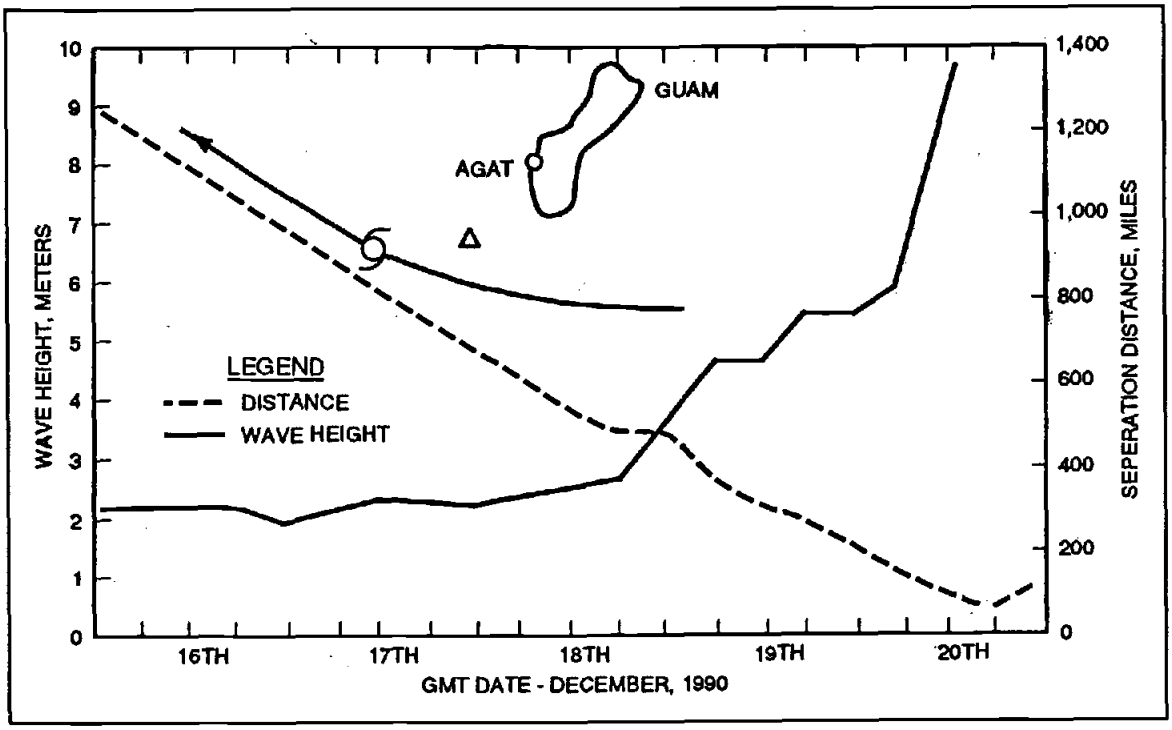

Figure 15. Typhoon Russ; path and observations

history of the separation distance between the buoy and the storm center and the measured significant wave height. The approach and arrival of Typhoon Russ are obvious in the data. The buoy failed when the center of the storm was a distance approximately the radius of maximum winds away, so the last few wave heights measured, though still increasing, probably represent the peak conditions. Typhoon conditions were also captured during typhoons Brian and Gay. Appendix D contains plots of the complete time series of wave heights, periods, and directions for all available data.

b. *Wave transformation.* Most of the data recovered represent the normal condition on the leeward side - flat calm. Instances of simultaneous operation of the offshore gauge and the three gauges along the reef flat (2A, 2B, and 4A) when significant energy was approaching from the west, were rare. Table 2 summarizes the times and reduced parameters selected for further

Table 2
Summary of Reef Flat Wave Transmission Events

Date-m/d/yr time-GMT	Significant Wave Height (m) Peak Period (sec) 1B	2A	2B	4A	Depth (m)
10/16/92 0200	1.77 12.5	0.26 102	0.36 102	0.29 205	0.9
10/16/92 0600	1.83 12.5	0.21 205	0.31 205	0.21 205	0.7
11/23/92 0600		0.26 68	0.45 68	0.51 205	0.8
11/23/92 1500	5.13 12.5				
11/24/92 0600	4.26 11.1	0.26 205	0.42 102		0.8
11/24/92 0800	4.52 11.1	0.26 205	0.45 205		0.9
08/06/93 1600	3.95 12.5			0.86 205	1.2
08/07/93 0200	3.51 12.5			0.79 205	1.1
08/07/93 0600	2.85 11.1			0.47 205	0.8
08/07/93 1400	3.05 12.5			0.71 205	1.2
08/07/93 2200	2.94 12.5			0.51 205	0.9

discussion. They are representative of energetic conditions for both low and high predicted tidal elevations. Direction of approach of the incident waves ranges from 217 to 299 deg true north. The measured depths listed are from Site 2B, and are somewhat (say 1/2 m) deeper than typical water depths on the reef flat because the gauge was placed in a local depression. The energy levels (as indicated by significant wave height) exhibit another unexpected behavior - they tend to increase as the waves propagate shoreward. Additionally, the peak period on the reef flat bears little resemblance to the incident deepwater wave period. In fact, the notion of a decay ratio for the

incident wave height is inappropriate; rather, a non-linear energy transformation occurs.

Figure 16 is a pressure time series plot from the gauges at Sites 5A, 2B, and 4D that illustrates the transformation process. In relatively deep water at the outer end of the channel (Site 5A), the record is that of "normal" swell waves, with periods of about 15 sec. On the reef flat (Site 2B), the characteristic nonlinear shape has evolved. A longer harmonic, near 100 sec, can be seen modulating the signal.[3] In the harbor (Site 4D) this long wave completely dominates the signal, while the wind waves are effectively blocked.

Figure 17a is the energy spectrum from Site 1B at 0600 hr on 16 October 1992, which is typical for fully developed wave conditions in deep water. Incident significant wave height was about 1.8 m. Underneath (Figure 17b) are the spectra from the reef gauges, showing the dramatic increase in low-frequency content moving shoreward. The aforementioned low frequency limit on the reef flat sensors precludes accurate identification of the peak period, but it is clearly more than 100 sec. The 12-sec (0.08-Hz) offshore peak is not apparent at Site 2A, shows as a secondary peak at Site 2B, and is barely visible at Site 4A. This trend is typical of all cases examined, as further illustrated in Figures 18a and 18b, for the conditions at 1600 hr on 6 August 1993.

Note the scale change relative to the previous figure; incident significant wave height is near 4 m in this case.

c. *Design waves and surge levels behind coral reefs.* No data were obtained by the onshore system during extreme - or even moderately severe - wave conditions; this objective was not met. The water levels recovered during typhoons Omar and Brian were those of a leeward shore, so no dramatic surge occurred. Figure 19 shows the depth time series for the gage at

[3] The 2.5-Hz sampling rate has "stretched" the bottom two plots relative to the first, 1-Hz-sampled plot.

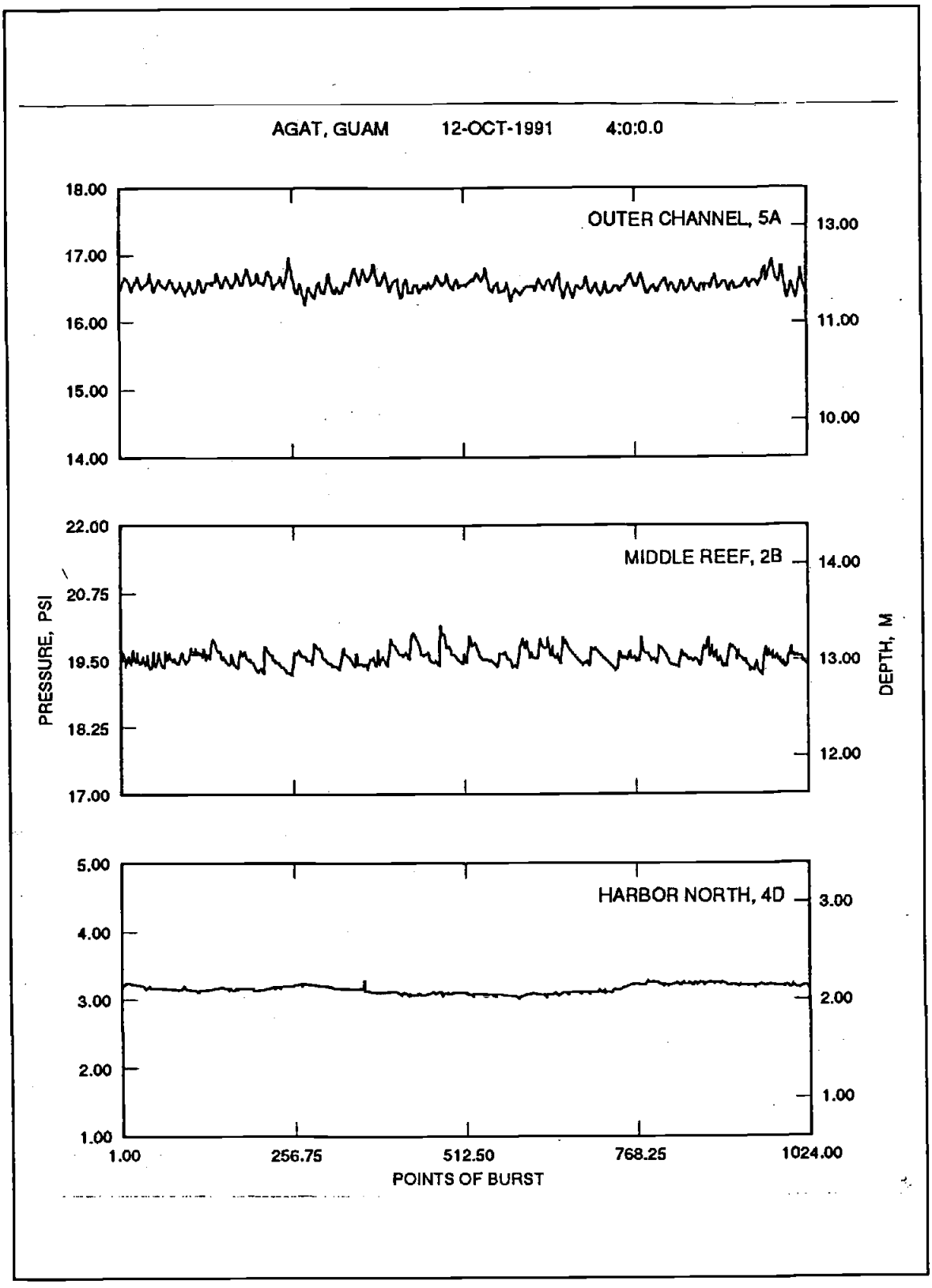

Figure 16. Wave transformation; pressure time series

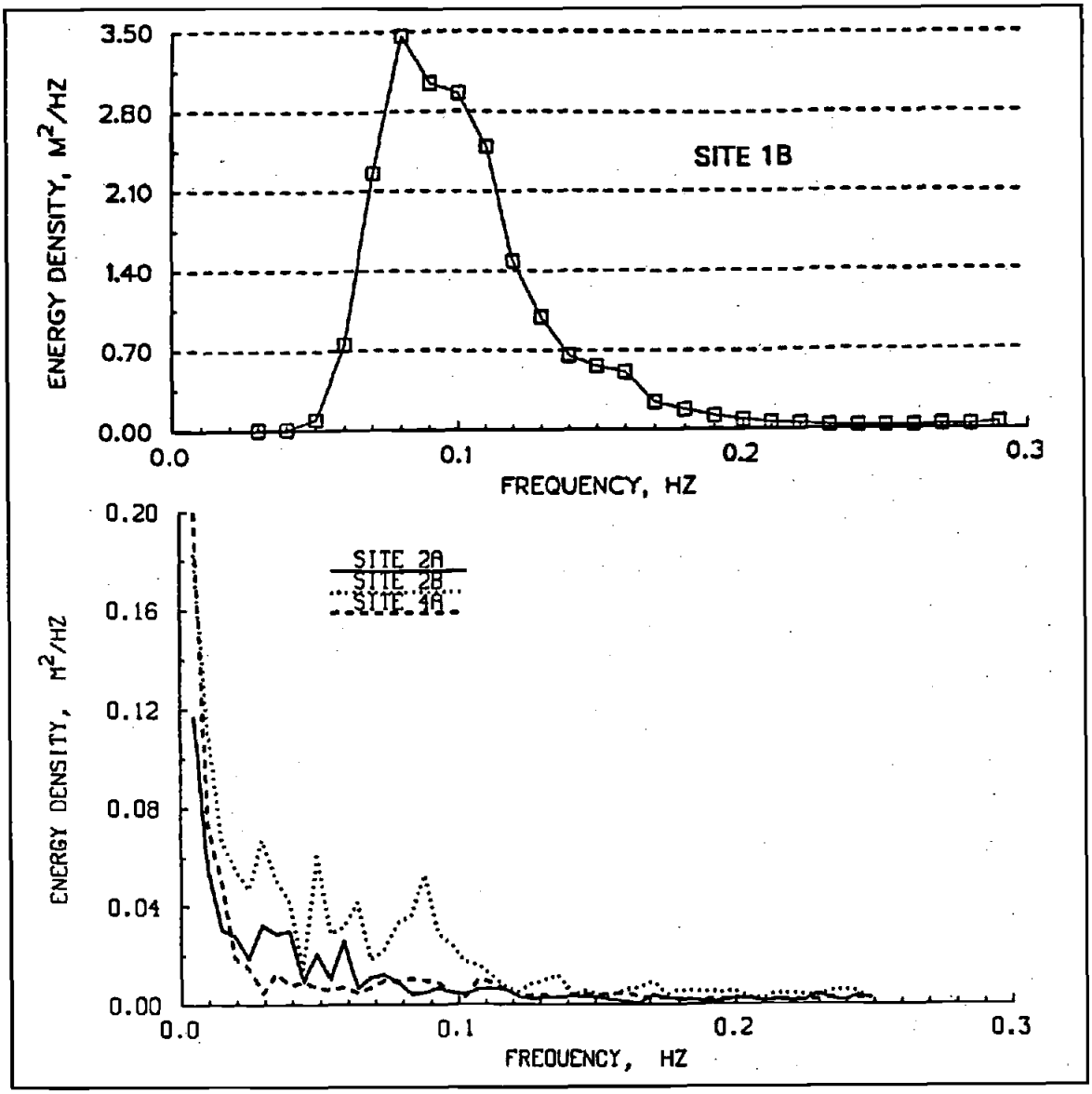

Figure 17. Energy spectra for Sites 1B (a) and 2A, 2B, and 4A (b) on 10/16/92 @ 0600 hr

Site 2-M for the landfall of Omar and the four-day period during and after the landfall of Brian. The mean water level on the high tide (mhw) after Omar's passage is perhaps 1/2 m above the previous mhw. Superimposed high-frequency oscillations (i.e., relatively high when compared to tides, but low relative to wind waves) are about the same magnitude as the surge. This

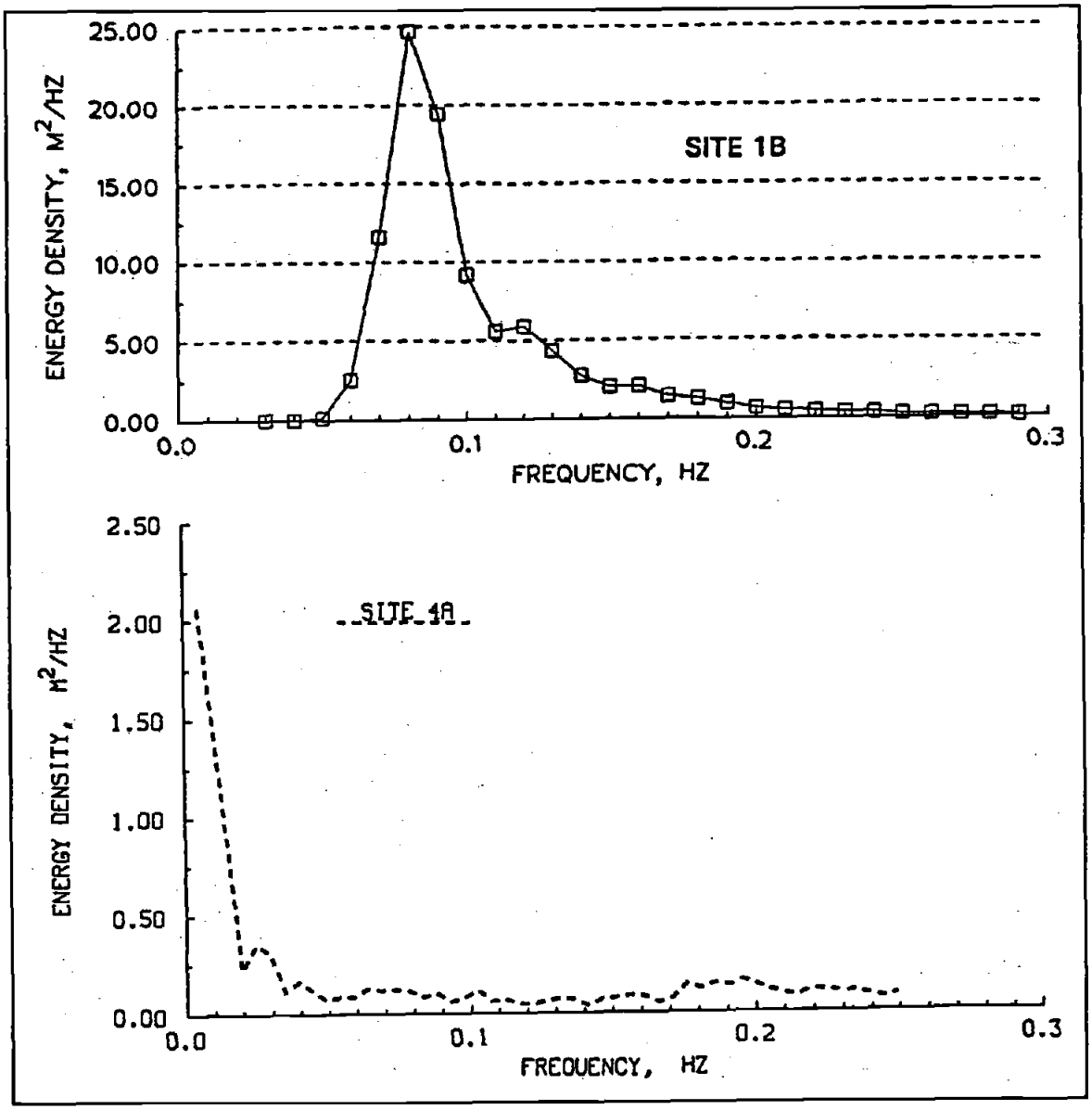

Figure 18. Energy spectra for Sites 1B (a) and 4A (b) on 8/06/93 @ 1600 hr

indicates that design water levels for the reef flat should include both these long wave motions and the average water levels.

d. Validation of the HARBS model. Insufficient data were obtained from the sensors inside the harbor to provide validation of HARBS. Because the

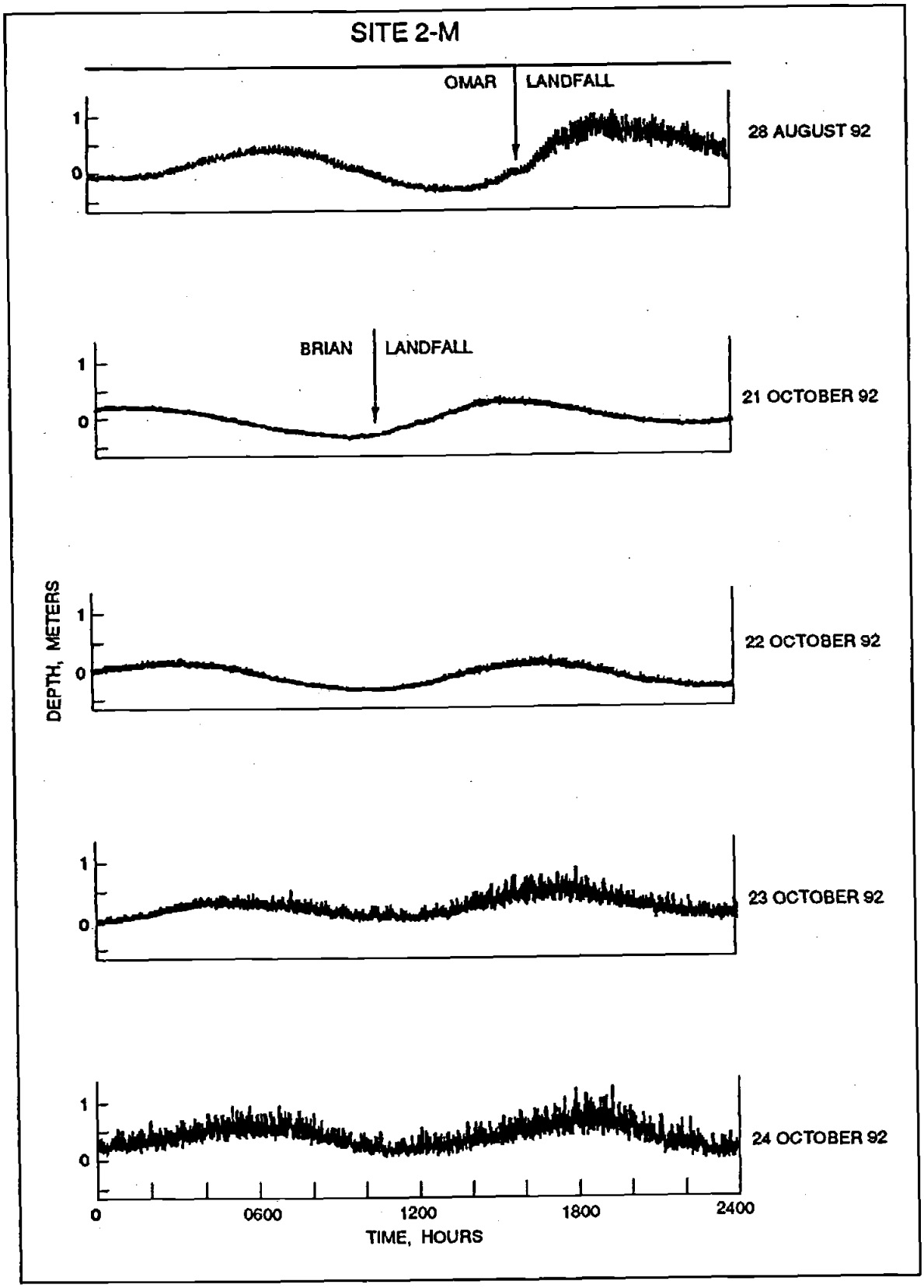

Figure 19. Pressure time series at Site 2-M for typhoons Omar and Brian

model was run for wind waves between 8 and 20 sec, the observed long-wave phenomenon was not modeled.

e. *Wave transformation down steep-sided channels.* Simultaneous operation of sensors 5A and 5B was always during low wave conditions. Insufficient data were obtained to meet this objective for waves of engineering significance.

f. *Site inspections.* The reef flat is not actually flat on the human scale, but pockmarked with sand-filled holes and cracks ranging from centimeters to meters in scale. A thin veneer of sand covered much of the higher surfaces. A dive inspection revealed that the bottom of the entrance channel is covered with a thick layer (over 1 m) of sand, as is the bottom of numerous fissures further offshore. These fissures, on the order of 5 m deep and some tens of meters across, run for hundreds of meters in a generally cross-shore direction offshore of the reef face to the top of a near vertical wall that begins around -30 m. Some 30 m further down the wall, a massive wedge of sand begins its steep (about 1 on 1) descent downward and offshore.

Though the breakwater is classified as a rubble mound, the shallow depths and clarity of the water allowed it to be built essentially as a laid-up structure. The armor stones were individually placed and fitted, often after repeated trials and hand shaping with chisels. The result is a surface that could accommodate the average sedan (see Figure 20). The only discrepancy observed in the inspections occurred on the northern end of the revetted shoreline, at the northwest corner of the harbor. A stone at the toe of the revetment in about 1 m of water, estimated to weigh about 200 kg, was displaced about 1/2 m seaward some time between harbor construction and September 1990. No other damage was observed over the course of the study. No effects were observed on adjacent shorelines.

The one significant change in the project was in the boat basin itself. Between the completion of the breakwater and completion of the marina

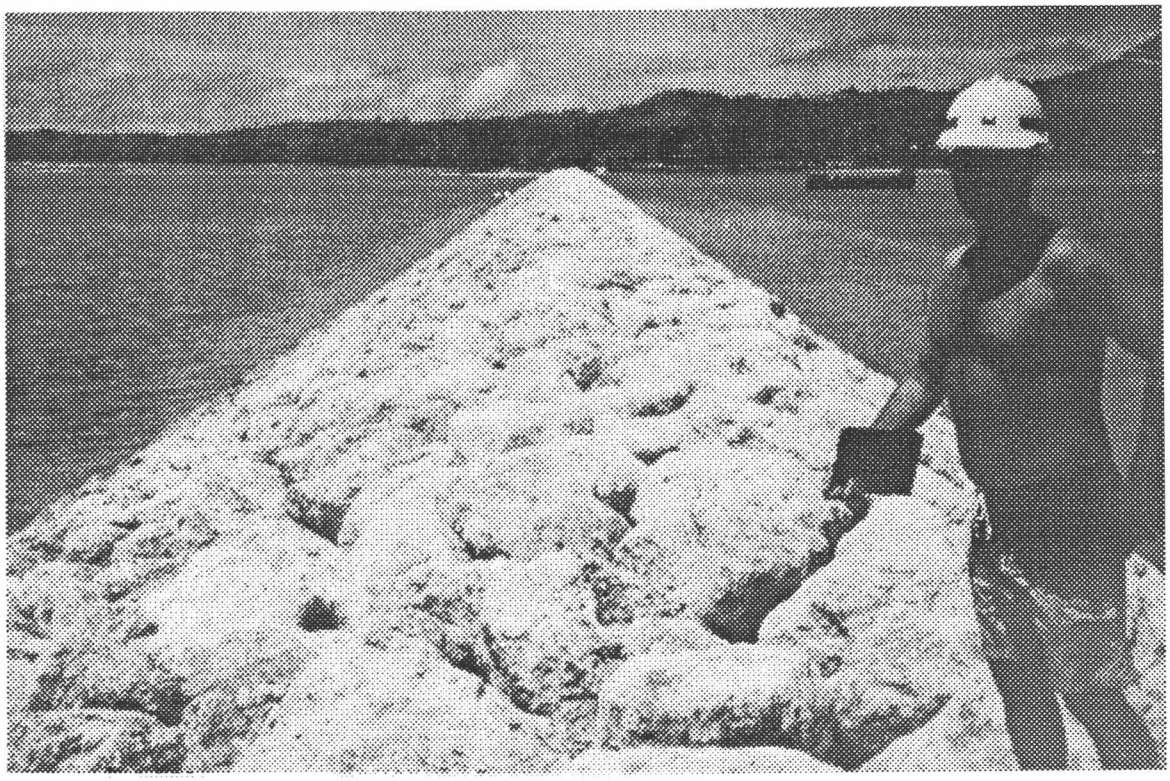

Figure 20. Breakwater surface

facilities in 1990, approximately 1,000 cu m of sediments accumulated in the northern end of the boat basin. Depths were reduced to about a meter in places, making those slips unusable for all but outboard vessels.

g. *Wave-induced circulation on the reef flat.* A "dry run" of the episodic measurement approach was conducted on 7 August 1992 during calm conditions to test the instruments and practice the deployment technique. For Typhoon Omar, pressure sensors were deployed at Sites 2-M, 3-O, and 4-M (see Figure 11) for a period of 5 days beginning on 27 August. Some current data were collected on the 27th, the day before the typhoon hit, but the velocities were too small to be reliably measured.

Two pressure sensors were deployed (at Sites 2-M and 3-O) on October 20 through 24 for Typhoon Brian. Currents were measured on the

20th (before the storm's arrival) but were again too small to be reliably measured. On 23 October, 2 days after the storm passage, currents on the order of 30 cm/sec were measured, when waves from the departing Brian, combined with a more distant Typhoon Colleen, were over 3 m. The solitary, relatively weak measured current contrasts sharply with a verbal report of a "ripping 15 mph" current in the harbor during the peak of Typhoon Guy. Unfortunately, no pressure gages or current meters were deployed for Typhoon Guy to corroborate the observation.

Measurement of significant currents on the reef was not successful, but the reef oscillations associated with them were (see Figure 19). Figure 21 is a 1-hr "blow-up" of the oscillations at Sites 2-M and 3-O at 1800 on 25 October. Components approaching 1/2 m in height are obvious at periods ranging from under a minute to several minutes.

DISCUSSION

Some of the quantitative objectives of the study were not met because of the lack of measured data during the rare high-energy events and because assumptions about the nature of the wave energy on reef flats proved wrong. However, observations have resulted in valuable qualitative information that should be considered when planning or designing projects in a similar environment.

There is no indication that *wind* waves on a reef flat will exceed the depth-limited breaking criteria used for sloping beaches. The highest wave height to water depth ratio in Table 2 is about 0.72, slightly lower than the 0.78 breaking wave criteria used in design. However, this energy-based significant wave height includes all of the low-frequency energy as well, and is really associated with the seiche amplitudes. The height of the highest wind waves on the reef flat, a figure needed in calculating stone stability, will probably not even exceed one half the water depth, as long as the water depths are shallow. However, as the water depth increases due to surge, the breaking wave height limit will increase. Without

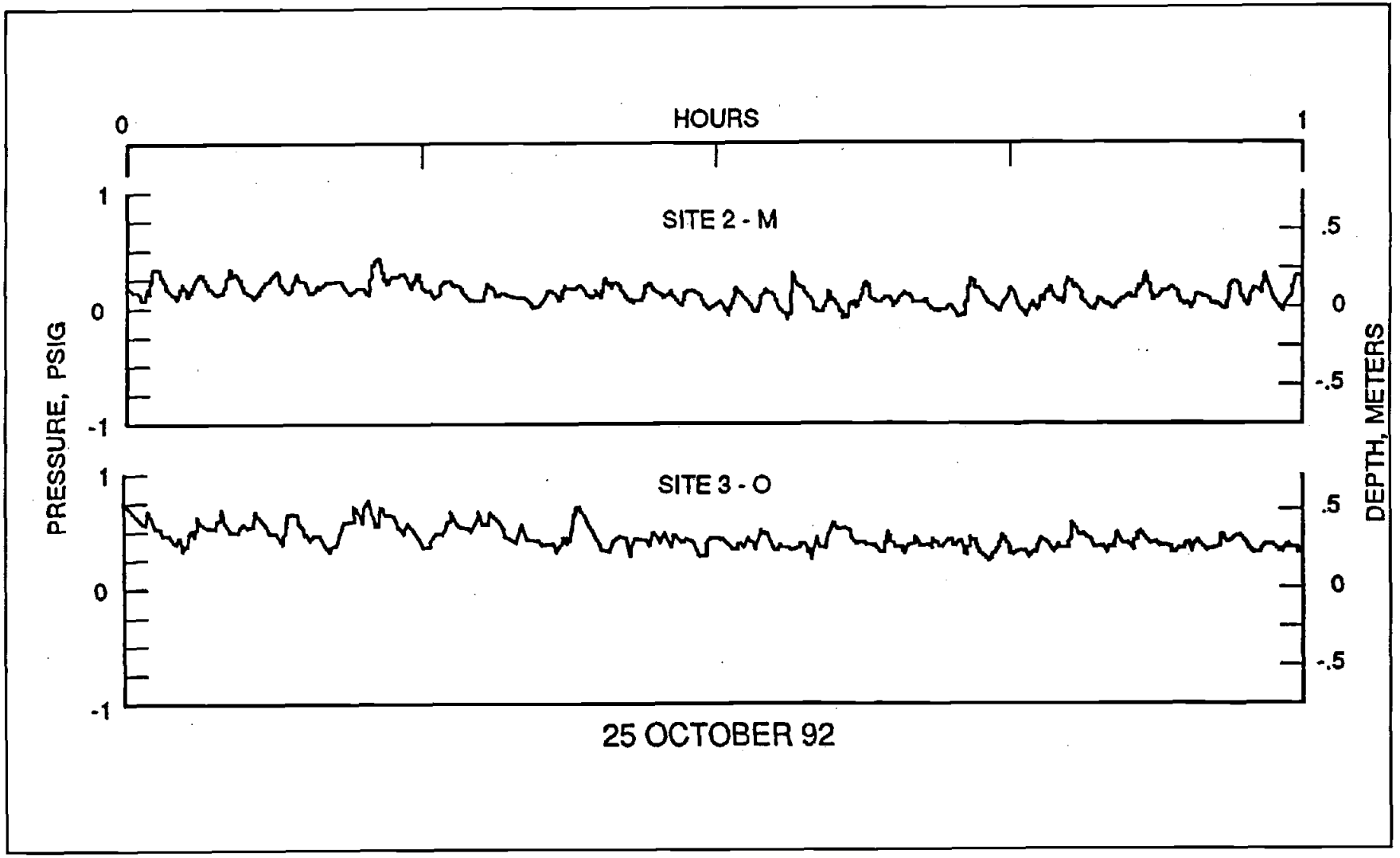

Figure 21. One-hour "blow-up" of oscillations at Sites 2-M and 3-O, 25 October

verification of a lower breaking limit under typhoon conditions, the standard depth-limited criteria should be retained for design.

No measurement of surge levels during typhoons approaching from the west was obtained that exceeded the initial design estimate of 1.4 m. Estimates of surge from measurements or models of planar beaches are unlikely to apply. Some information on the wave-induced setup is available from laboratory studies reported in Smith (1993). Data from a two-dimensional physical model study of a reef-type profile are compared to numerical predictions of wave height and water level behind the reef. Setup on the reef flat on the order of 10 percent of the incident wave height was predicted for cases typified by the prototype measurements in Table 2. (Though the reef profile modeled is described as representing Agat Harbor, the bathymetry is dissimilar enough from the prototype that detailed comparisons with data in this report are not likely to be productive.) For the 9.8-m incident waves measured during Typhoon Russ, wave setup of about 1 m is likely, in addition to atmospheric effects. In any case, wind waves propagating shoreward are not the only, and maybe not even the predominant, environmental loading for structures on reef flats. The physical model simulated the low-frequency energy observed on the reef flat, and predicted heights on the order of 1/4 to 1/2 the incident wind wave height. Forces on structures due to the currents associated with these long waves should be considered as well as wave forces.

A candidate description of the long waves is a seiche of the open-ended basin represented by the continuous stretch of reef flat between the prominent point (Nimitz Beach) in the south and the small islands at Gaan Point in the north. Figure 2 provides an aerial view of this feature. If it is approximated as a rectangular basin length × width × height, with dimensions 600 m × 2,400 m × 1 m , the equation for the seiche periods (neglecting friction) is

$$T = 4\left[gh\left(\frac{4m^2}{w^2} + \frac{(2n - 1)^2}{\ell^2}\right)\right]^{-1/2} \qquad (3)$$

where n and m are the modes of oscillation for the cross and longshore dimensions, respectively, and g is gravity. Table 3 gives the first two modes for the cross and longshore oscillations, independently and combined.

Table 3
Seiche Modes for a Rectangular Basin

n	m	T (sec)
1	0	766
0	1	1533
2	0	255
0	2	766
1	1	685
2	1	252
1	2	542
2	2	242

Note that the first crosshore and second alongshore modes coincide. Friction effects would tend to reduce the seiche periods somewhat, so an oscillation on the order of several to ten minutes, as observed, could be predicted to occur. This is within the range commonly associated with surf beats on other coasts. While no measurements or observations are available to verify their presence in the incident waves, surf beats are most likely the forcing mechanism for the low-frequency energy on the reef flat.

The peak magnitude of the currents associated with these oscillations is

$$v = \frac{H}{2}\sqrt{\frac{g}{h}} \tag{4}$$

or on the order of 1 m/sec for seiche amplitudes on the order of 30 cm. While these are significant, they are less than the observed velocities. In addition, seiche oscillations would be periodic, reversing direction each cycle. Another mechanism must account for the pulsing currents.

The qualitative description of the wind waves propagating across the flat can be shown to be consistent with quantitative estimates. If the reef flat water depth, h, is assumed to be 1 m, a 30 cm/ 10 sec wave has an Ursell number of about 300, and is best described with cnoidal theory. The square of the modulus of the elliptic integral k^2 is about $1 - 10^{-5}$, or

very near to unity, at which cnoidal theory reduces to solitary wave theory (*Shore Protection Manual* 1977). Shoreward mass transport per unit crest width for a solitary wave is $[(16/3)\, h^3\, H]^{1/2}$, or about 1.3 m^3/m. For the reef flat dimensions above, this amounts to over 300 m^3/sec moving shoreward.

The shortest path (hydraulically) for the return flow to take is toward the ends of the reef flat, where breaking and setup are not occurring. Since the harbor is connected to deep water by the entrance channel, the low water level is brought conveniently close - from the return flow's perspective. If just one third of the return flow takes this "short-cut" through the harbor and entrance channel back to sea, velocities across the 100-m-wide opening would be on the order of 1 m/sec. This is sufficient to balance the out-of-phase flow from the seiche, and double the in-phase flow, resulting in a pulsing flow of up to around 4 knots. This is a little less than observed, but no allowance has been made for the setup return flow. Figure 22 schematically illustrates the circulation mechanism hypothesized. Highest velocities would occur where the gradient is steepest, which is near the shoreward side of the harbor basin. This pattern could explain the displacement of the toe stone at the northwest corner of the basin, an area exposed to the highest velocity currents flowing into the harbor.

The sediment that entered the harbor came from the veneer of sand that is evident in many places overlaying the old coral on the reef flat. It was transported there by the currents flowing through the harbor, which acts as an effective settling basin. Given the evidence of significant offshore sediment transport through the natural pathways, this process will continue for the current harbor configuration. Since the transport is episodic, it is impossible to predict the short-term rate of influx. If it is a persistent problem, alternative geometries that would reduce influx of sediment while maintaining the desirable flushing characteristics could be investigated.

CONCLUSIONS

The following conclusions were reached as a result of this study:

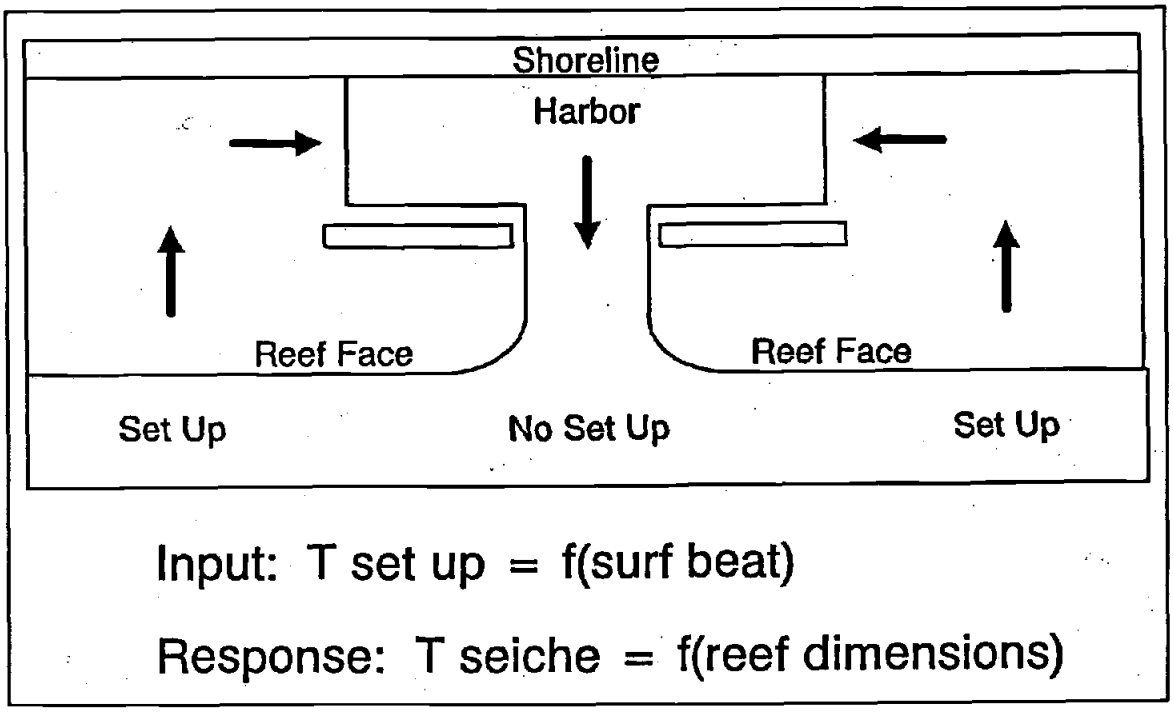

Figure 22. Schematic representation of reef flat circulation/oscillation

a. With the exception of the NDBC buoy located offshore, most data recovered from this monitoring effort represent mild conditions. The buoy recorded waves near 10 m before failing during Typhoon Russ.

b. Wind waves dissipate most of their energy in breaking at the reef face. Wave energy propagates across reef flats as bores, moving water shoreward that returns seaward through breaks in the reef face. Agat Harbor and its entrance channel provide such a pathway.

c. Wave heights on the reef flat do not increase appreciably as wave height offshore increases, but the amplitude of seiche of the entire reef flat is affected by incident energy. It is probable that wave groups (surf beats) with periods near the principal seiche modes of a reef flat will induce harmonic coupling.

For this system, coupling can occur at periods on the order of several to ten minutes.

d. The combination of seiche, return flow from wave setup, and mass transport of bore-like waves can result in large currents running parallel to shore. For structures located on the reef flat, forces due to the resulting currents can be of larger magnitude than forces due to the wind waves themselves. Currents on the order of 3 m/sec were observed visually under moderately rough wave conditions. This observation is consistent with calculations of currents due to combined seiche and solitary waves 30 cm in height. Currents are probably responsible for displacement of one stone at the toe of the structure.

e. Typhoon surge levels were not measured, but are likely to be a meter or more, based on model data.

f. It is difficult to extrapolate these results to more extreme events. During a typhoon, wind shear on the water would play an important role, but the approach angle would determine whether this augments or cancels the current. A high surge may increase seiche amplitudes, but tend to linearize waves propagating on the flat, reducing mass transport. The design storm may well be one that passes eastward of the island on a northwesterly track, bringing little surge but strong northwesterly wind and swell after it passes the island. Under these conditions, it is not unreasonable to anticipate currents exceeding 5 m/sec on the reef flat.

g. The detached breakwater design promotes flushing of the harbor, but can result in significant influx of sediment during high-current events.

Wave Transmission and Reflection for a Porous Rubble Mound Breakwater

David D. McGehee

11th International Harbour Congress,
Royal Flemish Society of Engineers, Antwerp Belgium,
June 1996

WAVE TRANSMISSION AND REFLECTION FOR A POROUS RUBBLE MOUND BREAKWATER

INTRODUCTION

The Monitoring Completed Coastal Projects (MCCP) Program was established by Headquarters, U.S. Army Corps of Engineers (HQUSACE) in 1981 to evaluate the performance of the Corps in planning, design, construction, and operation and maintenance of selected Civil Works coastal projects. The program's objective is to acquire information through intensive monitoring of coastal projects for improving:

a. Project purpose and attainment.

b. Design procedures.

c. Construction methods.

d. Operation and maintenance techniques.

The 1984 nomination of Burns Harbor for inclusion in the MCCP stressed the continuing need to maintain the crest elevation of the breakwater as the principal problem with the project. The assumption at that time was that the loss of elevation was due to foundation failure, inadequate armor stone stability, or both. Wave conditions inside the harbor were inconveniencing operations and causing damage to vessels. The original monitoring plan focused on three technical areas: 1) structural stability, 2) geotechnical stability, and 3) waves and water levels. As the study progressed, the interaction of these three areas became apparent (McGehee and Moritz 1996). This paper will present the results of the measured wave transmission and reflection characteristics of the breakwater, and a

comparison to results of a two dimensional (2-D) physical model test performed during the design of the structure (Jackson 1967).

Site Description: Burns Harbor, Indiana is located on the southern end of Lake Michigan (Figure. 23). The configuration of Lake Michigan exposes the harbor to significant wave energy from the northern quadrant. Maximum fetch is about 300 miles, to the north. Extreme weather usually occurs during passage of cold fronts associated with extratropical cyclones. While these storms can generate high winds, they typically move across the lake before seas become fully developed, so extreme waves tend to be duration-limited rather than fetch limited. Water levels fluctuate seasonally on the order of a meter due to regional precipitation patterns and near a meter during storms from wind setup/setdown. The natural shoreline consists of high dunes of medium sand. The lake bottom is covered with silty sand; slopes are on the order of 1:100 offshore of the harbor.

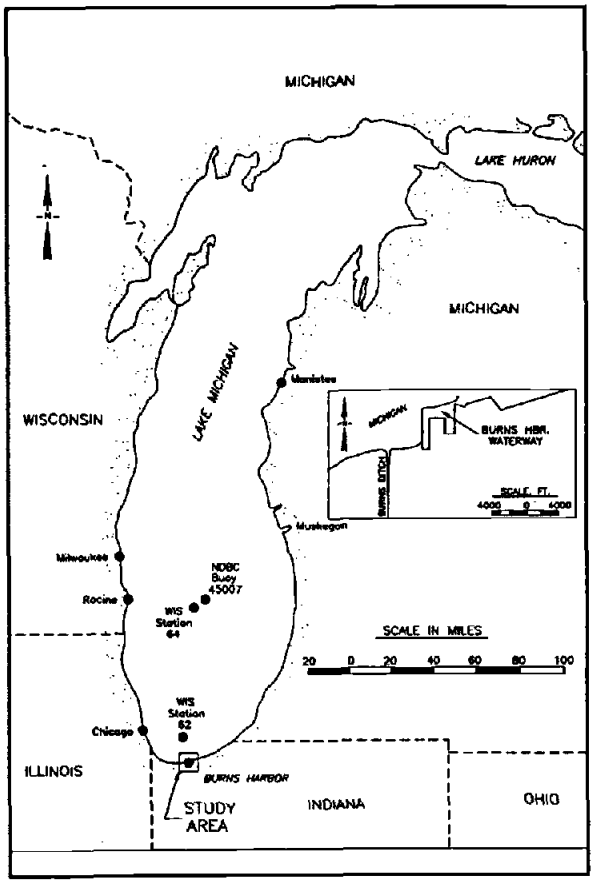

Figure 23. Location of Burns Harbor, Indiana

Project Description: The harbor consists of an L-shaped breakwater with a 1200-ft-long western arm and a 4640-ft-long northern arm (Figure 24). A cellular sheet pile extension connects the western arm to the shore. The depth of the lakeside toe of the northern arm ranges from 30 ft to -41 ft Low Water Datum (LWD). The authorized project depth is 30 ft in the entrance channel, and 28 ft in the harbor, though actual depths are typically more. The interior perimeter of the harbor has both riprap revetment and vertical steel sheetpile sections.

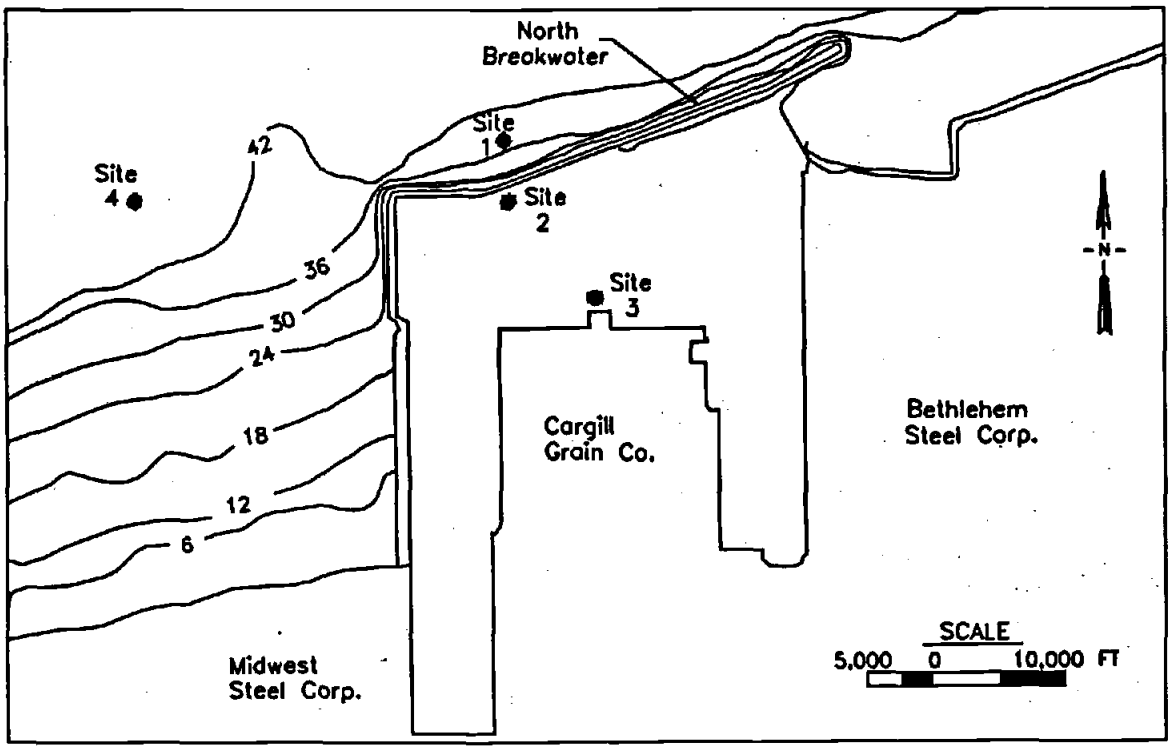

Figure 24. Plan of Burns Harbor with wave guage locations

The breakwater is a multilayer rubble-mound structure with two layers of random-placed Bedford limestone armor (W stone). Figure 25 is a typical cross section for the northern arm. Design crest elevation is +14 ft LWD. Side slopes on both lake and harbor sides are 1:1.5. The core stone ranges from 5 to 90 lb and projects about 15 ft beyond the W/10 stone to form a bedding layer for the armor. A sand core forms the lowest layer.

The parallelipiped, cut stone armor units, which range from 10 to 16 tons on the trunk and from 15 to 20 tons on the head, are typical for coastal structures in the Great lakes, but the two layer random placement was unusual at the time of its design. A high core design with laidup placement of a single layer of armor is more typical. Burns Harbor was the first breakwater built in the Great Lakes with this style of armor placement.

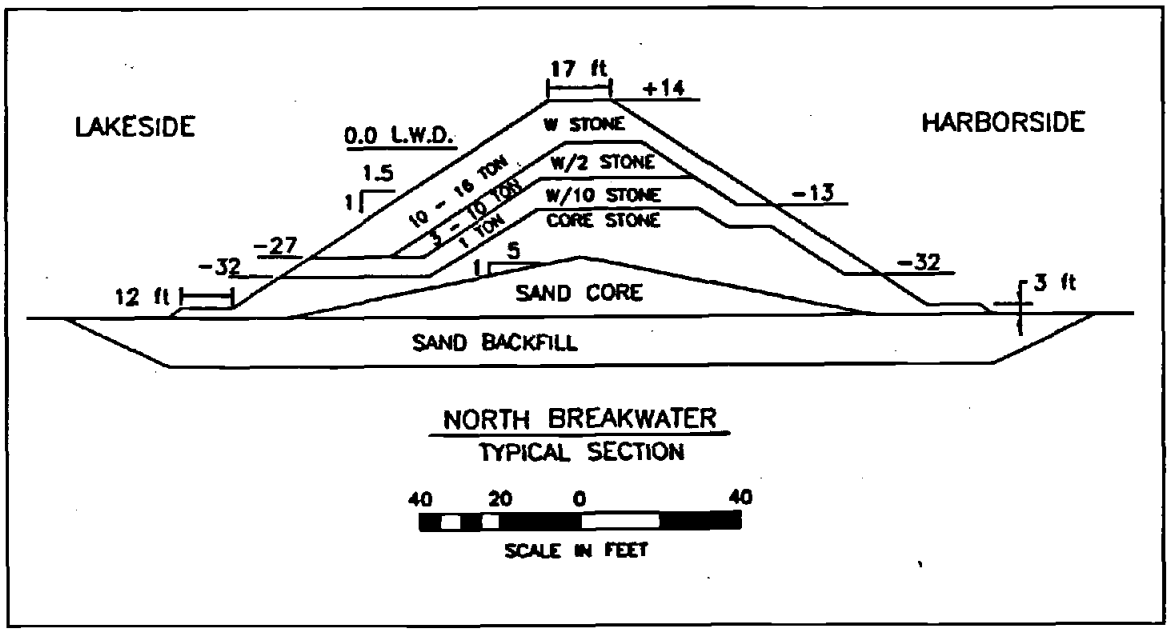

Figure 25. Typical breakwater cross section

WAVE AND WATER LEVEL DATA

The purposes of the wave measurement and analysis effort were to 1) evaluate the original selection of the design wave; 2) measure the breakwater's reflection and transmission characteristics; 3) evaluate the 2-D physical model transmission results; 4) monitor the actual wave conditions in the harbor; and 5) determine the mode by which wave energy entered the harbor. The purpose of the water level analysis was to evaluate the selection of the design water level.

Wave Data Collection: Wave gages were installed at locations 1 through 4 as shown on Figure 24. Site 1 is located directly in front of the breakwater and measures the combined incident plus reflected wave field. Site 2 is behind the breakwater at approximately the same station and measures the total wave energy transmitted into the harbor. It was situated to minimize influence by wave energy coming through the entrance. Site 3 is directly in front of the highly reflective grain dock that experienced damaging wave conditions. Site 4 was

selected to measure incident waves approaching the breakwater. It is located to the west of the breakwater in front of a beach assumed to produce negligible reflection.

Ideally, all gage sites would have been instrumented simultaneously, but the budget constrained the number of available gages. The gages were self-contained, single-point pressure sensors mounted on steel frames on the lake bottom. Sampling schemes were constrained by battery and memory capacity. In order to obtain data over a winter storm season when retrieval is impractical, waves were sampled at 1 Hz for 1024 seconds every 3 hours. Mean depth over the gage was also obtained for each wave record from the bottom-mounted wave gages at Sites 1 through 4.

Wave Data Reduction: Spectral analysis of the pressure time-series provides a one-dimensional energy spectrum of the water surface. In the following discussion, the terms wave height and period will refer to an energy-based wave height, H_{m0}, calculated from the zeroth moment of the one-dimensional energy spectrum (generally equivalent to significant wave height, H_s), and the period T_p associated with the peak of the energy spectrum.

Data return was about 80 percent over the combined deployment intervals. A height threshold of 0.2 m was applied to the reduced data, since estimates of H_{mo} and T_P for low energy conditions are questionable, and waves below 0.2 m have no engineering significance for this study. Figure 26 is a typical sea surface energy spectrum from Site 1 on 8 February 1987.

Wave Reflection/Transmission: Figure 27 shows the incident plus reflected energy-based significant wave height (Site 1) plotted as a function of the simultaneously measured incident wave height (Site 4) for incident waves over 0.5 m when hindcast winds were from the northern quadrant. The results of the analysis show that reflection for low waves, less than about 2 m, was essentially negligible, but was significant for waves above this level. The actual reflection is not, of course, a step function at 2 m, but this value serves as a useful and convenient threshold, since smaller waves are unlikely to have any impact on the structure.

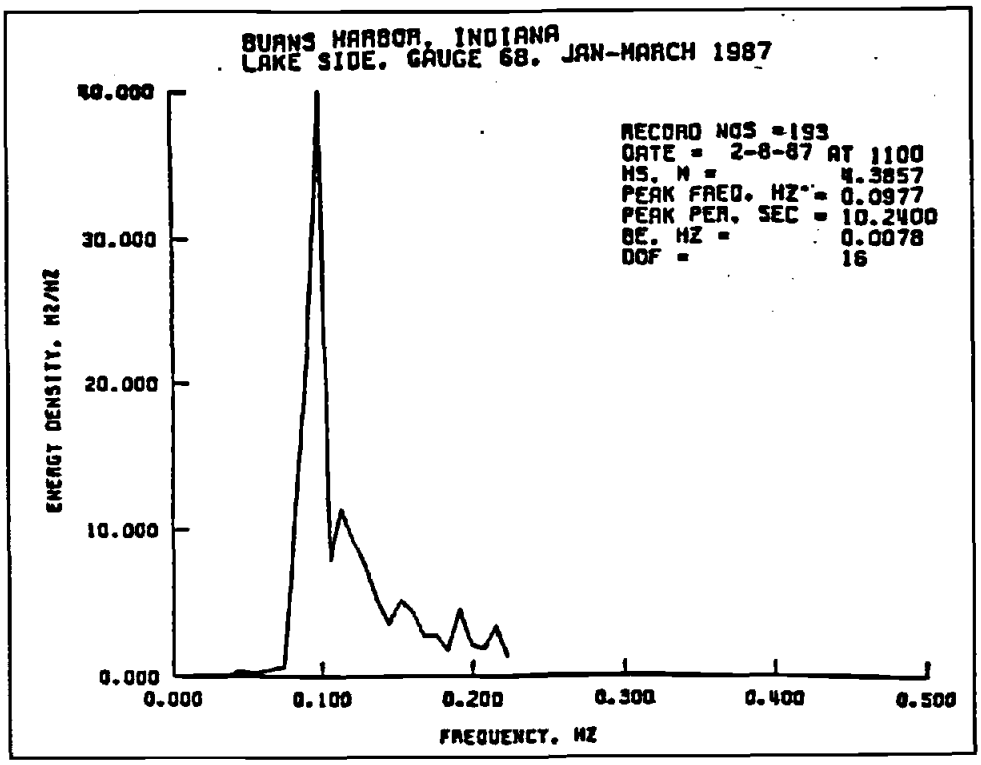

Figure 26. Typical sea surface energy spectrum for Site 1, 8 February 1987

The reflection coefficient, K_R, is defined for monochromatic waves as:

$$K_R = \frac{H_R}{H_I} \tag{5}$$

Since the measured values of significant wave height are based on an energy-derived parameter, an assumption is made that energy is conserved; i.e.,

$$(H_{I+R})^2 = H_I{}^2 + H_R{}^2 \tag{6}$$

leading to an equivalent expression for K_R,

$$K_R = \left[\frac{(H_{I+R})^2 - H_I{}^2}{H_I{}^2}\right]^{\frac{1}{2}} \tag{7}$$

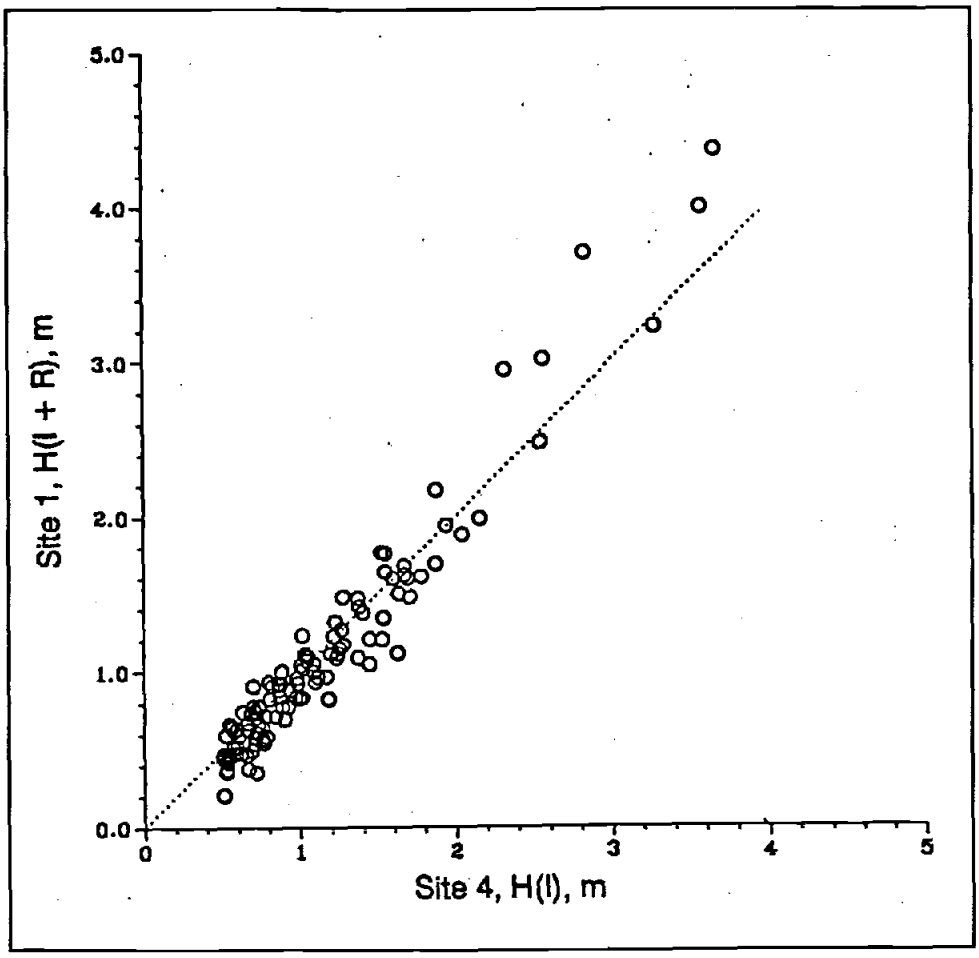

Figure 27. Significant wave heights (H_s) at Site 1 versus Site 4

Figure 28 plots the square of wave heights at Sites 1 and 4 for incident waves over 2 m. A least squares fit to the data is also plotted and corresponds to

$$(H_{I+R})^2 = -1.08 + 1.39H_I^2 \quad (8)$$

The 90 percent confidence bands for Equation 8 are also shown on Figure 28, but it is debatable how meaningful that statistic is for such a small sample. Visual inspection confirms that measured values are within about a meter of the predictor equation. The resulting reflection coefficient, K_R, is plotted in Figure 29 as a function of incident significant wave height, and is approximated by the equation

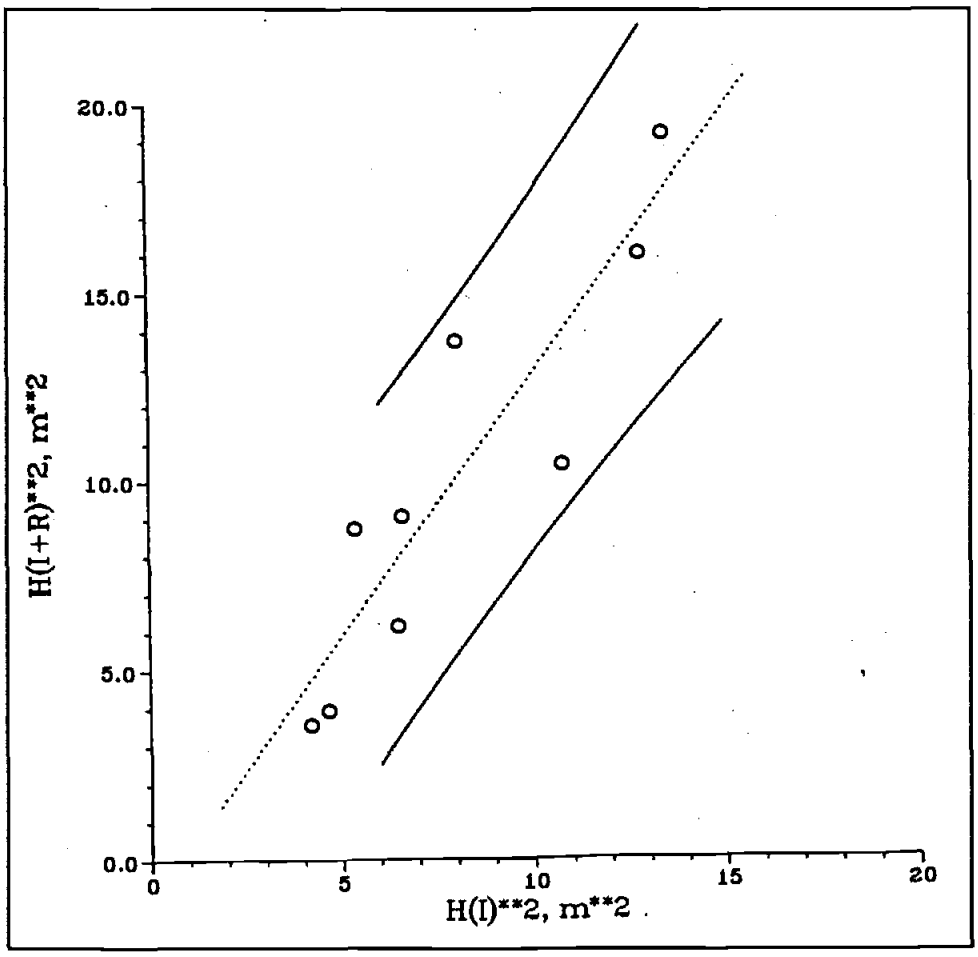

Figure 28. Least squares regression of significant wave height squared at Site 1 versus Site 4

$$K_R \cong \left\{ \begin{array}{l} 0\ , \qquad H_I \le 2.0m \\ 0.62\sqrt{1-\dfrac{2.77}{H_I^2}}, H_I > 2.0m \end{array} \right\} \tag{9}$$

The wave transmission coefficient is the ratio of transmitted to incident wave heights. But all transmitted wave measurements (Site 2) were obtained when incident plus reflected energy were measured at Site 1. To compensate for the additional energy, wave heights measured at Site 1 were adjusted by the calculated reflection relation given in the previous equation. These calculated incident wave heights, designated as "Site" 1A, were used in conjunction

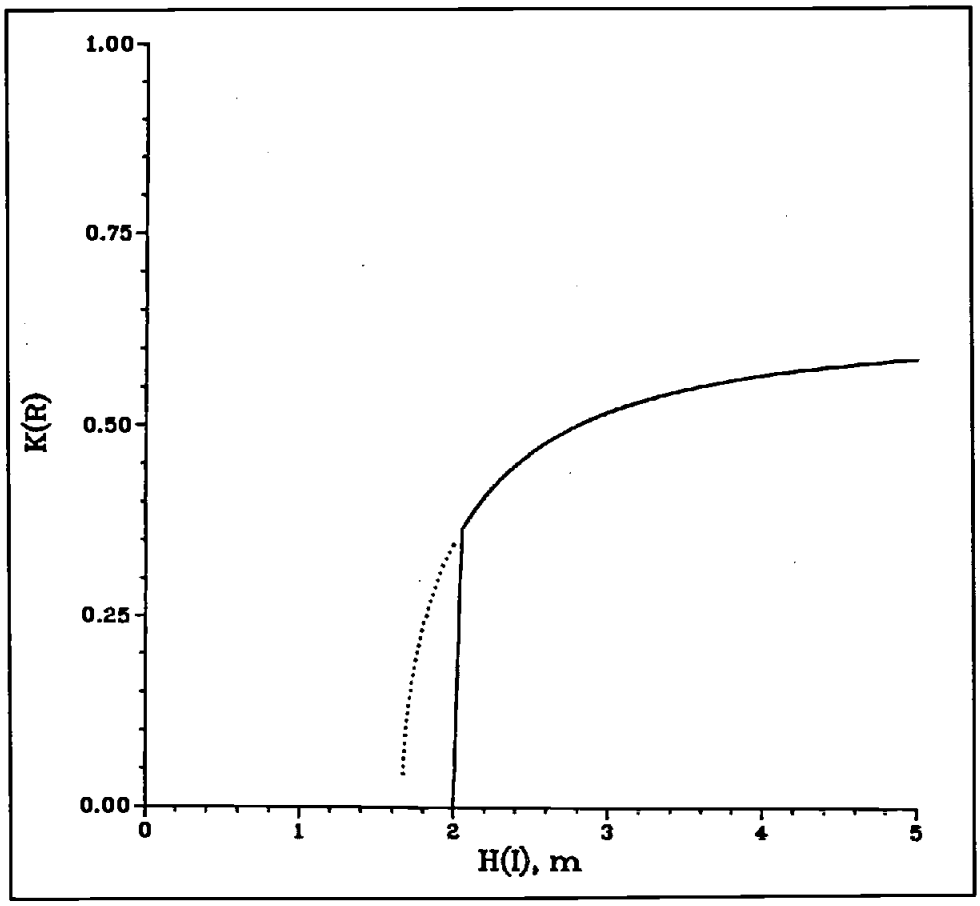

Figure 29. Reflection coefficient, K_R, versus incident significant wave height

with simultaneously measured transmitted wave heights (Site 2) to calculate transmission characteristics. The results are presented in Figure 30, where K_T is plotted as a function of incident wave height, and is represented by the equation

$$K_T = 0.192 - 0.052 H_I + 0.018 H_I^2 \tag{10}$$

Figure 31 is another plot of K_T, but plotted against wave power. The scatter is reduced compared to Figure 30, partly due to better representation of higher waves with short periods that have little impact on the structure. Because both theory and the measurements showed a dependence of K_T on wave period as well as height, and wave power incorporates

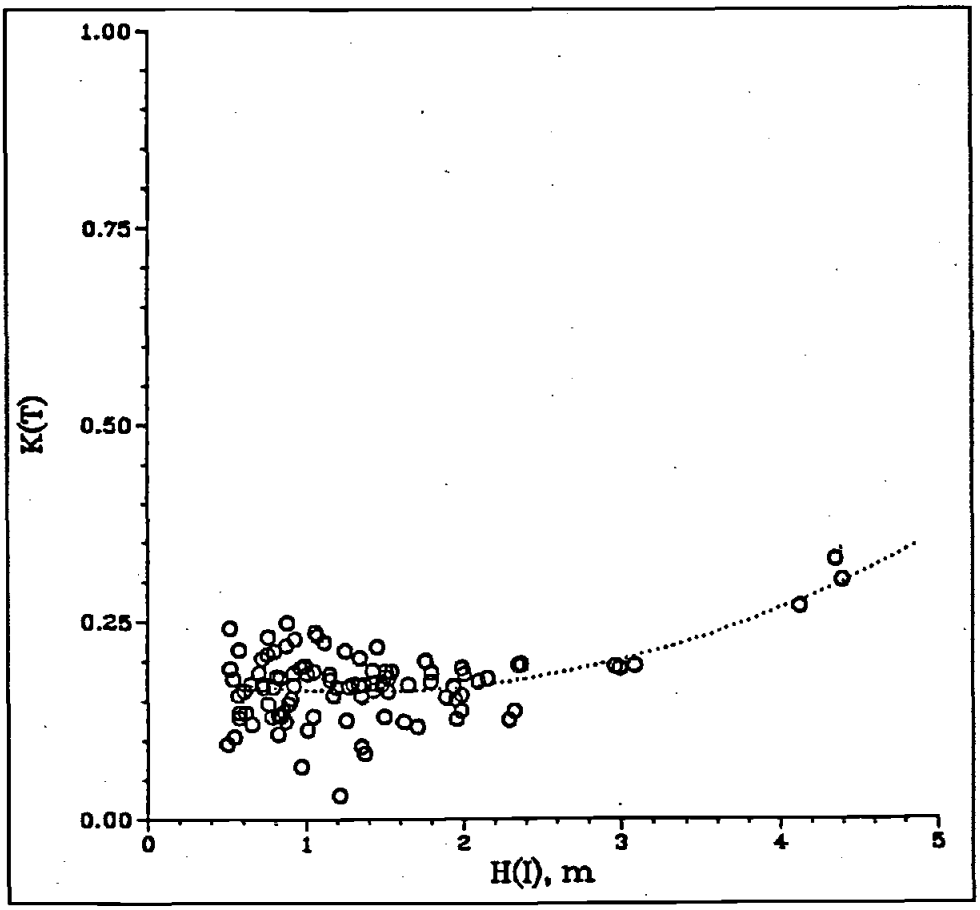

Figure 30. Transmission coefficient, K_T, versus incident significant wave height

both parameters, correlations based on wave power may be a more useful way of defining and calculating transmission for porous structures.

Figure 32 is a comparison of the prototype and the 2-D model transmission coefficients. The prototype data ranged from 4.1 to 11.6 sec, but only those prototype waves with periods greater than 10 sec, comparable to the 11 sec model waves, are plotted. The 2-D model measured wave transmission at two locations at distances *L/2* and *L* behind the breakwater, where *L* was the shallow water wavelength. Transmitted wave heights were generally higher at the *L* position than the *L/2* position. The transmitted wave measurements in the prototype were made at a fixed distance of about 75 m from the center of the breakwater.

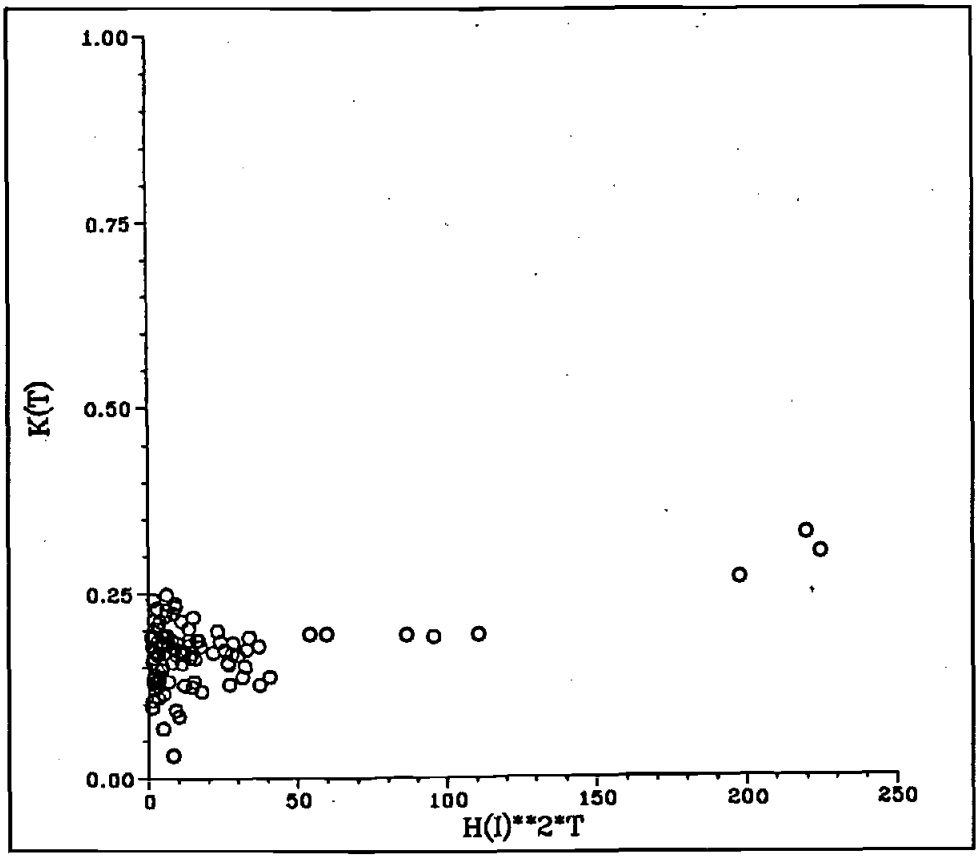

Figure 31. Transmission coefficient, K_T, versus incident significant wave power

This location falls halfway between *L/2* and *L* for the longer waves of interest (the order of 100 m). It is uncertain if the increasing trend with distance behind the structure exists in the prototype, so *L* and *L/2* model data sets are plotted.

Only eight prototype incident wave data points meet the criteria of having periods greater than 10 sec, and these are compared to 10 modeled incident wave heights. The uncorrected transmission coefficient

$$K_T = \frac{H_{(Site\ 2)}}{H_{(Site\ 1)}} \tag{11}$$

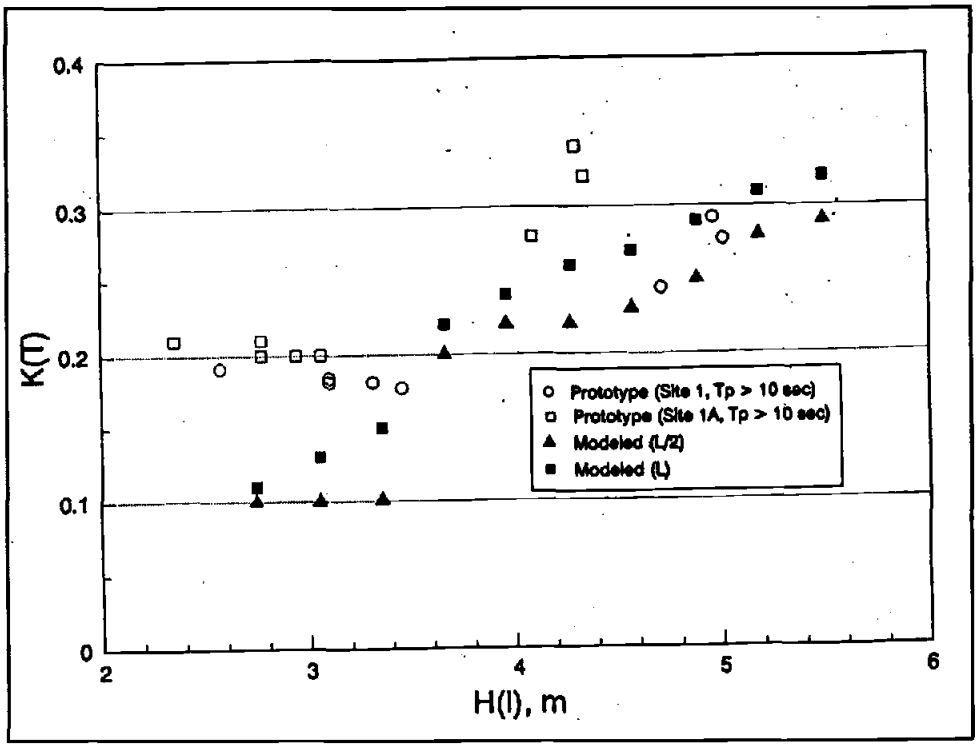

Figure 32. Measured and modeled transmission coefficient, K_T, versus wave height when $T_p > 10$ sec

is also plotted to clarify the effect of applying the reflection correction to the measured data at Site 1 (and because there is no documentation on the treatment of reflected waves in the model). The general trend of all four data sets is increasing transmission with increasing wave height, though the prototype data from Site 1A (i.e. adjusted for reflection) reveals highest transmission, with a maximum of 0.33 for the 4.35 m incident wave; the model reaches 0.32 for the 5.5 m wave. The data from Site 1 more closely follows the model results.

The model significantly underpredicted transmission for waves below 3 m, regardless of whether the reflected waves are included. Long period waves below 3 m are transmitted through the structure without overtopping, and are strongly influenced by the structure's porosity. Results of later research showed that the core material in scaled physical models should be oversized relative to the linear scaling relationship to compensate for viscosity effects (Keulegan, 1973). The core material in the 1966 study was sized linearly, like the

cover layers, and the underprediction may result from the effect of the increased viscous drag, relative to the prototype, at these scales.

Another factor that would tend to increase the measured energy at Site 2, and thus the prototype transmission coefficient, is the effect of energy coming through the entrance, in spite of the attempt to minimize this influence by its position. Finally, the lake level during the more extreme events exceeded the 4 ft LWD used in the model study.

The measured data for waves over 3 m are from a storm that occurred on 8-9 February, and 9 March, 1987. Lake levels for the February storm, as measured at the Calumet gage, exceeded 1.8 m (6 ft LWD). This increased water level undoubtably affected the transmission. Lake levels at Burns Harbor during the March event, as measured at Site 1, were very near the 4.0 ft LWD used in the model study.

Evaluation of the model's performance presupposes that the model cross section duplicates the prototype; i.e., that the actual structure was constructed as designed. The stability analysis has shown that significant amounts of armor have been added to the structure without a concomitant increase in structure elevation or volume. Therefore, the existing structure must contain a higher percentage of armor, and the less porous layers must be correspondingly lower in the cross section than the design structure. Whether this increased porosity is sufficient to account for the increased transmissivity cannot be determined with the existing data, but it is certainly a contributing factor.

The model data show an abrupt discontinuity around 3.5 m. It is near this point that the model study indicated overtopping occurred. It seems likely the additional energy coming over the model structure caused the increase in total transmittance. There is not as obvious a jump in the prototype data, though it could be argued that an increase in the rate of transmittance occurs between 3 and 4 m. It is likely that this corresponds to the onset of significant overtopping in the prototype as well. The model predicts total transmittance better in the combined transmission/overtopping regime.

Direct comparison of the model and prototype is hampered by the following factors:

Model Data

- regular waves

- uncertainty in correction for reflection
- scale effects (core sizing)

Prototype Data

- irregular waves
- uncertainty in incident wave height (on the order of 1 m)
- peak periods different from model wave periods
- transmitted gage position different
- higher actual cross section composition
- uncertainty in mean water levels during storms

SUMMARY

Measurements were made of waves at four sites inside and outside a harbor protected by a porous rubble mound breakwater. The breakwater's wave reflection characteristics were obtained by analyzing simultaneous measurements from Sites 1 and 4. To describe the relationship between measurements at these two sites, an energy-based method was used to determine a reflection coefficient, K_R, as a function of incident wave height. The transmission function of the breakwater, K_T, was similarly calculated from simultaneous measurements at Sites 1 and 2. Since the measurements at Site 1 contained both incident and reflected energy, they were transformed by the reflection function, K_R, before calculation of K_T. Finally, the measured transmission characteristics were compared graphically to the physical model results.

Estimating Tsunami Amplitudes and Periods

David D. McGehee and Charles K. Sollitt

Submitted to *Journal of Waterway, Port, Coastal and Ocean Engineering,*
American Society of Civil Engineers, New York, NY,
October 1997

ESTIMATING TSUNAMI AMPLITUDES AND PERIODS

BACKGROUND

The present tsunami warning system for U.S. coastal areas relies on identification of submarine epicenters from seismic signals. Tsunami arrival time can be reasonably estimated for coastlines far from the seismic source, but reliable amplitude information is lacking in warnings. For coastal regions near the source, the tsunami could precede the warning. In McGehee and McKinney (1995) (referred to hereafter as M & M), a method was described for estimating the amplitude of an approaching tsunami during the first few minutes of the arrival of the leading edge of the first wave using pressure measurements in shallow water. The pressure measurements can be obtained in real-time from the existing network of near-shore wave gages operated by the U.S. Army Corps of Engineers (CE) in cooperation with various coastal states (McGehee and Hemsley 1993; Seymour et al. 1993). The M & M technique relies on detection of an unusually large (positive or negative) sea-surface slope to trigger a warning, and an estimation of the wave amplitude by linear extrapolation of the "trigger" slope over an assumed quarter period of the tsunami wave. Without prior knowledge of the wave period, a range of expected periods, from 10 to 40 minutes, is used to provide corresponding lower and upper bounds for the amplitude. Since the extrapolation is linear, the range of estimates varies by the same factor of four as the range of periods. M & M tested the method with data from the 4 October 1994 Shikotan tsunami, as measured from a CE wave gage at Kahului, HI. Upper and lower bounds that bracketed the actual (approximately 1 m) tsunami height within 1/4 m were predicted from the pressure data.

Four techniques are now suggested to improve the quality of the estimate. They include: inputting the tsunami's actual period, as measured from its passage at more distant locations; utilizing sinusoidal and solitary models to better simulate the wave profile; estimating the tsunami period from the (temporal) derivative of the measured surface elevation; and selecting slope thresholds based on onshore damage criteria. The following

discussion assumes the pressure time series has already been filtered to eliminate wind-wave energy, as described in more detail below.

TECHNIQUES

Operational improvements: Substitution of the actual tsunami period for the broad lower and upper period bounds should reduce the estimated bounds and improve the accuracy of amplitude estimates. Two sources of information are available prior to the arrival of the tsunami at the site of interest: estimation from the seismic signal, and direct measurement of the tsunami at a remote site which the tsunami has already passed. While progress is being made in relating the tsunamigenic potential of an earthquake from the seismic spectrum (Talandier and Okal 1989; Walker and Bernard 1993), effective prediction of the tsunami amplitude, let alone its frequency, from the seismic signal is still a subject of research (Raymond, Hyvernaud, and Talandier 1991; Pendick 1993; Schindele et al. 1995).

For the second option, reliable measurements of the tsunami wave period can potentially be obtained (after at least one wave has passed) from three sources: pressure sensors at other CE wave gages closer to the source of the tsunami, the newer coastal tidal stations operated by the National Ocean Service (NOS) of the National Oceanic and Atmospheric Administration (NOAA), or NOAA's proposed deep-water pressure sensors using acoustic and satellite telemetry (Bernard 1991; Gonzalez et al. 1996). Assimilation of these measurements into propagation models of varying sophistication is already a practice of the current warning procedure (Blackford and Kanamori 1995). What is proposed is an additional effort to transmit the earliest measured period to each of the remaining measurement sites to enhance their "stand-alone" warning capability independent of the performance of the propagation model.

Better models: In M & M, the measured slope that exceeds a "normal" threshold is held constant, so the wave is, effectively, modeled as triangle. The second improvement utilizes a more realistic wave form of the tsunami to predict the crest elevation. It can be applied

using the assumed lower and upper bounds for the tsunami period, or even more effectively, in conjunction with the measured period.

An obvious improvement over a constant slope projection is a sinusoidal, or linear wave model. The majority of the existing subsurface pressure sensors envisioned for application of this technique are located in about 10 m water depth, h. Linear theory has proven adequate for many engineering applications, even in shallow water. However, the more appropriate model for tsunamis of any significant magnitude (say, 1 - 5 m) in this depth may be cnoidal, which reduces to linear theory for smaller amplitudes, or to solitary wave theory for larger waves at the breaking limit. By considering these two "extremes", two results can be obtained which should bracket the actual wave height for most situations.

Sinusoidal: For simplicity, the origins of the x (horizontal) space coordinate is taken at the sensor, of the z (vertical) space coordinate at the still water surface, and for time $t = t_o$, the start of the tsunami as detected from the slope exceedance test. If the tsunami is assumed to have amplitude, $a = H/2$, and angular frequency, $\sigma = 2\pi /T$, at any subsequent time, t, the water surface elevation, $\eta(t)$, is of the form

$$\eta(t) = a\sin(\sigma t) \tag{12}$$

so that the tsunami amplitude, a, is

$$a = \frac{\eta(t)}{\sin(\sigma t)} \tag{13}$$

From linear theory, the measured pressure, p, from a sensor at depth h is

$$\frac{p}{\rho g} = \left[\frac{\cosh k(h+z)}{\cosh(kh)}\right]\eta + h + \bar{\eta} \tag{14}$$

where ρ is the water density, g is gravity, $\bar{\eta}$ is the tidal elevation, and η is the elevation of the water surface due to the tsunami. For long waves, the pressure response function approaches 1. That is,

$$\frac{\cosh k(h+z)}{\cosh(kh)} \rightarrow 1 \quad ...as.... \quad kh \rightarrow 0 \tag{15}$$

so that,

$$\eta = \frac{p}{\rho g} - h - \bar{\eta} \tag{16}$$

The mean depth of the sensor, h, can be determined simply from a long-term (on the order of a month) mean of the pressure time series. The tidal component can be obtained from tide tables, so η, neglecting wind surge, setup/down, etc., is determinable.

The upper and lower bounds of the tsunami amplitude can be found by substituting the upper and lower estimates of the tsunami period, T, into Equation 13. The amplitude bounds can be recalculated every time step, after initial detection. Use of a sinusoidal model is less conservative than the linear model, since the amplitude estimated by Equation 13 for any assumed period, T, is reduced from the linear estimate by the ratio

$$\frac{a_{sinusoidal}}{a_{linear}} = \frac{\frac{\eta(t)}{\sin(2\pi t/T)}}{T\eta(t)/t} = \frac{t}{T\sin(2\pi t/T)} \tag{17}$$

which is always less than 1 for $t < T$. It also reduces the range between the lower and upper bounds, which is a factor of 4 (identical to the range in estimated periods) for the linear model. In the sinusoidal model, the range between the upper and lower bounds is

$$\frac{\sin(\frac{2\pi t}{T})}{\sin(\frac{2\pi t}{4T})} \tag{18}$$

which has a maximum at 4 as t approaches 0, and a minimum of 2.6131... as t approaches $T/4$, at the first crest or trough.

Cnoidal: As for shallow water sinusoidal waves, the pressure attenuation under a solitary wave can be ignored and the mean depth and tide level subtracted, so the water surface elevation, η, can be obtained directly from the pressure time series. The governing equation for solitary theory (Shore Protection Manual 1984) is

$$\eta = H sech^2 \Theta \tag{19}$$

where

$$\Theta = K(x - c\tau) \tag{20}$$

and

$$K = \sqrt{\frac{3H}{4h^3}} \tag{21}$$

In Equations 19 and 21 above, H, the solitary wave height measured from the trough (always at or above the still water level) to the crest, is the desired quantity. The wave celerity, c, is evaluated as

$$c = \sqrt{g(h+H)} \tag{22}$$

Equations 19 -21 describe a solitary wave with the x-origin at the wave crest, and the time origin, τ, at the passage of the crest. As in the sinusoidal model, the sensor can be assumed to be at $x = 0$. A coordinate conversion is utilized to select a new time variable, t, whose origin occurs when the leading edge of the wave arrives at the sensor. Equation 20 becomes

$$\Theta = K[-c(t-T/2)] \tag{23}$$

Though the solitary wave period's theoretical value is infinite, there are two alternatives for estimating a finite value for T. One, use the previously selected upper and lower bounds of the tsunami period, or input the wave period from another source, as described above. Two, assume the wave is constant form and translational, then $T = L/c$. While L is also theoretically infinite, effectively, 95 % of the wave's volume lies within the distance (Demirbilek 1991)

$$L = \frac{2.12h}{\sqrt{H/h}} \tag{24}$$

If the first exceedance of the slope threshold is assumed to be the leading edge of the wave ($\eta_0 = 0$), then the measured water surface change, η_1, at some later time, t_1, then can be expressed

$$\eta_1 = Hsech^2[-Kc(t_1-T/2)] \tag{25}$$

The only unknown in the above equation is H.

More analysis: The third improvement involves extracting additional information from the pressure signal to estimate the wave height directly, without assuming or inputting a wave period. Thus, it can be applied if the pressure sensor detecting the tsunami is the only source of information for a warning. It requires additional analysis of the rate of change of the pressure signal to estimate the tsunami period and/or its amplitude, using either of the two wave models.

Sinusoidal: Taking the time derivative of Equation 16,

$$\frac{\partial \eta}{\partial t} = \frac{1}{\rho g}\frac{\partial p}{\partial t} - \frac{\partial h}{\partial t} - \frac{\partial \bar{\eta}}{\partial t} \tag{26}$$

The mean water depth over the sensor is a constant, and the change in tidal elevation can be neglected over the time scale of a few minutes of interest in a warning situation, so the rate of change of the pressure signal is essentially due to the tsunami signal alone. Combining Equations 12 and 26,

$$\frac{\partial \eta}{\partial t} = \sigma a \cos(\sigma t) \tag{27}$$

The first maximum of the slope magnitude (to include a crest or trough-leading wave) occurs at $\eta = 0$, when $t = 0$, or

$$\left|\frac{\partial \eta}{\partial t}\right|_{max} = \frac{1}{\rho g}\left|\frac{\partial p}{\partial t}\right|_{max} = \sigma a \tag{28}$$

Substituting the maximum slope into Equation 27 and solving for the angular frequency yields,

$$\sigma t = \cos^{-1}\left[\frac{\left|\frac{\partial \eta}{\partial t}\right|}{\left|\frac{\partial \eta}{\partial t}\right|_{max}}\right] \tag{29}$$

so the predicted tsunami period is

$$T = \frac{\cos^{-1}\left[\frac{\left|\frac{\partial \eta}{\partial t}\right|}{\left|\frac{\partial \eta}{\partial t}\right|_{max}}\right]}{2\pi t} \tag{30}$$

The amplitude can be found from Equation 13, or from Equation 28 as

$$a = \frac{|\frac{\partial \eta}{\partial t}|_{max}}{\sigma} \tag{31}$$

Cnoidal: Unlike the linear wave form, the point of maximum slope occurs at some point after the leading edge. For calculating that point, the original time and space origins at the crest will be retained. Taking the time derivative of Equation 19,

$$\frac{d\eta}{d\tau} = \frac{d\eta}{d\Theta}\frac{d\Theta}{d\tau} \tag{32}$$

The first term is

$$\begin{aligned} \frac{d\eta}{d\Theta} &= H\frac{d(sech^2\Theta)}{d\Theta} \\ &= -2\eta \tanh\Theta \end{aligned} \tag{33}$$

and the second term is

$$\begin{aligned} \frac{d\Theta}{d\tau} &= \frac{d[K(c\tau - x_0)]}{d\tau} \\ &= K(c - \frac{dx_0}{d\tau}) \end{aligned} \tag{34}$$

The second term in the brackets is the horizontal water velocity (assumed uniform vertically), which can be approximated anywhere along the profile as $c\eta/h+\eta$, so

$$\begin{aligned} \frac{d\Theta}{d\tau} &= Kc - \frac{Kc\eta}{h+\eta} \\ &= \frac{Kch}{h+\eta} \end{aligned} \tag{35}$$

the maximum slope occurs when the second derivative is zero.

$$\frac{d^2\eta}{d\tau^2} = [\frac{d^2\eta}{d\Theta^2}\frac{d\Theta}{d\tau} + \frac{d\eta}{d\Theta}\frac{d(\frac{d\Theta}{d\tau})}{d\Theta}]\frac{d\Theta}{d\tau} = \tag{36}$$

The first term in the brackets is found by differentiating Equation 33,

$$\begin{aligned}\frac{d^2\eta}{d\Theta^2} &= -2\tanh\Theta\frac{d\eta}{d\Theta} - 2\eta\frac{d(\tanh\Theta)}{d\Theta} \\ &= 4\eta - \frac{6\eta^2}{H}\end{aligned} \tag{37}$$

and the last term in the brackets by differentiating Equation 35.

$$\begin{aligned}\frac{d(\frac{d\Theta}{d\tau})}{d\Theta} &= \frac{d(\frac{Kch}{h+\eta})}{d\Theta} \\ &= \frac{2Kch\eta\tanh\Theta}{(h+\eta)^2}\end{aligned} \tag{38}$$

Substituting Equations 33, 35, 37, and 38 into Equation 36 and solving for H,

$$\begin{aligned}[4\eta - \frac{6\eta^2}{H}][\frac{Kch}{h+\eta}] + \frac{[-2\eta\tanh\Theta][2Kch\eta\tanh\Theta]}{(h+\eta)^2} &= 0 \\ 2 - \frac{3\eta}{H} - \frac{2\eta(1-\frac{\eta}{H})}{h+\eta} &= 0 \\ H = \frac{\eta^2+3h\eta}{2h} \quad \ldots\ at\ (\frac{d\eta}{d\tau})_{max}&\end{aligned} \tag{39}$$

Better Thresholds: The fourth improvement involves selecting the threshold of slope exceedance that triggers a warning. In M & M, a heuristic threshold was selected that was the approximate maximum slope for a 10 m range, semidiurnal tide, which is an order of magnitude higher than the normal tide range at Kahului. Other modes of energy besides tides and wind waves may be evident in a pressure time series that cause large slope changes, but are not caused by tsunamis and do not warrant a civil defense response. An empirical method is described in Seymour (1996) using data from the long-term (up to 2 decades) pressure records from gages operated by the CE-managed Coastal Data Information Program (Flick et al. 1993). By analyzing the measured slopes in the historical time series, a threshold can be selected just above the normal (i.e., non-threatening) conditions, but below any dangerous/damaging conditions, regardless of the source of the wave energy.

Another definition of a "trigger" is the maximum slope for a tsunami of sufficient height to produce damage or threat onshore. That is, select the threshold of runup that is considered dangerous, and calculate the characteristics of the tsunami that would exceed it. From Synolakis (1987) the runup, R, is expressed as a function of h_s and H_s, the water depth and wave height at the toe of an idealized beach, where the bottom slope changes from a constant offshore value to a steeper, but constant onshore value.

$$\frac{R}{h_s} = 1.109\left(\frac{H_S}{h_s}\right)^{0.582}$$
$$H_s = h_s\left[\frac{R/h_s}{1.109}\right]^{1/0.582} \tag{40}$$

If wave power, P, conservation from linear theory is assumed, the relationship between H_s and H, the wave height farther offshore where the pressure sensor is located, is

$$P_{offshore} \propto H^2\sqrt{gh} = H_s^{\,2}\sqrt{gh_s} \propto P_{onshore}$$
$$H = H_s\left(\frac{h_s}{h}\right)^{1/4} \tag{41}$$

The solution to Equation 41 can be used in Equation 28 to select the trigger slope for the sinusoidal model. For the solitary model combine Equations 19, 21, 22, and 32,

$$\left(\frac{\partial \eta}{\partial \tau}\right)_{max} = -2\eta \tanh\Theta \frac{Kch}{h+\eta}$$
$$= -2\sqrt{\frac{3H}{4h^3}}\sqrt{g(h+H)}\frac{\eta h}{h+\eta}\pm\sqrt{1-\frac{\eta}{H}} \qquad (42)$$

RESULTS

Evaluation: The time series used in M & M to evaluate performance was obtained from the 4 October 1994 Shikotan tsunami using pressure sensors located inside and offshore of Kahului Harbor, HI. The measurement system in Kahului Harbor was intended to measure wind wave and harbor seiche energy down to 0.0033 Hz, and was not designed to capture the continuous, multi-hour time series. Data collected during the passage of the tsunami were obtained by remotely accessing the system via telephone modem, interrupting the pre-programmed sampling scheme, and manually downloading the system buffers, approximately every two hours. The assumptions used in M & M for the actual start time of adjacent segments were subsequently found to be erroneous.[4] Consequently, time series originally thought continuous (Figure 33, M & M's Figure 3A, which is referenced to Pacific Standard Time) are in fact separated by gaps of approximately 15 minutes. This problem has been corrected in the following analyses.

Filtering of the pressure signal is required to remove the wind wave energy from the 1-Hz samples and "expose" the tsunami signal. If a warning capability is envisioned, filtering must be accomplished in the time-domain. In M & M, a sliding boxcar mean was used; the segment length for averaging was either 180 or 300 sec, and the boxcar was advanced in

[4] A footnote in M&M explains that timing errors were suspected, but were not critical to evaluation of the basic detection and linear extrapolation routine.

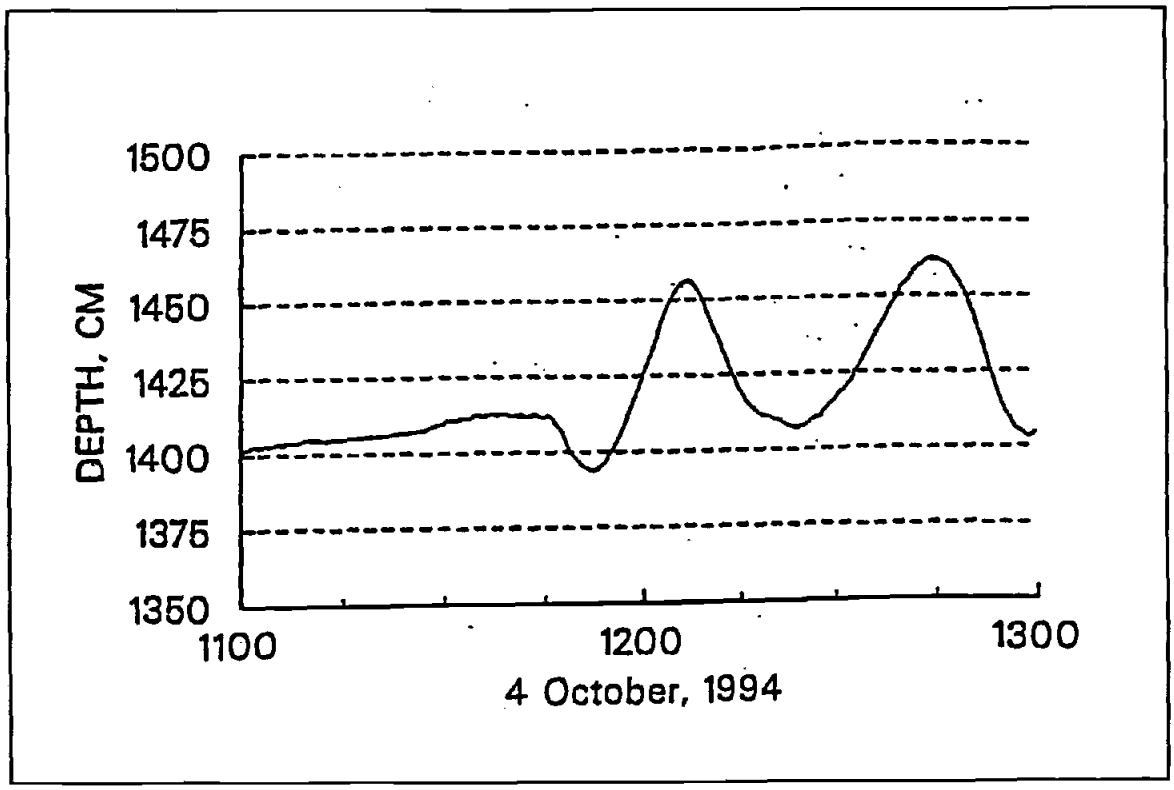

Figure 33. Original filtered offshore water level time series (Figure 3A in M & M)

15 or 30 sec increments to calculate the next point. For this paper, a band-pass (0.0003 - 0.008 Hz) four-pole Butterworth filter is used. This eliminates the delay (15 or 30 sec) in generating the filtered time series and removes the lower frequency tidal signal to isolate the tsunami.

Figure 34 shows the filtered offshore and in-harbor pressure time series segments correctly time-coded. Most unfortuitously, a gap occurs just at the arrival of the tsunami offshore (Figure 34A). While various order splines can be used to interpolate the missing signal, any attempt to evaluate a warning capability based on the interpolated portion of the offshore signal would be inconclusive. Other evaluations, such as the performance of other filters or the most appropriate wave model, can be made on the well-developed portion (after 1200 PST) of the offshore tsunami signal. The start of the second harbor segment at 12:36:17 (Figure 34B) occurs immediately before the end of the first offshore segment (not tsunami evident) and just minutes before the initial arrival of the tsunami in the harbor at

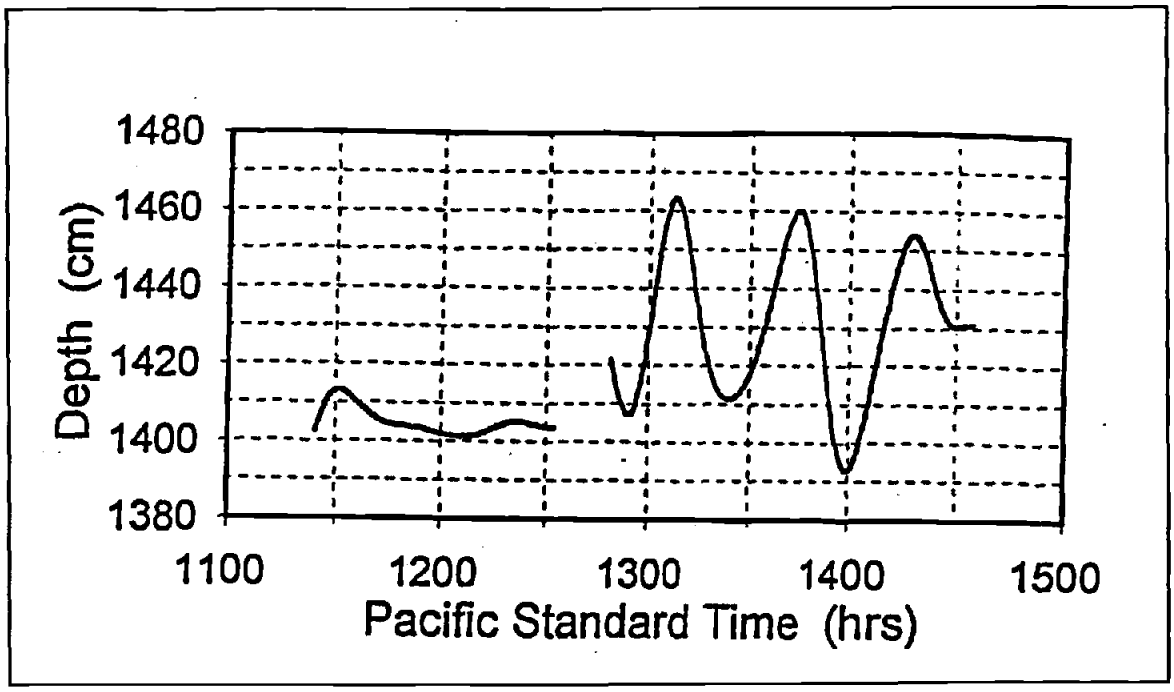

Figure 34A. Corrected filtered offshore water level time series

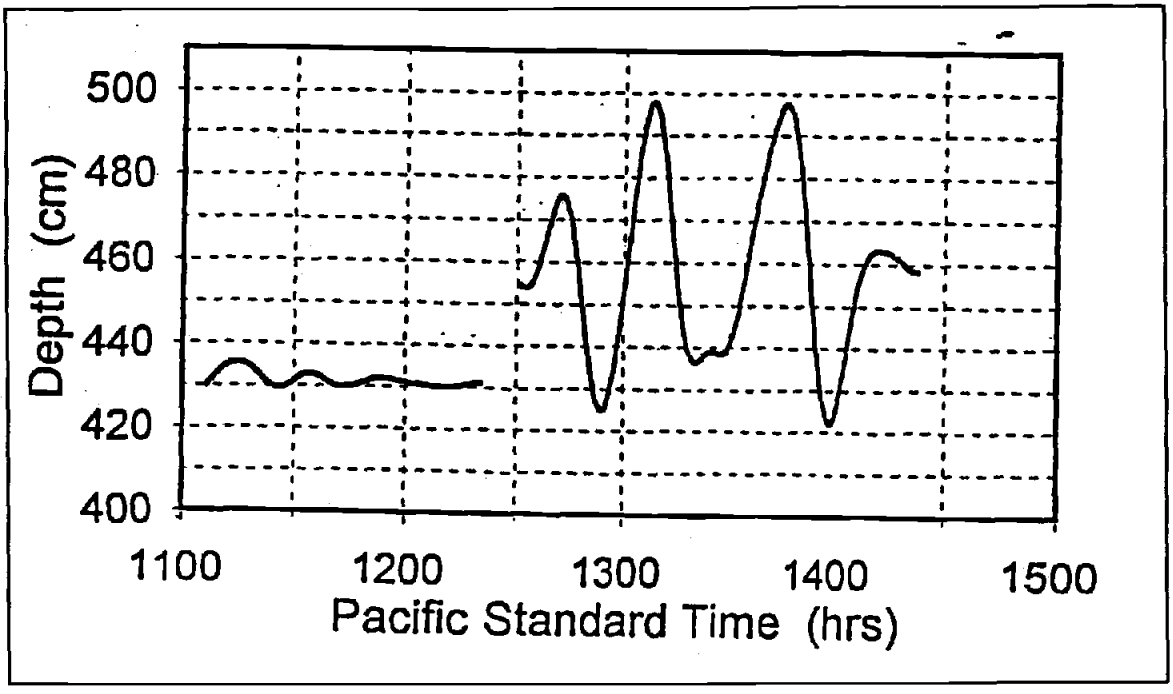

Figure 34B. Corrected filtered onshore water level time series

around 1241. It is this second segment of the filtered harbor time series that is demeaned and used to evaluate the predictions, below.

Table 4 provides a 5-second subset of the time series, beginning two seconds before the 0.375 mm/sec slope threshold from M & M is first exceeded. Column 1 is **n**, the point number of the time series, and time in seconds after the start of the segment; column 2 is t, as used in Equation 13, beginning at point number 265, when the threshold is first exceeded. Column 3 is η, the filtered, demeaned time series, and column 4 is the discrete slope, i.e., $(\eta_{n-1} - \eta_n)/1$ sec.

Table 4
Measured Water Level, Slope, and Predicted Crest Elevation (Subset)

n	t	h	Dh/Dt	h*
263	na	-1.382	0.0373	na
264	0	-1.344	0.0375	na
265	1	-1.307	0.0377	12.365
266	2	-1.269	0.0380	12.403
267	3	-1.231	0.0382	12.440

Beginning at point number 265, Equation 13 and an input period will provide an amplitude estimate. At that time, the slope is still increasing, so Equation 30 cannot be used to estimate the tsunami period from the data. If no other period information is available, the 10 - 40 min assumed range is the only option. At $t = 1$ (i.e., one second after the tsunami is detected), the corresponding lower and upper bounds of the amplitude from Equation 13 are 2.3 cm and 13.1 cm, respectively, an underprediction of 4.2 cm. Using the slope extrapolation method of M & M at the same point gives a range from 4.3 cm to 21.3 cm. This brackets the actual value of the crest, but with the expected wider bounds. Succeeding predictions will literally improve by the second.

If a reliable estimate of the tsunami period is known *a priori* from, for example, another gage in the CE network, better amplitude estimates should result. Rigorous spectral

analysis requires a time series much longer than the longest period of interest, but a delay of many hours to obtain an accurate peak period may be a poor trade-off during an actual event. Using the 6864-second (1.9 hours) filtered segment of the *offshore* signal as an example of a short sample of an "upstream" tsunami event, a Fourier transform yields a spectral peak at 2288 sec (~38 minutes).[5]

Column 5 is η^*, the predicted elevation of the crest, using the amplitude predicted from Equation 13, with $T = 2288$ sec. Since the model assumes time zero coincides with the zero-crossing of the elevation, the numerator is the change in elevation from -1.3 cm, the value of η at t_o. After dividing, -1.3 cm is added to a to reference η^* to the same datum used for the actual crest. Columns 3 and 5 are plotted in Figure 35 (against **n**), from the beginning of the segment to point 800, just beyond the first crest of the tsunami.

After occurrence of the (local) maximum slope, both the tsunami period (Equation 30) and amplitude (Equation 31) can be predicted. Table 5 contains a 15-sec interval of the time series, beginning just before the occurrence of η_{max} at point 436,[6] then skips to a 5-sec interval in the vicinity of the following crest: 17.3 cm at point 694. Columns 1-4 are the same as in Table 4. Column 6 is T in sec, as predicted each time step from Equation 30. Column 7 is η (T), the crest elevation predicted from the amplitude provided from Equation 13 (or identically, Equation 31) with the instantaneous value of T from column 4 in the denominator. As described above, the crest prediction is referenced to the same datum as the measured crest by using η - 7.4 in the numerator. After dividing, the 7.4 cm offset is added back. Column 7 is also plotted in Figure 35. The solitary model (Equation 39) predicts one amplitude value of 11.3 cm at point 437.

Discussion: In addition to reducing the delay in calculating slopes, the band-pass filter is superior to the moving-window filter from M & M in suppressing high-frequency noise seen in Figure 33. It also eliminates the delay (15 or 30 sec) in generating the filtered time series

---

[5] The measured tsunami period in shallow water is highly affected by local bathymetry. For example, a deepwater measurement of this tsunami from several hundred kilometers offshore of Oregon resulted in a dominant period of 24 minutes. (Personal conversation with Mr. Edward Bernard of NOAA's Pacific Marine Environmental Laboratory, Seattle, WA.)

[6] The point associated with η_{max} is actually the center of a 16-sec interval of constant (to four decimal places) maximum slope.

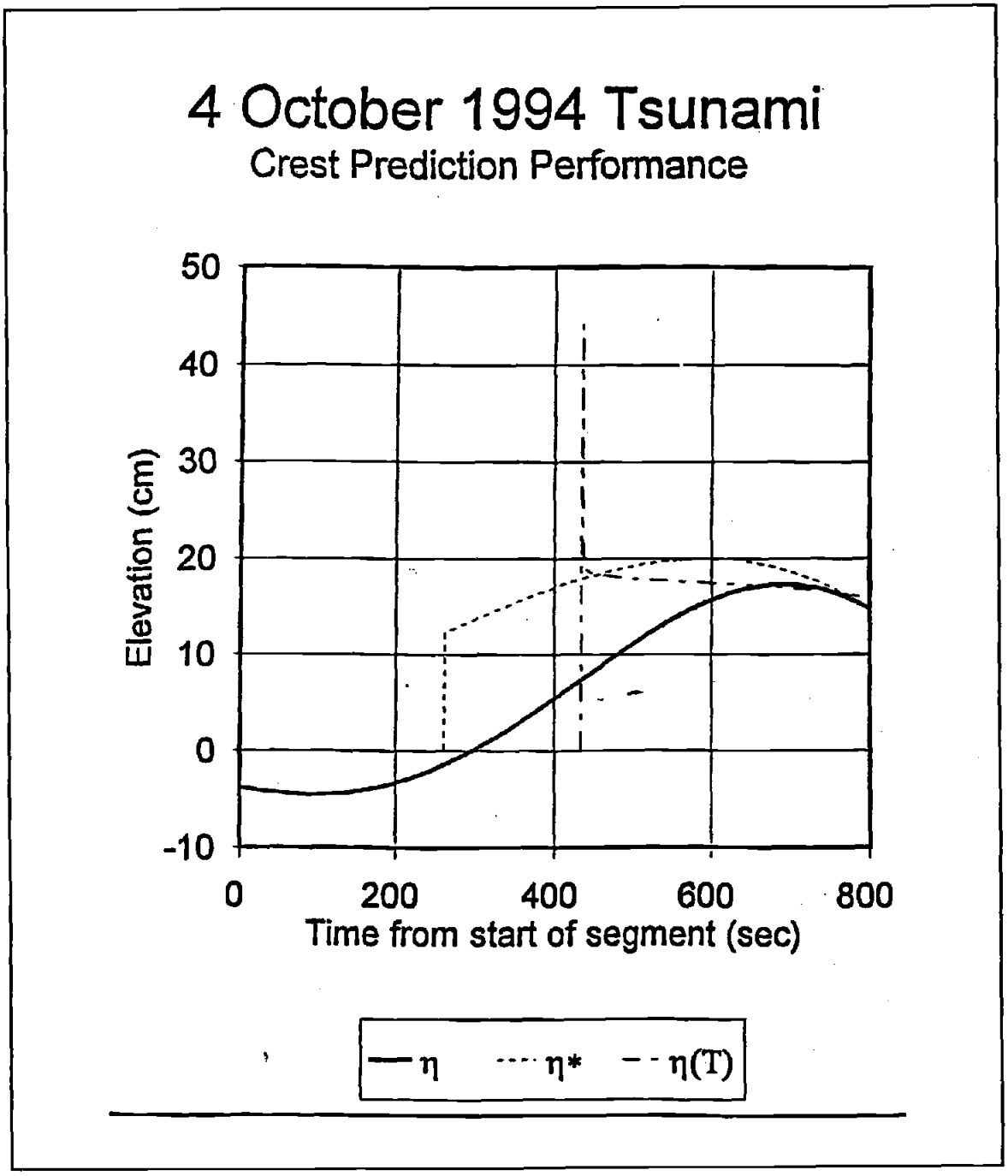

Figure 35. Measured water level and predicted crest elevations

Table 5
Measured Water Level, Slope, Predicted Period, and Crest Elevation (Subset)

n	t	ηη	Δη/Δt	η*	T	η(T)
436	0	7.413	0.0583	17.904	0.000	0.000
437	1	7.471	0.0583	17.928	3962.929	44.186
438	2	7.530	0.0583	17.953	1568.621	21.969
439	3	7.588	0.0583	17.977	1385.192	20.267
440	4	7.646	0.0583	18.002	1314.296	19.609
441	5	7.705	0.0583	18.026	1276.382	19.257
442	6	7.763	0.0583	18.050	1252.677	19.037
443	7	7.821	0.0583	18.074	1236.407	18.886
444	8	7.879	0.0583	18.097	1224.523	18.776
445	9	7.938	0.0582	18.121	1215.444	18.692
446	10	7.996	0.0582	18.145	1208.270	18.625
447	11	8.054	0.0582	18.168	1202.446	18.571
448	12	8.112	0.0582	18.191	1197.613	18.526
449	13	8.170	0.0582	18.215	1193.527	18.488
450	14	8.229	0.0581	18.238	1190.013	18.456
...	...	...	...	...	...	...
692	256	17.333	0.0008	18.894	1032.684	16.996
693	257	17.333	0.0004	18.872	1032.002	16.989
694	258	17.333	-0.0001	18.849	1031.317	16.983
695	259	17.333	-0.0005	18.826	1030.629	16.977
696	260	17.332	-0.0009	18.803	1029.936	16.970

with a moving window, and removes the lower frequency tidal signal for clearer representation of just the tsunami. The first warning that the threshold has been exceeded with the heuristically selected 0.375 mm/sec threshold comes more than 7 minutes before the arrival of the first crest.[7] The theoretical t_0 for a 38-minute wave would occur at point 122, where

[7] The typical CE wave gage is located 1-2 km offshore. Assuming linear theory and an average depth between the gage and shore of 5 m, the crest will take an additional 140 to 280 sec to arrive at shore. In practice, 10-minute warning times should be realizable.

the signal can be seen (Figure 35) to begin its upward climb, but the slope is just 0.05 mm/sec, in the same range as normal tides. Even with reliable period information, applying the sinusoidal model too early will result in a poor prediction.[8] Starting when the slope maximum occurs, the sinusoidal model conforms nearly exactly to the measured wave form. Note also from Figure 35, that the half-period from the trough to the crest is roughly 600 sec, which is consistent with the predicted periods in Table 5. After a large error in the first second, the model converges rapidly to a very accurate estimate of the ultimate crest elevation.

The solitary model underpredicts the crest significantly. Unlike Equation 13 or 31, Equation 39 is a function of depth and, since the zero-crossing point is not "reset," the predicted crest elevation is directly affected by the selection of datum. Demeaning the signal by the mean value of the second segment (455.5 cm) produces a different prediction than if it was demeaned by 426.5 cm, the mean of the preceding segment. For example, when η is small relative to h, Equation 39 reduces to 1.5 η. If the datum was shifted downward by 20 cm, the actual crest would be 37.3 cm, the maximum slope would occur at 27.5 cm, but the predicted crest would be 41.3 cm, an overprediction.

While the two extremes of cnoidal theory did not produce major differences in this instance, the sinusoidal and solitary models vary considerably for larger wave heights. Say, a minimally destructive tsunami with a height of 1 m and a period of about 30 min is measured with a typical wave gage in 10 m of water. The theoretical maximum (temporal) slope for the sinusoidal model, from Equation 28, is

$$\left|\frac{\partial \eta}{\partial t}\right|_{max} = \sigma a = \frac{2\pi}{1800}(1/2) = 1.7 \ mm/\text{sec} \tag{43}$$

The solitary wave maximum slope for the same parameters can be found by rearranging Equation 39 to provide η in terms of H and h.

$$\eta = \pm\frac{3h}{2}\left[\sqrt{\left(\frac{8H}{9h}+1\right)}-1\right] \tag{44}$$

[8] Not shown in the tables, but by way of illustration: two minutes after starting at point 122, Equation 13 predicts a crest of barely 1 cm.

Substituting the given parameters gives a value of $\eta = \pm 0.65$ m at the maximum slope. To find the value of that maximum slope, solve Equation 32 with the appropriate values, which yields a value of about 200 mm/sec, or two orders of magnitude higher than the sinusoidal model. Inversely, a measured slope of this magnitude would result in a predicted crest somewhere between 1 m (solitary) and 29 m (sinusoidal). Obviously, it would be critical to select the right model in a working warning system! To preclude unusable ranges for larger tsunamis, it is essential to use an accurate value for the mean depth and the tide to evaluate η, when the maximum slope occurs.

CONCLUSIONS

In McGehee and McKinney (1995), a simple method was described for estimating the amplitude of an approaching tsunami with a nearshore, subsurface pressure sensor. In this paper four techniques were suggested to improve the timeliness and the accuracy of the estimate. They are: inputting the tsunami's actual period, as measured from its passage at more distant locations; utilizing sinusoidal and solitary models to better simulate the wave profile; estimating the tsunami period from the (temporal) derivative of the measured surface elevation; and selecting slope thresholds based on onshore damage criteria.

The performance improvements for the first, second, and third suggestions were evaluated with a pressure time series from the 4 October 1994 Shikotan tsunami measured inside and offshore of Kahului Harbor, HI. The tsunami height measured nearly 1 m at it's maximum, but the predictions were tested on the first, smaller wave to arrive in the harbor. The pressure signal was processed with a band-pass filter to remove wind wave and tidal components.

Using the sinusoidal model and no outside information, it is possible to get very accurate warnings more than four minutes before the arrival of the crest at the sensor. An heuristic slope exceedance threshold of 0.375 mm/sec triggered a first warning more than 7 minutes before the arrival of the crest at the sensor. At that point, using the sinusoidal model with the tsunami wave period, *as post-measured at that site*, underpredicted the crest

for the earliest estimates, but gave reasonable agreement within five minutes of the arrival of the crest. Selecting a lower threshold gave more (over 9 minutes) warning, but the quality of the estimated amplitude declined. Waiting one more minute until occurrence of the maximum slope improved the accuracy significantly. Starting the sinusoidal model at the maximum slope, it rapidly converged to within 10 % of the actual crest value in 5 seconds. The solitary model underpredicted the crest in this analysis, but its performance is sensitive to selection of datum. Improved determination of mean depth and tidal elevation at the sensor are critical to reasonably predict larger tsunamis.

SUMMARY

Three case studies were presented that rely on measured wave data to either understand an environmental processes, evaluate design tools and provide engineering solutions. The first study documented an extensive monitoring effort of a harbor located on a coral reef flat. Several typhoons were captured in both deep and shallow water. Analysis of the data identified low frequency oscillations of the entire reef flat basin, and associated currents was the dominant form of hydraulic energy during extreme events.

In the second study measurements were made of waves at four sites inside and outside a harbor protected by a porous rubble mound breakwater. The reflection and transmission functions of the breakwater were calculated from the measurements. Finally, the measured transmission characteristics were compared graphically to the physical model results. The measured wave transmission was higher than predicted.

In the third study, techniques were suggested to improve the timeliness and the accuracy of warnings of an approaching tsunami using a subsurface pressure sensor. Their effectiveness were evaluated with a pressure time series from the 4 October 1994 Shikotan tsunami measured inside and offshore of Kahului Harbor, HI. Using no outside information, it is possible to trigger a first warning more than nine minutes, and a very accurate amplitude estimate more than four minutes, before the arrival of the crest at the sensor. Improved determination of mean depth and tidal elevation at the sensor are critical to reasonably predict larger tsunamis.

These three studies demonstrate the impact of the analysis approach, the sampling methodology, and the sensor characteristics on the utility of wave measurements in engineering research. In fact, the single most important conclusion of the thesis is the need to develope a *data analysis plan* prior to developing a *data collection plan*, and allow the needs and limitations of both to drive the selection of an appropriate sensor/instrument system.

BIBLIOGRAPHY

Bernard, E. N. (1991). "Tsunami hazard: a practical guide for tsunami hazard reduction." *Natural Hazards*, 4, 2-3.

Blackford, M., and Kanamori, H. (1995). "Tsunami warning system workshop report (Sept. 14-15, 1994)." *NOAA Technical Memorandum ERL PMEL-105*.

Boc, S. J., and McGehee, D. (1989). "Agat Small Boat Harbor, Guam - Monitoring Plan." *Proceedings, Coastal Zone* '89. American Society of Civil Engineers, Charleston, SC.

Chen, H. S., and Houston, J. R. (1986). "Calculation of water oscillations in coastal harbors - HARBS and HARBD user's manual," Instruction Report CERC 86-7, U.S. Army Engineer Waterways Experiment Station, Vicksburg, MS.

Demirbilek, Z. (1991). "Class notes: Ocean Wave Mechanics, OE 671." Texas A & M University, College Station, TX.

Earle, M. D., McGehee, D., and Tubman, M. (1996). "Field wave gaging program, wave data analysis standard," Instruction Report CERC-95-1, U.S. Army Engineer Waterways Experiment Station, Vicksburg, MS.

Farrar, P. D., and Chen, H. S. (1987). "Wave response of the proposed harbor at Agat, Guam: Numerical model investigation," Technical Report CERC-87-4, U.S. Army Engineer Waterways Station, Vicksburg, MS.

Flick, R., Seymour, R., Guza, R., and McGehee. D. (1993). "California's coastal data information program: a successful federal, state, and university cooperation," *Proceedings, Coastal Zone '93, 8th Symposium on Coastal and Ocean Management*, ASCE, New Orleans, LA.

Gonzalez, F., Mero, T., Mofgeld, H., and Rabinovich, A. (1996). "Far-field measurements of the 4 October 1994 Shikotan tsunami." *Perspectives on Tsunami Hazard Reduction - Proceedings, 1995 IUGG Tsunami Symposium*, IUGG/AGU, Boulder, CO.

Jackson, R. A. (1967). "Stability of Proposed Breakwater, Burns Waterway, Indiana; Hydraulic Model Investigation" - Technical Report No. 2-766 - U.S. Army Engineer Waterways Experiment Station - Vicksburg, MS

Keulegan, G. H. (1973). "Wave Transmission Through Rock Structures: Hydraulic Model Investigation" - Technical Report H-73-1 - Hydraulics Laboratory - U.S. Army Engineer Waterways Experiment Station - Vicksburg, MS

Longuet-Higgins, M. S., Cartwright, D. E., and Smith, N. D. (1963). "Observations of the directional spectrum of sea waves using the motions of a floating buoy," *Ocean Wave Spectra*, 111-36.

McGehee, D., and Hemsley, J. (1993). "Implementing a national wave monitoring network - some lessons and plans." *Proceedings, Waves '93, 2nd International Symposium on Ocean Wave Measurement and Analysis*, ASCE, New Orleans, LA.

McGehee, D., and McKinney, J. (1995). "Measurement of the October 4, 1994 tsunami with pressure transducers." *Perspectives on Tsunami Hazard Reduction - Proceedings, 1995 IUGG Tsunami Symposium*, IUGG/AGU, Boulder, CO.

McGehee, D. D., Moritz, H., Prickett, T., Shirley, J. (1997). "Burns Harbor, Indiana, Monitoring Study; Volume I: Overview of Approach and Results" - Technical Report CHL-97-5, U.S. Army Engineer Waterways Experiment Station - Vicksburg, MS.

McGehee, D. D. and Rhee, J. P. (1996). "Results of Analysis of Wave Measurements at Burns Harbor" - in "Burns Harbor, Indiana, Monitoring Study; Volume II: Detailed Approach and Results" - U.S. Army Engineer Waterways Experiment Station - Vicksburg, MS.

Pendick, D. (1993). "Slow motion slip may drive tsunami surprise." *Science News*, 143, 135.

Raymond, D., Hyvernaud, O., and Talandier, J. (1991). "Automatic detection, location and quantification of earthquakes: application to tsunami warning." *Pure and Applied Geophysics*, 135, no.3, 361-382.

Schindele, F., Raymond, D., Gaucher, E., and Okal, E. (1995). "Analysis and automatic processing in near-field of eight 1992-94 tsunamigenic earthquakes: improvements towards real-time tsunami warning." *Pure and Applied Geophysics*, 144, no.3-4, 381-408.

Seymour, R. (1996). "Sea level rate of rise as an early warning of tsunamis." *Proceedings, Hazards '96*, Toronto, Ontario.

Seymour, R., Castel. D., McGehee, D., Thomas, J., and O'Reilly, W. (1993). "New technology in coastal wave monitoring." *Proceedings Waves '93, 2nd International Symposium on Ocean Wave Measurement and Analysis*, ASCE, New Orleans, LA.

Shore Protection Manual. (1977). 3rd ed., 2 Vol, U.S. Army Engineer Waterways Experiment Station, U.S. Government Printing Office, Washington, DC.

Shore Protection Manual, 4th ed., 2 Vols. (1984). U.S. Army Corps of Engineers (USACE) Waterways Experiment Station, Vicksburg, MS.

Smith, J. M. (1993). "Nearshore wave breaking and decay," Technical Report CERC-93-11, U.S. Army Engineer Waterways Experiment Station, Vicksburg, MS.

Steele, K. E., Wang, D. W., Teng, C., and Lang, N. C. (1990). "Directional wave measurements with NDBC 3-meter discus buoys," 1804-01.05, U.S. Department of Commerce, National Data Buoy Center, Stennis Space Center, MS.

Synolakis, D. (1987). "Runup of solitary waves." *Journal of Fluid Mechanics*, 185, 522-545.

Talandier, J., and Okal, E. (1989). "An algorithm for automated tsunami warning in French Polynesia based on mantle magnitudes." *Bulletin of the Seismological Society of America*, 79, 1177-93.

U.S. Army Engineer District, Honolulu. (1981). "Final Detailed Project Report and Environmental Statement; Agat Small Boat Harbor, Territory of Guam," Honolulu, HI.

Walker, D. A., and Bernard, E. N. (1993). "Comparison of T-phase spectra and tsunami amplitudes for tsunamigenic and other earthquakes." *Journal of Geophysical Research*, 98(C7), 12,557-12,565.